EXPERIMENTAL INVESTIGATION AND SYSTEMS MODELING OF FRACTIONAL CATALYTIC PYROLYSIS OF PINE

A Thesis
Presented to
The Academic Faculty

By

Anil Goteti

In Partial Fulfillment
Of the Requirements for the Degree
Master of Science in the
School of Chemical and Biomolecular Engineering

Georgia Institute of Technology

December 2010

EXPERIMENTAL INVESTIGATION AND SYSTEMS MODELING OF FRACTIONAL CATALYTIC PYROLYSIS OF PINE

Approved by:

Dr. Matthew J. Realff, Advisor
School of Chemical and Biomolecular
Engineering
Georgia Institute of Technology

Dr. John D. Muzzy, Co –advisor
School of Chemical and Biomolecular
Engineering
Georgia Institute of Technology

Dr. Christopher W. Jones
School of Chemical and Biomolecular
Engineering
Georgia Institute of Technology

Dr. Pradeep K. Agrawal
School of Chemical and Biomolecular
Engineering
Georgia Institute of Technology

Dr. Rhett J. Mayor
School of Mechanical Engineering
Georgia Institute of Technology

Date approved: November 5, 2010

ACKNOWLEDGEMENTS

Contents

LIST OF FIGURES

ix

LIST OF TABLES

SUMMARY

The fractional catalytic pyrolysis of pine was studied both experimentally and through models. A preliminary stage economic analysis was conducted for a wood chip pyrolysis facility operating at a feed rate of 2000 wet ton/day for producing bio-oil.

In the experimental study, multiple grams of bio oil were produced in a single run to facilitate the more extensive characterization of the oil produced from pyrolysis of biomass impregnated with different catalysts. Two reactors configurations, a screw extruder and a tubular pyrolysis reactor, were explored to perform fractional catalytic pyrolysis of biomass. The main aim of performing a wood pyrolysis reaction in a modified screw extruder is to facilitate the simultaneous collection of bio-oil produced from staged temperature pyrolysis of three main components of wood, cellulose, hemicellulose and lignin, at a reasonable scale. Apart from complete characterization of bio-oil, this will enable us to study the effect of various selected catalysts on the quality of bio-oil and the percentage of char produced, and the influence of process parameters on chemical composition of the pyrolysis oils. These experiments were later performed in a tubular pyrolysis reactor due to the difficulty of making different parts of the extruder work well together. The goal of these experiments is to produce bio-oil in multiple grams from fractional catalytic pyrolysis of wood. This will enable us to study the effect of catalyst on the chemical composition of the oil and percentage of char produced.

In the modeling studies, a model of an auger reactor comprised of three different zones run at different temperatures to facilitate the collection of oil from pyrolysis of three major components of wood, namely cellulose, hemicelluloses and lignin, was developed. The effect of residence time distribution (RTD), and zone temperatures based on kinetic models on the yield of products

was studied. Sensitivity of the Arrhenius rate constants calculated from synthetic data with respect to small variations in process parameters was evaluated.

In the economic analysis of a wood chip pyrolysis facility, mass and energy calculations were performed based on a feed rate of 2000 wet tons/day of wood chips to the dryer. The cost of bio-oil at 10% return on investment was proposed and the sensitivity of the selling price of bio-oil with respect to capital and operating costs was analyzed.

The experimental study will serve as a benchmark in exploring the above mentioned reactor configurations further. Alkali metal carbonates were used to study the quality of oil produced from pine pyrolysis. It was established that these catalysts, when added in the same molar ratio basis, increase the percentage of char. However, complete characterization of these oils for different catalysts needs to be done.

Systems modeling of pyrolysis in an auger reactor established that the kinetic parameters (depending on experimental set up) and the RTD (Residence Time Distribution) parameters play a crucial role in determining the yield of oil. Variations in temperature of zone 3 play a crucial role in varying the output of oil whereas variations in temperatures of zones 2 and 1 do not significantly impact the output of oil. For a given reaction kinetic scheme for the pyrolysis reactions, calculated values of the kinetic rate constants are not sensitive to errors in experimental conditions. It was also established that the experimental error in calculation of the RTD parameters can induce error in calculation of the Arrhenius constants but these values can still predict the yield of products accurately.

In the economic analysis of wood chip pyrolysis, the selling price of the bio-oil according to the cost calculation is projected to be $1.49/gal. The production cost of bio-oil is $ 1.20/gal. The

cost of bio-oil is extremely sensitive to variations in operating cost (for example, cost of feed stock and selling price of char) and is not significantly affected by the variations in capital cost.

CHAPTER 1

INTRODUCTION

About 97% of all transportation energy in the United States is derived currently from nonrenewable petroleum (Davis et. al., 1998). Energy for transportation consumes 63% of all oil used in the United States. Foreign oil accounts for more than half of all oil used in the United States. The fact that oil is nonrenewable and the fact that the United States is heavily reliant on foreign sources for energy are excellent incentives for developing renewable energy sources. The accelerated rate of growth of energy consumption in Asia, particularly China and India, raises this incentive for all countries. In addition, the burning of fossil fuels, which produces carbon dioxide, has serious environmental consequences. In contrast to fossil fuels, the use of biomass for energy provides significant environmental advantages. Plant growth needed to generate biomass feedstocks removes atmospheric carbon dioxide, which offsets the increase in atmospheric carbon dioxide that results from biomass fuel combustion. There is currently no commercially viable way to offset the carbon dioxide added to the atmosphere (and the resultant greenhouse effect) that result from fossil fuel combustion. The climate change effects of carbon dioxide from fossil fuels are now generally recognized as a potential serious environmental problem. To meet the goals of the Kyoto agreement, the United States was asked to reduce greenhouse gas (GHG) emissions to a level 7% below the 1990 emissions in 2008. Carbon dioxide is the predominant contributor to the increased yield of GHGs. The combustion of fossil fuels accounts for two-thirds of global anthropogenic CO_2 emissions, with the balance attributed

to land use changes which could happen as a result of land converted for biofuel growth (Mohan et.al, 2006).

Renewable energy is of growing importance in satisfying environmental concerns over fossil fuel usage. Wood and other forms of biomass are one of the main renewable energy resources available. In contrast to other renewables, that give heat and power, biomass represents the only source of liquid, solid and gaseous fuels (Bridgewater et.al, 2000). Biomass, which comprises 47% of total renewable energy consumption worldwide, is the single-largest renewable energy resource currently being used. Recently, it surpassed hydropower as an energy source (http://www.feedstockreview.ornl.gov/pdf/billion_ton_vision.pdf). Wood and other biomass can be treated in a number of different ways to provide such fuels. Thermochemical and bio-chemical processes are the two most important routes to convert woody biomass into fuel. Also, wood is used for fueling steam engines and turbines that generate electricity. Fast pyrolysis of woody biomass, a thermochemical process for conversion of woody biomass to bio-oil, will be the focus in this study.

The first objective of the thesis is the development of a procedure for generating multiple grams of bio-oil in a single run to facilitate the more extensive characterization of the oil produced from pyrolysis of biomass impregnated with different catalysts. Two reactor configurations namely, a screw extruder and a tubular pyrolysis reactor will be explored to perform fractional catalytic pyrolysis of biomass. The effect of various selected catalysts on the quality of bio-oil and the percentage of char produced, and the influence of process parameters and catalytic conditions on chemical composition of the pyrolysis oils will be investigated.

The second objective of the thesis is the development of a model of an auger reactor comprised of three different zones run at different temperatures. The effect of residence time distribution

(RTD), and zone temperatures based on kinetic models on the yield of products will be studied. The sensitivity of Arrhenius rate constants calculated from synthetic data with respect to small variations in process parameters will be evaluated. Mass and energy balances on the auger reactor will be performed and the energy requirement for each unit process will be calculated.

The third objective is the economic assessment of the woody biomass pyrolysis plant based on a feed rate of 2000 wet tons/day of wood chips. An estimate of the cost of the bio-oil per gallon for a 10% Return on Investment (ROI) based on the feed rate will be evaluated.

CHAPTER 2

LITERATURE SURVEY

2.1 Wood composition

The chemical composition of wood is different from non-renewable fuels. Wood and other plant biomass primarily consists of oxygen containing polymers. Carbohydrate polymers and oligomers (65%-75%) and lignin (18%-35%) are the major structural chemical components of wood. Organic extractives and inorganic minerals are typically minor low molar mass extraneous materials (4%-10%). Figure 2.1 gives a schematic of general components in plant biomass (Mohan et.al, 2006).
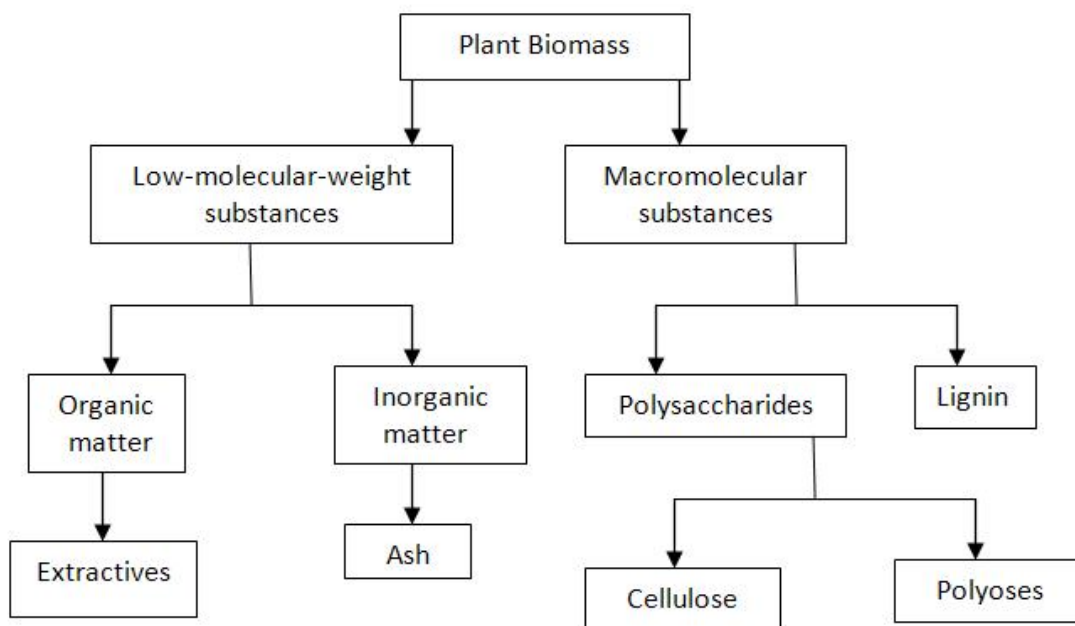
Figure 2.1: General composition in plant biomass (Mohan et. al, 2006)

The percentage weights of cellulose (a polymer glucosan), hemicelluloses (also known as polyose), and lignin vary in different biomass species of wood. The products of biomass

4

pyrolysis are a combination of pyrolysis of the three major components of wood, namely cellulose, hemicellulose and lignin and extractives, each of which has its own kinetic characteristics. In addition reactions of primary pyrolysis products and between pyrolysis products and the original feedstock molecules could result in secondary reaction products (McCarthy et. al, 2000).

2.2 Thermochemical processes

Thermochemical and biochemical (fermentation and anaerobic digestion) processes are the two major methods of converting biomass to fuel. In this thesis, the focus is on fast pyrolysis, a subset of thermochemical processes. Figure 2.2 provides a schematic of different thermochemical processes to convert biomass into fuel (Bridgewater.et.al, 2000) and is described as follows:

- Combustion of woody biomass to provide direct heat to boilers for steam generation, and hence electricity generation

- Gasification of woody biomass at temperatures greater than 700^0C, to produce a synthesis gas (H_2 and CO). Synthesis gas that can be used for electricity generation in a turbine or an engine, or can be directly combusted to generate heat.

- Pyrolysis of woody biomass into liquid fuel, gas and charcoal in the absence of oxygen. These products are feedstocks for electricity generating applications and other processes as illustrated in Figure 2.2.
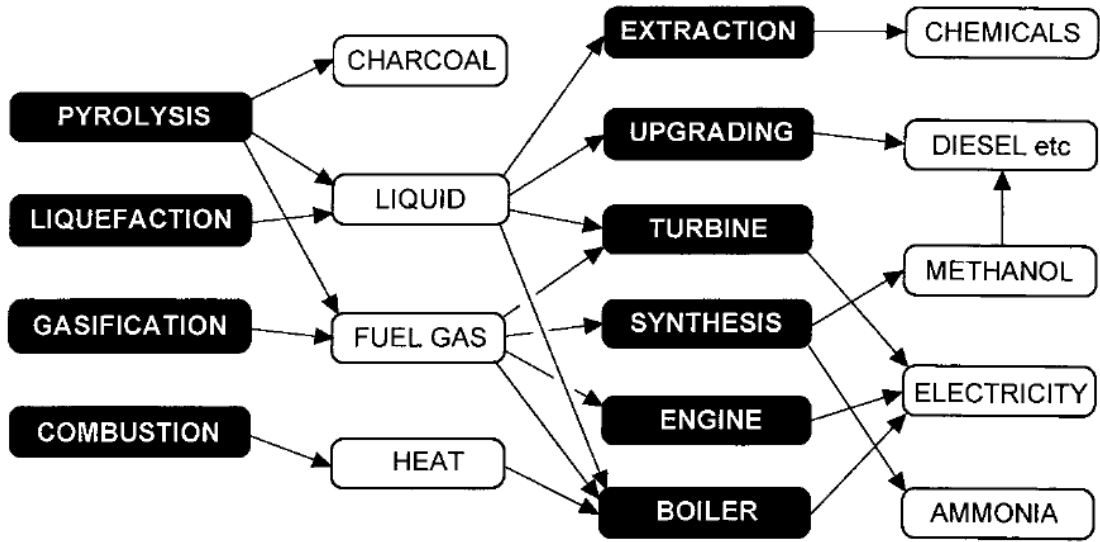
Figure 2.2: Thermochemical biomass processes and products (Bridgewater et. al, 2002)

2.3 Pyrolysis

Pyrolysis is the thermal decomposition of materials in the absence of oxygen or when significantly less oxygen is present than required for complete combustion (Mohan et. al, 2006).

The pyrolysis process can be divided into three subclasses depending on the operating conditions: conventional slow pyrolysis (carbonization), fast pyrolysis, and flash pyrolysis. The range of important operating parameters for pyrolysis processes are given in Table 2.1.

Table 2.1: Operating parameters for pyrolysis processes (Demirbas et al., 2002)

	Slow Pyrolysis	Fast Pyrolysis	Flash Pyrolysis
Pyrolysis temperature (^{0}C)	300-700	600-1000	800-1000
Heating rate(^{0}CS^{-1})	0.1-1	10-200	>1000
Particle size (mm)	0.5-50	<1	<0.2
solid residence time (s)	300-500	0.5-10	<0.5

6

Table 2.2 summarizes the typical product yields obtained by different modes of pyrolysis of wood on a dry basis (Bridgewater et al., 1991).

Table 2.2: Typical product yields (dry wood basis) obtained by different modes of pyrolysis of wood (Bridgewater et al., 1991)

		Liquid	Char	Gas
Slow pyrolysis	low temperature, very long residence time	30%	35%	35%
Fast pyrolysis	moderate temperature, short vapor residence time	75%	12%	13%
Flash pyrolysis	high temperature, no residence times	5%	10%	85%

2.4 Fast Pyrolysis

In fast pyrolysis, the rate of heating is faster compared to slow pyrolysis. This process is used to produce bio oil in large quantity compared to slow pyrolysis or flash pyrolysis. The critical feature of the fast pyrolysis is to bring the reaction interface of the biomass particle to optimum process temperature and minimize its exposure to lower temperatures which favors the formation of charcoal. The essential features of a fast pyrolysis process for producing liquids are (Bridgewater et al., 1999):

- Faster rate of heating (about 10-200 $^0CS^{-1}$) and heat transfer rate at reaction interface. This can be achieved by finely ground biomass feed.

- The residence time of the vapor is short, typically less than 2 seconds

- Vapors produced in the pyrolysis reaction have to be rapidly cooled to produce bio oil

- Fast pyrolysis is performed at a controlled reaction temperature of around 500 ^0C. The temperature of the vapor phase is 400-450 ^0C

Therefore, chemical reaction kinetics, heat and mass transfer processes, as well as phase transition play an important role in fast pyrolysis (Bridgewater et al., 1991).

7

2.5 Biomass Pyrolysis Reactors

This section describes the different reactor configurations that have been investigated to perform fast pyrolysis both at lab scale and pilot scale.

2.5.1 Lab scale pyrolysis devices

The pyrolysis reactors can be classified as either continuous-mode or pulse-mode depending on the heating mechanism (Levy et. al, 1972). Furnace pyrolyzer is an example of continuous-mode pyrolyzer which usually consists of a cylindrical oven held at constant temperature into which a miniaturized sample boat is introduced.

Pulse mode pyrolyzers comprise five basic types:

(1) Filament pyrolyzers-usually resistively heated platinum ribbons or coils (Levy.et. al, 1972)

(2) Curie-point pyrolyzers-inductively heated ferromagnetic wires (Buhler et. al, 1970)

(3) Microreactor (Muzzy et. al, 2008)

(4) Laser pyrolyzers (Folmer et. al, 1969)

(5) Plasma pyrolysis reactors (Tang et. al, 2005)

(6) Solar pyrolysis reactor (Lede et al., 1998)

The pulse-mode pyrolyzers applying a step temperature ramp are generally preferred for analytical purposes because they provide rapid heat transfer and the vapors produced in the reaction are quickly driven away from the heating zone, minimizing the possibility of secondary reactions.

2.5.1.1 Resistively heated microfurnace or tube pyrolyzer

A tube prolyzer provides an isothermal condition into which the samples are introduced using a little cup or a solid plunger syringe (White et al., 1991). This reactor is not preferred for precise

analytical work due to a lack of control of the time/ temperature profile of the sample (Blackledge et al., 1992). The boat pyrolysis reactor presented in chapter 4 is an extended version of a micro-furnace. Refer to chapter 4 for further details.

2.5.1.2 Resistively heated filament pyrolyzer

Filament pyrolyzers (Ericsson et. al, 1985) can acquire a controlled pyrolysis temperature extremely quickly. An initial pulse of heating at a high voltage produces a current through the metal filament (usually a Pt- coil) causing it to heat rapidly until the programmed pyrolysis temperature is reached. The pyrolysis temperature is maintained by reducing the voltage. (Blackledge et. al, 1992).

2.5.1.3 Microreactor

The micro-reactor is designed to accept a powdered feedstock which is spread over a hot surface. After a specified time, the residual solids are scraped off the hot surface. The volatiles are collected in a condenser. A typical charge to the reactor is 50 mg in order to achieve rapid thermal equilibrium with the hot surface. The microreactor is intended to study the pyrolysis of wood and it components under "idealized" conditions in order to obtain a fundamental understanding of the pyrolysis reactions taking place (Muzzy et. al, 2008).

2.5.1.4 Laser pyrolyzer

The laser pyrolyzer consists of a laser focused through a microscope objective lens onto a targeted area which is pyrolyzed using either a continuous wave or a number of high energy pulses (Greenwood et. al, 1998). The thermal interaction between laser and material initiates the pyrolysis reaction which produces pyrolysis products (Meruva et. al, 2003). The intense, short duration laser beam enables rapid temperature rise times, followed by rapid cooling, thus reducing the potential for secondary reactions.

2.5.1.5 Plasma pyrolysis reactor

A plasma pyrolysis reactor can be used to perform flash pyrolysis. The temperature attained in a thermal plasma is very high (usually 2500-9500^{0}C) for biomass pyrolysis (Tang et. al, 2005). The high energy density associated with thermal plasma can solve the problems generally encountered in conventional pyrolysis reactors, such as low gas and high char yield (Bridgewater et al., 2003). Nevertheless, they are seldom used on a commercial scale due to high electrical power consumption (Brown et. al., 1979).

2.5.1.6 Solar pyrolysis reactor

Pyrolysis of biomass using concentrated solar energy offers a potential way of converting biomass to fuel. A vortex type reactor, such a cyclone reactor, utilizes concentrated solar energy to heat up the biomass particle and also the walls of the reactor against which the biomass particles slide with high velocity. The friction between two solids removes the pyrolysis vapor immediately due to the centrifugal force effects. However, use of concentrated solar energy imposes many restrictions on the reactor design which requires significant modification of the existing vortex reactor (Lede et al., 1998).

2.5.2 Pilot scale reactor

The different reactor configurations that can be applied for fast pyrolysis are described below.

2.5.2.1 Circulating fluidized bed reactor

Conduction and convection are the dominant mode of heat transfer in this reactor. The particle size of the biomass used for pyrolysis in these reactors is typically less than 3mm to obtain a good liquid yield. This is to reduce the heat transfer limitation within the particle. The biomass particles in the reactor are fluidized by a gas (Bridgewater et. al, 1999). A circulating bed of hot sand acts as a heating medium for the biomass particles introduced into the reactor. Good

temperature control and high heat transfer rate from the sand to biomass particles are the most important characteristics of this reactor. The recirculated product gas, sand, and biomass particles move together in the fluidized bed reactor. (Luo et al., 2004).

2.5.2.2 Ablative reactor

In an ablative reactor, wood is pressed against a surface which is maintained at a high temperature leaving an oil film which evaporates rapidly. The rate of heat supply to the reactor is the major rate limiting step as the process typically uses wood particles of larger size compared to a fluidized bed reactor. Therefore, there is no requirement for a carrier gas, but the reactor is more complex as the entire process is mechanically driven (Bridgewater et.al, 1999). The reactor wall is maintained at temperatures typically less than 600 ^{0}C and the centrifugal force causes the wood particles to press against the hot reactor wall (Diebold et. al, 1988).

2.5.2.3 Vacuum furnace reactor

Long solid residence time and short vapor residence times are the important characteristics of this reactor which simulates fast pyrolysis. Total liquid yields are typically lower (60-65%) compared to fluidized beds (75-80%). These reactors have the ability to process larger particles than most fast pyrolysis reactors. However, larger particles and use of vacuum leads to higher equipment and processing cost (Bridgewater et al., 1993).

2.5.2.4 Rotating cone reactor

A rapid heating rate and short residence time of the solids are the essential features of a rotating cone reactor than can facilitate fast pyrolysis with negligible char formation (Wagenaar et. al, 1994). The particle size of the biomass used in this reactor is relatively fine, like any transported bed-reactor, for a better liquid yield. The liquid yields are typically 60-70% of the feed rate of

the reactant (Bahng et.al, 2009). Carrier gas is needed for burning the char and for sand transport, but the amount of carrier gas required is much less compared to the fluidized bed reactor.

2.5.2.5 Auger reactor

In an auger reactor, the biomass feedstock is transported using a screw conveyor in a cylindrical heated tube. Good mixing of the sand and the biomass, and good control of the residence time of the feed stock are the key features of an auger reactor. As the feedstock is transported through the tube, the temperature of the reactant is raised to the pyrolysis temperature (250-450^{0}C). The gases produced during the pyrolysis are condensed to collect bio-oil. Char and sand are collected at the end of extruder in a vessel and they are separated to reuse the sand.

An experimental setup is described in chapter 3 which is a modified version of an auger reactor (refer to chapter 3 for further details). Bridgewater et al. (1999) summarized the heating methods for different fast pyrolysis reactors and they are presented in Table 2.3. Also, the types of heat transfer and features of each reactor are summarized in Table 2.4.

Table 2.3: Fast pyrolysis reactors and heating methods (Bridgewater et. al, 1999)

Reactor Type	Method of heating
Ablative coil	Reactor wall heating
Ablative mill	Reactor wall (disc) heating
Ablative plate	Reactor wall heating
Circulating fluid bed	In-bed gasification of char to heat sand
Cyclone or Vortex	Reactor wall heating
Fluid bed	Heated recycle gas
	Hot inert gas
	Partial gasification
	Fire tubes
Horizontal bed	Fire tubes
Vaccum multiple hearth	Hearth heating
Rotating cone	Wall and sand heating
Transported bed	Recirculates hot sand heated by char combustion
Vacuum moving bed	Direct contact with hot surface

Table 2.4: Reactor types and heat transfer (Bridgewater et. al, 1999)

Reactor type	Suggested Mode of Heat Transfer	Advantages/Disadvantages/Features
Ablative	95% Conduction	Accepts large size feed stocks
	4% Convection	Very high mechanical char abrasion from biomass
	1% Radiation	Compact Design
		Heat supply problematical
		Heat transfer gas not required
		Particulate transport gas not always required
Circulating fluid bed	80% Conduction	High heat transfer rates
	19% Convection	High char abrasion from biomass and char erosion
	1% Radiation	leading to high char in product
		Char/Solid heat carrier separation required
		Solids recycle required; Increased complexity of system
		Maximum particle size up to 6 mm
		Possible liquids cracking by hot solids
		Possible catalytic activity from hot char
		Greater reactor wear possible
Fluid Bed	90% Conduction	High heat transfer rates
	9% Convection	Heat supply to fluidizing gas or bed directly
	1% Radiation	Limited char abrasion
		Very good solids mixing
		Particle size limit <2 mm in largest dimension
		Simple reactor configuration

2.6 Kinetics of pyrolysis

The kinetics of pyrolysis play a significant role in determining the yield of pyrolysis products. The kinetic rate constants are dependent on the heat and mass transfer mechanisms of a pyrolysis reactor which are dependent upon the design of the reactor. Since, one of the goals of the thesis is to model the yield of products in an auger reactor for a given kinetic scheme, different kinetic schemes given in the literature are reviewed in this section.

2.6.1 One component mechanism for primary pyrolysis

The majority of kinetic mechanism models consist of a single or three parallel reactions for the formation of the main product classes, namely gas, oil and char respectively. This mechanism was first proposed by Shafizadeh et al. (1977). This mechanism will be utilized in chapter 4 for predicting the yield of products from an auger reactor. Figure 2.3 describes the schematic of the mechanism proposed by Shafizadeh et al. (1977).
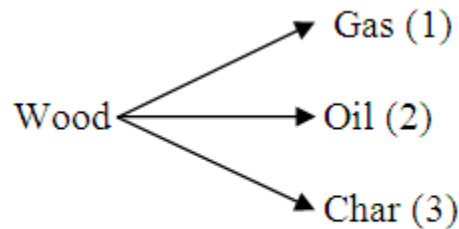
Figure 2.3: One component mechanism of primary pyrolysis of wood (Shafizadeh et al.,1977)

Di Blasi et al. (2008) presented a summary of the one component mechanisms of wood/biomass pyrolysis proposed on the basis of experiments carried out under isothermal or fast heating rate conditions from the literature and they are presented in Table 2.5.

Table 2.5: Kinetic constants for one-component mechanisms of wood/biomass pyrolysis (Di Blasi et al., 2008)

Feedstock (variety, size, mass)	Experimental system	T_r	Reaction mechanism	Kinetic constants: E (kJ/mol), A (s^{-1})
Oak, 650 µm	Isothermal tube furnace	573–673 K	$\frac{dY}{dt} = -kY$ $k = k_C + k_G + k_L$	$k = 2.47 \times 10^6 \exp(-106.5/RT)$ $k_L + k_G = 1.73 \times 10^6 \exp(-106.5/RT$ $k_C = 7.4 \times 10^5 \exp(-106.5/RT)$ $k_L = 4.12 \times 10^6 \exp(-112.7/RT)$ $k_G = 1.43 \times 10^4 \exp(-88.6/RT)$
Hardwood, 300–350 µm	Isothermal entrained-flow reactor	677–822 K	$\frac{dY}{dt} = -kY$	$k = 1.483 \times 10^6 \exp(-89.52/RT)$
Wild cherry	Isothermal tube furnace	538–593 K	$\frac{dY}{dt} = -k(Y - Y_{C\infty})$ $Y_{C\infty} = 0.25 - 0.30$	$k = 11.9 \times 10^{11} \exp(-173.7/RT)$
Sweet gum, hardwood, 45–88 µm, 100 mg	Screen heater (1000 K/min)	600–1400 K	$\frac{dY_V}{dt} = k(Y_{V\infty} - Y_V)$ $Y_{V\infty} = 0.93$	$k_L + k_G = 33.38 \times 10^4 \exp(-69/RT)$
—	—	—	$\frac{dY}{dt} = -kY$ $k = k_C + k_T + k_G + k_W$	$k_C = 1.08 \times 10^7 \exp(-121/RT)$ $k_T = 2 \times 10^8 \exp(-133/RT)$ $k_G = 1.3 \times 10^8 \exp(-140/RT)$ $k_W = 5.13 \times 10^6 \exp(-92.1/RT)$
Almond shells, 300–500 µm, 2 mg	Pyroprobe 100	733–878 K	$\frac{dY}{dt} = -kY$	$k = 1.885 \times 10^6 \exp(-108/RT)$ $k_C = 2.98 \times 10^3 \exp(-73/RT)$ $k_L = 5.85 \times 10^6 \exp(-119/RT)$ $k_G = 1.52 \times 10^7 \exp(-139/RT)$
Fir wood, 300–425 µm, 2 g	Isothermal batch fluid-bed	673–773 K	$\frac{dY_V}{dt} = k(Y_{V\infty} - Y_V)$ $Y_{V\infty} = 0.005$	$k_G + k_L = 2.40 \times 10^4 \exp(-94/RT)$
Pine, 100–125 µm	TGA Drop tube	553–673 K 773–873 K	$\frac{dY}{dt} = -kY$ $k = k_C + k_G + k_L$	$k = 1.4 \times 10^{10} \exp(-150/RT)$ $k_C = 3.05 \times 10^7 \exp(-125/RT)$ $k_L = 9.28 \times 10^9 \exp(-149/RT)$ $k_G = 1.11 \times 10^{11} \exp(-177/RT)$
Forest waste, $\leqslant 1000$ µm, 25 mg	Isothermal TGA	498–598 K	$\frac{dY}{dt} = -k(Y - Y_{C\infty}), Y_{C\infty} \cong 0.25$	$k = 7.68 \times 10^7 \exp(-124.87/RT)$
		973–1173 K	$\frac{dY}{dt} = -k(Y - Y_{C\infty}), Y_{C\infty} \leqslant 0.15$	$k = 6.33 \times 10^2 \exp(-91.53/RT)$
Beech, <80 µm, 9 mg	Tube furnace	573–708 K	$\frac{dY}{dt} = -kY$	(a) $k = 2.4 \times 10^5 \exp(-95.4/RT)$ (b) $k = 4.4 \times 10^9 \exp(-141/RT)$ $k_L + k_G = 1.5 \times 10^{10} \exp(-149/RT)$ $k_C = 3.3 \times 10^6 \exp(-112/RT)$ $k_G = 4.4 \times 10^9 \exp(-153/RT)$ $k_L = 1.1 \times 10^{10} \exp(-148/RT)$

It appears that there is a wide variation in the calculated values of rate constants. This might be the result of the different heating conditions established in different experimental devices or the mathematical treatment of the experimental data (Di Blasi, 2008).

2.6.2 Three component mechanism for primary pyrolysis

The three-component mechanism models consists of three major components of wood, namely: cellulose, hemicelluloses and lignin, undergoing three parallel reactions for the formation of the main product classes, namely gas, oil and char respectively (Di Blasi et al., 2008). In several cases dynamic measurements and the corresponding kinetic analyses examine one heating rate only, generally below 10 K/min. The use of thermogravimetric systems with slow heating rates and application of numerical methods for parameter estimations certainly contribute to reduce the differences between the estimated values of kinetic constants unlike one-component reaction mechanisms. The effects of the highly heterogeneous material, however, still remain and general mechanisms with a wide range of applicability are not available. We have to estimate 9 kinetic rate constants in total. A schematic explaining the three component mechanism is given in Figure 2.4.
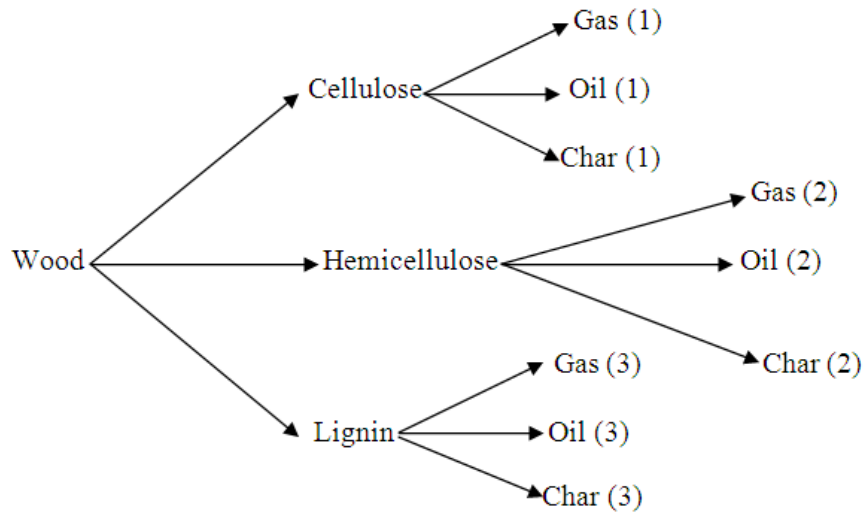
Figure 2.4: Schematic of a three component pyrolysis kinetic scheme (Maschio et al., 1994)

Alternatively, based on a description of the different zones in the isothermal weight loss curve, multi-component mechanisms of wood-biomass pyrolysis can be proposed. Branca et al.,(2003) proposed a three stage series mechanism, which takes into account the competitive formation of classes of compounds belonging to either the gas or the solid phase. A schematic explaining this mechanism is given in Figure 2.5.

$$k_1 = k_{V1} + k_B \;\; ; \;\; k_2 = k_{V2} + k_D \;\; ; \;\; k_3 = k_{V3} + k_C$$
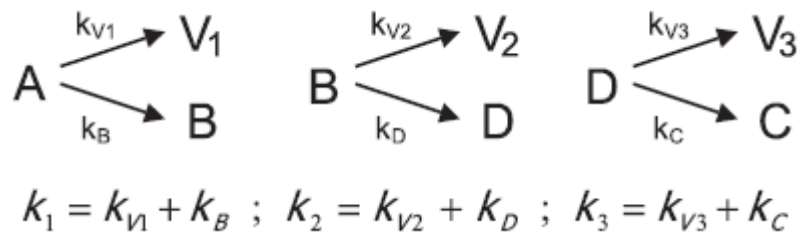
Figure 2.5: Multi component pyrolysis mechanism (Branca et al., 2003)

2.6.3 Secondary reactions

At high temperatures and long residence times, the vapor phase undergoes secondary reactions (Antal et al., 1985). These alter both the yields and composition of the wood/biomass pyrolysis products. Figure 2.6 explains the schematic of a typical one component primary pyrolysis of wood with secondary reactions.
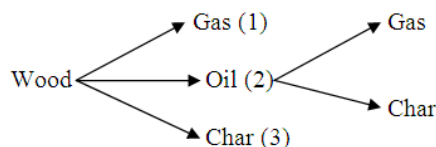
Figure 2.6: A global mechanism for the secondary reactions of vapor-phase species
(Antal et al., 1985)

2.7 Influence of Catalysts on wood pyrolysis

Bio-oil obtained from fast pyrolysis is usually acidic and has a high viscosity. The viscosity increases with storage time. Catalysts can greatly alter bio-oil properties. Different catalysts have been investigated to determine the influence on the quality of the bio-oil, including chemical composition, stability of oil, viscosity and total acid number.

Al-MCM-41-type mesoporous catalyst was used by Adam et.al (2005) to improve the bio-oil properties. TG/MS was used to monitor product evolution under slow heating conditions (20 °C/min) from 50 °C to 800 °C. Levoglucosan was completely eliminated, whereas acetic acid, furfural, and furans become important cellulose pyrolysis products compared to an unmodified Al-MCM-41 catalyst. The quantity of higher-molecular-mass phenolic compounds is strongly reduced in the lignin-derived products.

Atutxa et al.,(2005) used HZSM-5 zeolite catalyst in situ in a conical spouted-bed reactor in the flash pyrolysis of sawdust at 400°C. HZSM-5 promoted major changes in the yields of gas,

18

liquid, and chars. The gas yields increased as the catalyst amount was increased, while the liquid yields decreased significantly and the char yields decreased slightly.

Agblevor et al., (2010) developed a fractional catalytic pyrolysis process that produces stable, low-viscosity biomass pyrolysis oils that can be stored at ambient conditions without any significant increase in viscosity using HZSM-5 zeolite catalyst. The oil was produced from pyrolysis of poplar wood in a circulating fluidized bed. The oils can be distilled at both atmospheric pressure and under vacuum without char or solid formation. Fractional catalytic pyrolysis oils produced from hybrid poplar wood were stored at ambient laboratory conditions for more than 10 months, and the change in dynamic viscosities was within 6%.

Williams et al., (1994) performed pinewood pyrolysis in a fluidized-bed pyrolysis reactor with nitrogen as the fluidizing gas using ZSM-5 zeolite catalyst. Oils were highly oxygenated before catalysis. After catalysis, the oils had markedly less oxygenated species present, a higher aromatic content, and an increase in biologically active polynuclear aromatic (PAHs) species. Oxygen in the oxygenated compounds was catalytically converted mainly to H_2O at lower catalyst temperatures and CO_2 and CO at high catalyst temperatures. The amounts of PAHs increased as the catalyst temperature increased. The oxygenated compounds remaining in the oil formed over the ZSM-5 bed were mainly phenols and carboxylic acids.

Garcia et al., (2001) studied the influence of catalyst pretreatment on gas yield in catalytic biomass (sawdust) pyrolysis based on the Waterloo Fast Pyrolysis Process (WFPP) technology. This technology achieves a very fast biomass heating rate and a low gas residence time in the reaction bed. A Ni/Al coprecipitated catalyst was used in the reaction bed where biomass thermochemical decomposition occurred. A decrease was observed in the H_2 and CO yields at both 650 and 700 °C when the sawdust feed rate increased; this could result from catalyst

19

deactivation. Higher H_2 and CO yields were observed at both temperatures after the catalyst had been reduced using hydrogen for one hour.

Wang et al., (2010) performed catalytic pyrolysis of pine wood in a fixed-bed reactor heated slowly from room temperature to 700 °C under a stream of purging argon to examine the effects of the physically mixed K_2CO_3 or $Ca(OH)_2$ on the pyrolysis behaviors. K_2CO_3 demonstrated a stronger catalysis for decomposition of hemicellulose, cellulose and lignin constituents, leading to the reduced yield of liquid product in conjunction with the increased yields of gaseous and char products because of the promoted secondary reactions of liquid product. Potassium led to an increase in the cumulative yields of H_2, CO_2 and CO at 700 °C. $Ca(OH)_2$ somewhat promoted the decomposition of cellulose and lignin constituents, and the effect of $Ca(OH)_2$ on the yields of liquid and char was opposite to that of K_2CO_3. The addition of $Ca(OH)_2$ did not significantly change the total yield of gaseous product at 700 °C but enhanced the yield of H_2.

CHAPTER-3

TWIN SCREW EXTRUDER

3.1 Experimental Set up

3.1.1 Introduction

Continuous pyrolysis rather than batch pyrolysis is a preferred mode of operation. There is a twin screw extruder at Georgia Tech which was acquired to perform continuous catalytic pyrolysis of nylon 6 carpet in order to recover the monomer caprolactam. This extruder is being adapted to perform continuous catalytic pyrolysis of wood.

The extruder is from NFM Welding Engineers. The screws are 30 mm in diameter and are counter-rotating and non-intermeshing. This screw design should facilitate devolatilization. One of the screws is shorter than the other. The last section of this extruder before the die operates like a single screw in order to build up pressure to push material out the die. This feature is not needed for pyrolysis since the system will operate under a vacuum. The short screw has a length to diameter ratio of 54. As shown in Figure 3.1, the extruder has 3 vent ports along the barrel. By changing screw speeds the residence time in the barrel can be varied between 1 and 10 minutes. There are 10 independently controlled heaters along the length of the barrel.
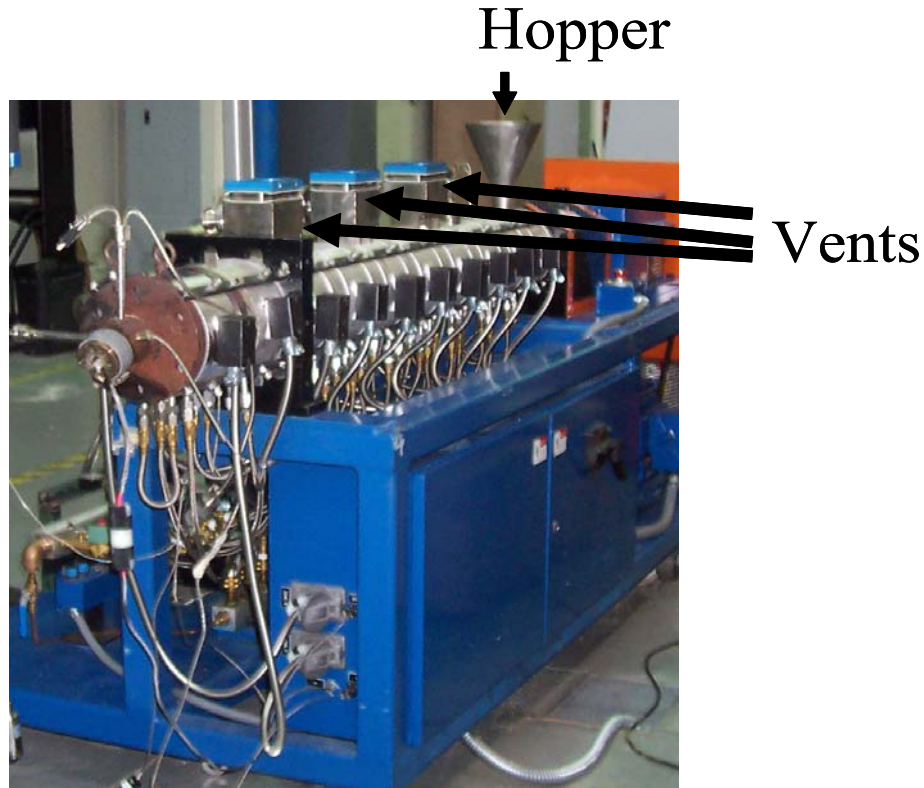
Figure 3.1: NFM Welding Engineers 30mm twin screw extruder

3.1.2 Raw Materials

Pine as sawdust was metered into the extruder without heating the barrel. No difficulty was encountered in metering the sawdust until the section where the short screw end was reached. At this point plugging occurred because the available volume for transporting the sawdust forward was reduced. Four approaches are being considered to resolve this problem.

- The first is to add a thermoplastic polymer, in this case high density polyethylene, which is quite stable at high temperature, in order to rely on melt flow or lubrication to carry material forward beyond the shorter screw.

- The second approach is to shorten the longer screw and it's barrel section in order to avoid a reduction in transport space along the barrel axis. This approach is second because it requires significant equipment modification.

- The third approach entails operating at pyrolysis temperatures which would reduce the amount of solids that needs to be transported forward.

- The fourth approach is to starve feed the extruder such that the final single screw section of the extruder is not overloaded with sawdust.

We have decided to blend high density polyethylene and ground pine and to perform the runs close to starve feed condition for easy transport of reactant through the extruder. The HDPE (high density polyethylene) was obtained from a local rotational molding company since it was available as a powder and should have a relatively low melt viscosity. The pine was obtained from American Wood Fibers, grade 4020, which is sold commercially as filler for plastics, primarily for making plastic lumber.

The cumulative particle size distribution of the pine, polyethylene and a blend of 20% pine and 80% polyethylene (by weight) are given in Table 3.1.

Table 3.1: Cumulative PSD of different components (Weight basis)

Diameter Range	% of pine (100% pine)	% of mixture (20% pine, 80% polymer)	% of polyethylene (100% polymer)
Less than 500μm	100	100	100
Less than 425μm	91.83	81.29	78.66
Less than 300μm	42.9	42.52	42.93
Less than 212μm	11.26	19.13	21.58
Less than 125μm	1.42	4.32	5.46

3.1.3 Modification

The extruder has to be modified in order to perform pyrolysis of pine. Following are the modifications done to the existing reactor to perform pyrolysis:

Blockage of all the holes: We need to run the extruder very close to pyrolysis conditions so that we can compare the results to micro-reactor experiments. There were many vents in the screw extruder and when it was operated at 280^0 C, there was bubbling of molten reactants through these vents. So all the holes at various zones in the screw extruder have been blocked. We did not observe any bubbling after the holes were blocked at the same operating conditions (Figure 3.2).

Figure 3. 2: Screw extruder after all holes were blocked

1.) Providing an inert environment: Volatile gases released at high temperatures during pyrolysis are extremely flammable and can prove detrimental to the screw extruder. Hence we added a N_2 gas purge through all the zones of the screw extruder creating an inert environment (Figure 3.3).

2.) Collection of Volatile gases: Volatile gases released during the experiment need to be collected immediately, if not, it would lead to secondary reactions and affect the quality of the bio-fuel. The N_2 purge would ensure that the residence time of the volatile gases in the reactor is short. A condenser was designed to facilitate the collection of volatile gases using liquid N_2 as coolant (Figure 3.4).

Figure 3.3: N_2 supply to the extruder just below the valve

Figure 3.4: Condenser to collect volatile gases using liquid nitrogen as coolant

3.) Closing feeder and hopper system: Initially the feeding system was open, leaving a pathway for air to enter the system. We had to design a new system to close the feeder and hopper system that would restrict the supply of air through the hopper. We faced many constraints in this issue with respect to the size of the fittings for the feeder and hopper system. Though we managed to get the material of required size, it had problems with the temperature of zone 1. The material was unstable at the operating conditions of zone 1. This material had to be modified and the temperature of zone 1 had to be reset to a lower temperature to avoid further problems (Figure 3.5).

Figure 3.5: Closed screw feeder from covered hopper, black transfer hose and extruder hopper

4.) Measuring vacuum: A Vacuum pump was provided to suck the volatile gases generated in the reactions through the zones. The volatile gases are made to pass through the condenser due to a vacuum pump where they condense. We collect bio-oil in the test tube provided at the end of the condenser (Figure 3.6).

Figure 3.6: Vacuum pump with a gauge

Once the above five modifications were completed, the screw extruder was set to run under pyrolysis conditions. We did a sample run to check the working of all the parts of the screw extruder. We faced further unexpected problems in our first run. They are as follows:

- The feeder was placed on the metal cover of the screw extruder. At high temperatures the cover became unstable causing it to move from its initial position. This led to the breakage of the feeder system and spilling of material all around the reactor.

- The N_2 supply was close to the feeder which resisted the feeding of reactant through the hopper. Most of the material was gushing out of a small screw hole in the hopper. Minute amounts of reactant was being propelled though the extruder.

- The metal cover of the screw extruder was replaced by another metal cover. The stability of this cover was confirmed at high temperature so that it will not damage the feeder

hopper system (Figure 3.7). The feeder hopper system was repaired and made air tight once again. The position of the N_2 supply was exchanged with a pressure transducer in zone 2 so that it would not affect the feed supply through the hopper. This result was confirmed when a sample experiment was run with the feeder-hopper system open to air.

Figure 3.7: Stabilized cover to screw extruder

3.1.4 Modifications in the future

If the collection system through a single vent in the auger reactor is successful, following will be the modifications done to the reactor.

- There are three independent collection systems, one for each vent on the extruder. These collection systems have condensers with liquid nitrogen as the coolant.

- An enclosed tank needs to be installed to collect the char and carrier fluid exiting the die. After running sawdust in the extruder, it was determined that the sawdust clogged the system at the tip of the short screw. We concluded a fluid is needed to facilitate the transport of solids beyond this point. High density polyethylene powder has been obtained as this carrier fluid.

A schematic of the extruder with the proposed modifications is given in Figure 3.8 (Muzzy et al., 2009).
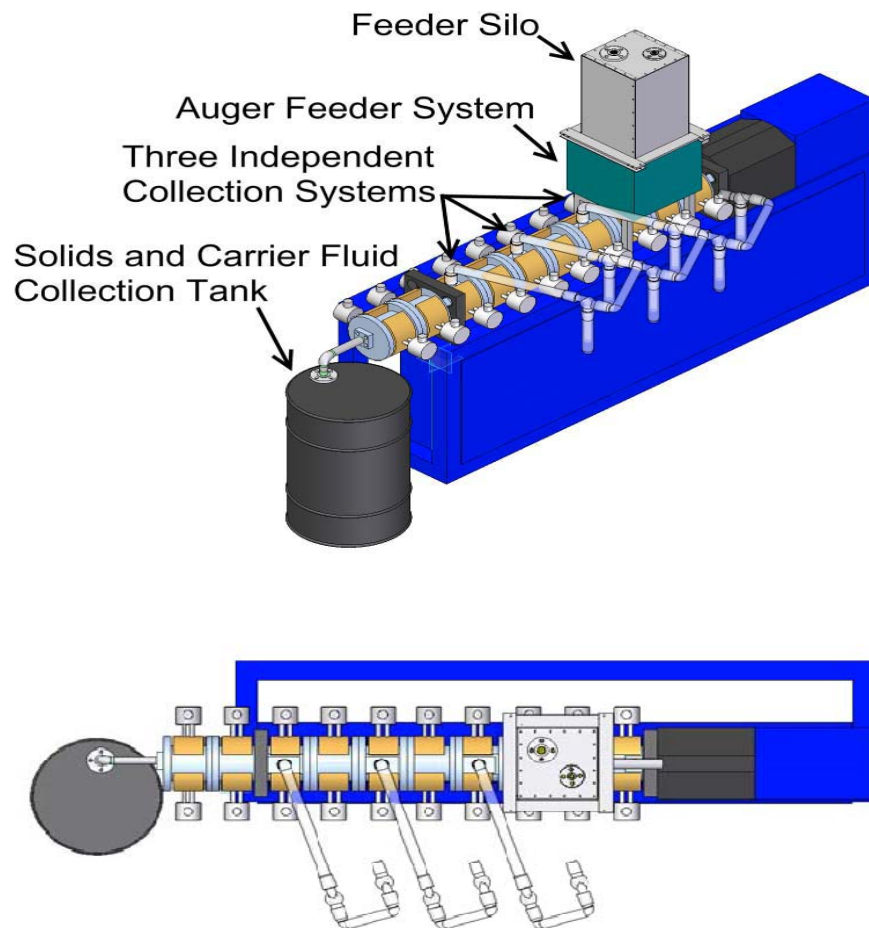
Figure 3.8: Schematic of the modified screw extruder (side and top view) (Muzzy et al., 2009)

3.2 Experimental run

3.2.1 Objective

The objective of the experiment is to perform a staged temperature pyrolysis of ground pine in a continuous process to condense pyrolysis vapors of cellulose, hemicelluloses and lignin separately. The value of the auger pyrolysis reactor is that we can produce multiple grams of oil in one run. This will facilitate more extensive characterization of the oil produced, including measuring viscosity over time to check the stability of the oil. The schematic explaining the objective of the experiment is given in Figure 3.9.
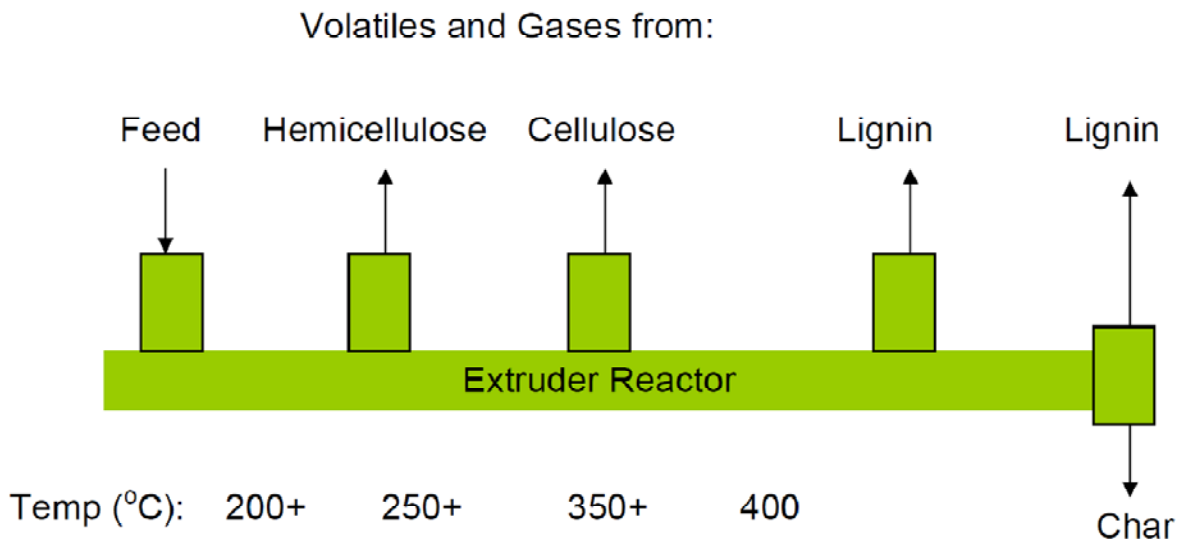
Figure 3.9: Proposed temperature profile along the extruder barrel in order to achieve fractionated pyrolysis (Muzzy et al., 2009)

3.2.2 Procedure

In operation the HDPE powder is blended with dried pine powder and placed in a covered feed hopper. The blend is metered into the extruder by controlling the feed screw speed. The transfer line is a sealed rubber hose in order to keep air out of the system. The extruder is "starve fed",

which means the screw feeder delivers the powder at a lower flow rate than the extruder can transport it downstream. Therefore the channel between the screws and barrel are not completely full of material in order to facilitate the release of volatiles. Nitrogen is fed to the extruder through the second vent port to flush out any air that might be present. A temperature profile is set along the barrel to melt the HDPE and then establish the desired pyrolysis temperatures. The extruder has three vent ports along the barrel which can be used to collect volatiles produced at different temperatures. However, at this time only one condenser exists so the first port is blocked and the second port is used for adding nitrogen. The condenser is attached to the third vent port. The condenser has two liquid nitrogen cold traps in series. The condenser is connected to a vacuum pump which can be throttled to maintain specific vacuum pressures. The HDPE is extruded out the die. Since the barrel section before the die only has one screw, this section of the extruder completely fills with molten HDPE, sealing off the die.

The modifications in section 3.1.3 were completed and the extruder is ready to perform pyrolysis. Conditions used in the first experimental run are described below:

- There are 3 zones and each zone has two heating sections. The temperature of the first heating section of zone 1 is maintained at 130^0C and the second heating section is maintained at 180^0C. Zone 2 is maintained at 250^0C and zone 3 is maintained at 300^0C.

- 20% ground pine and 80% polyethylene is used as the feed to the extruder.

- The screws were operated at a speed of 30 rpm which is equivalent to a feed rate of 0.99 kg/hr.

- The pressure of the vacuum created by the vacuum pump is -10 inches of Hg.

- The flow rate of nitrogen was maintained at 20 ft^3/hr at standard operating conditions.

- The extruder was run for 45 minutes and a sample of bio-oil was collected from the condenser.

The very first sample of bio oil collected from extruder. This sample was sent for elemental analysis. The results obtained from the Galbraith Laboratory are presented in Table 3.2.

Table 3. 2: Elemental analysis of oil obtained from extruder by Galbraith laboratory

Sample	C	H	N	O	Water %
Sample-extruder	53.71	5.27	<1%	34.75	49.69

These preliminary results indicate that the values obtained for elemental analysis are close to the values obtained from the micro-reactor. However, the composition of oil is expected to be different from the micro-reactor as the residence time and heat transfer mechanism is different from the micro-reactor. The oil is subjected to further analysis for detailed information about the product composition (Muzzy et al., 2009)

3.3 Problems leading to non-functioning of extruder

The problems observed in the extruder in the initial stages were rectified and a few runs were performed on the extruder. However, after running the extruder for a few more experiments we observed serious problems with the condenser. They are presented as follows:

- The extruder was operated for ten times to collect samples at different operating conditions. This led to the damage of the base portion of the condenser due to which there was escape of pyrolysis gases. The gases generated along the extruder could not be efficiently captured by the condenser (Figure 3.10).
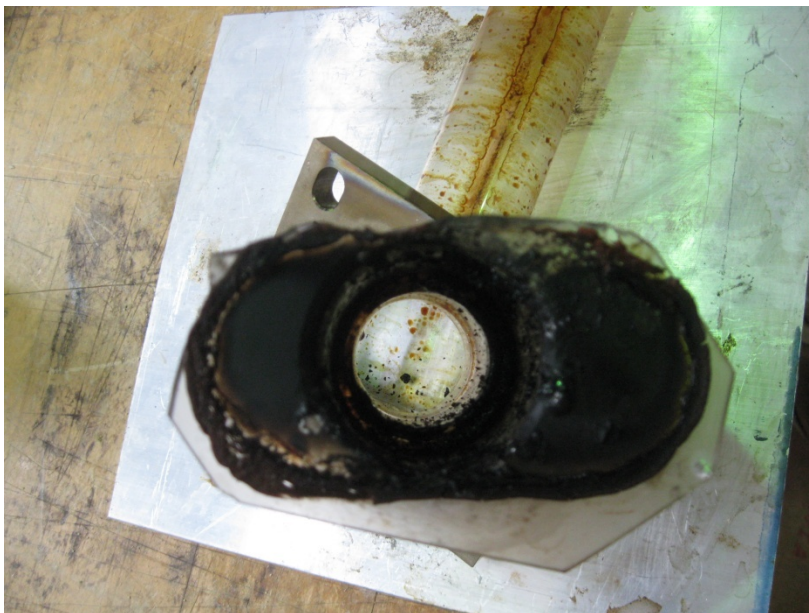
Figure 3.10: Damaged base of the condenser along with a melted gasket

- The gasket used to seal the base of the condenser to one of the extruder vents completely degraded due to which the bottom could not be fixed in a particular position.

- The gases travelling through the 50 cm long condenser portion condensed before they could actually reach the coolant section. The condensed gases stuck to the wall of the condenser and might lead to secondary reactions. We could collect some sample in the condenser but the major portion of the sample was stuck to the wall of the condenser.

- The glass tube used to collect the bio-oil sample when removed from the liquid nitrogen bath cracked due to the rapid change in temperature gradient.

Figure 3.11: Vapors condensing on the walls and sticking to it

- The gases rising through the vertical section of the glass transfer tube to the condenser also condensed and the liquid flowed back into the vent. This led to the formation of char at the entrance of the vent. It is a well known that char formation would lead to secondary reactions and would affect the quality of bio-oil (see Figure 3.12).

Figure 3.12: Char formation at the bottom

- The feeder and the hopper system was disrupted when the extruder was operated at lower vacuum conditions (-1 psi of Hg) compared to initial runs (-10psi of Hg). When the feeder system was opened, we found that the entire section was blocked with the polyethylene and pine mixture. One of the plausible explanations could be that the volatile gases escaped through the feeding vent. The temperature of these gases being hot, led to partial melting of the polyethylene mixture and it stuck to the walls of the feeding tube. It offered resistance to the free flow of the mixture which leads to blockage (see Figure 3.13).

Figure 3.13: Material sticking to the walls of the feeder

All the problems mentioned above call for better a design of the condenser system. Since it was taking a long time to fix these problems and the output quality of the oil would still be uncertain after fixing these problems, we chose to switch to a tubular pyrolysis reactor that will enable us to produce more oil (Refer to Chapter 4 for a detailed explanation of the tubular pyrolysis reactor).

3.4 Summary and Conclusions

A screw extruder is a good system for performing a staged temperature pyrolysis of ground pine in a continuous process to extract pyrolysis vapors of cellulose, hemicelluloses and lignin separately. The value of the auger pyrolysis reactor is that we can produce multiple grams of oil in one run. This will facilitate more extensive characterization of the oil produced, including measuring viscosity over time to check the stability of the oil. However, more work needs to be done on the vapor collection system for efficient collection of vapors from pyrolysis of pine at different temperatures.

CHAPTER 4

EXPERIMENTAL INVESTIGATION OF PINE PYROLYSIS USING TUBULAR PYROLYSIS REACTOR

4.1 Experimental Set up

The tubular pyrolysis reactor, used to produce bio-oil, consists of a long glass tube made of quartz to withstand high temperature (Figure 4.1). A sample of ground pine is measured (using weight balance) and placed on a boat shaped glass container. This container is placed in the middle of the glass tube. This boat shaped container consists of a tripod stand at the bottom to ensure that the boat does not wobble when placed inside the quartz tube. This boat contains a slot in the middle to insert a thermocouple. The function of thermocouple is to measure the actual temperature of wood placed inside the boat as the reaction proceeds. Heat is supplied to the glass tube radially by a tubular furnace. The tubular furnace is connected to the digital meter where the temperature of the tubular furnace can be set to a specific temperature. The digital meter also indicates the temperature of the tubular heater to ensure that it is maintained at the set temperature. An inert atmosphere is maintained in the glass tube by a supply of nitrogen gas. Flow rate of the nitrogen can be controlled using a flow meter. Nitrogen carries the volatiles and gases released during the pyrolysis to the two condensers, in series, located at the other end of the glass tube. These condensers are placed inside liquid nitrogen which acts as a coolant. These vapors from pyrolysis are condensed inside the condenser. The gas which does not condense exits (located inside fume hood) through a pipe connected at the end of the second condenser. All the joints in the reactor are sealed using O-rings to avoid leakage of pyrolysis gases during reaction at high temperature through gaps.

Figure 4.1: Tubular pyrolysis reactor consisting of wood sample, pyrolysis tube, condenser and heater
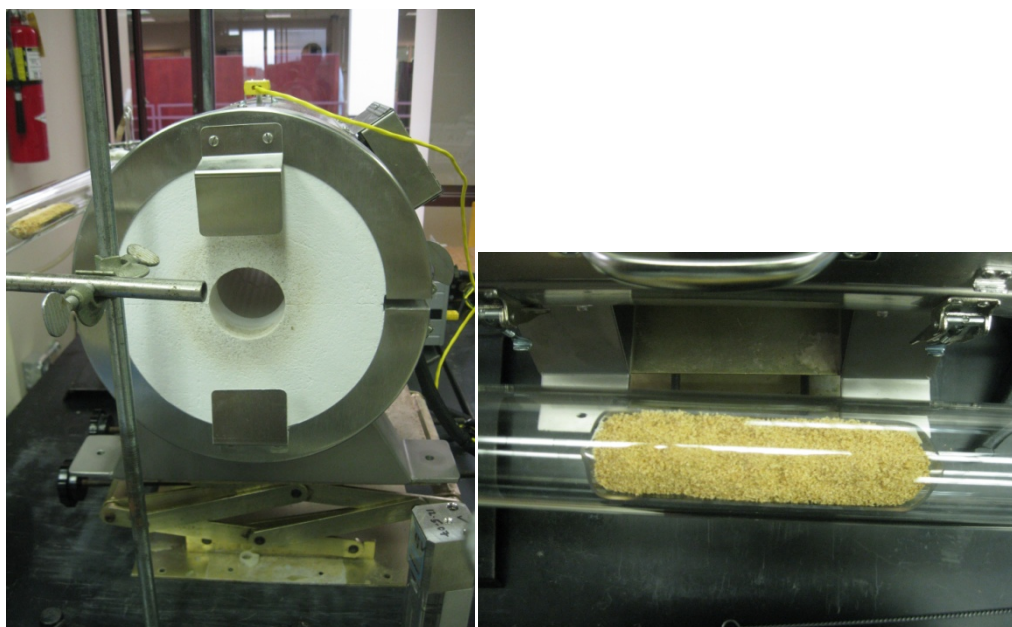
Figure 4.2: Furnace cross section used to supply heat to the pyrolysis reactor radially and wood sample placed in a boat shaped container inside the tubular reactor
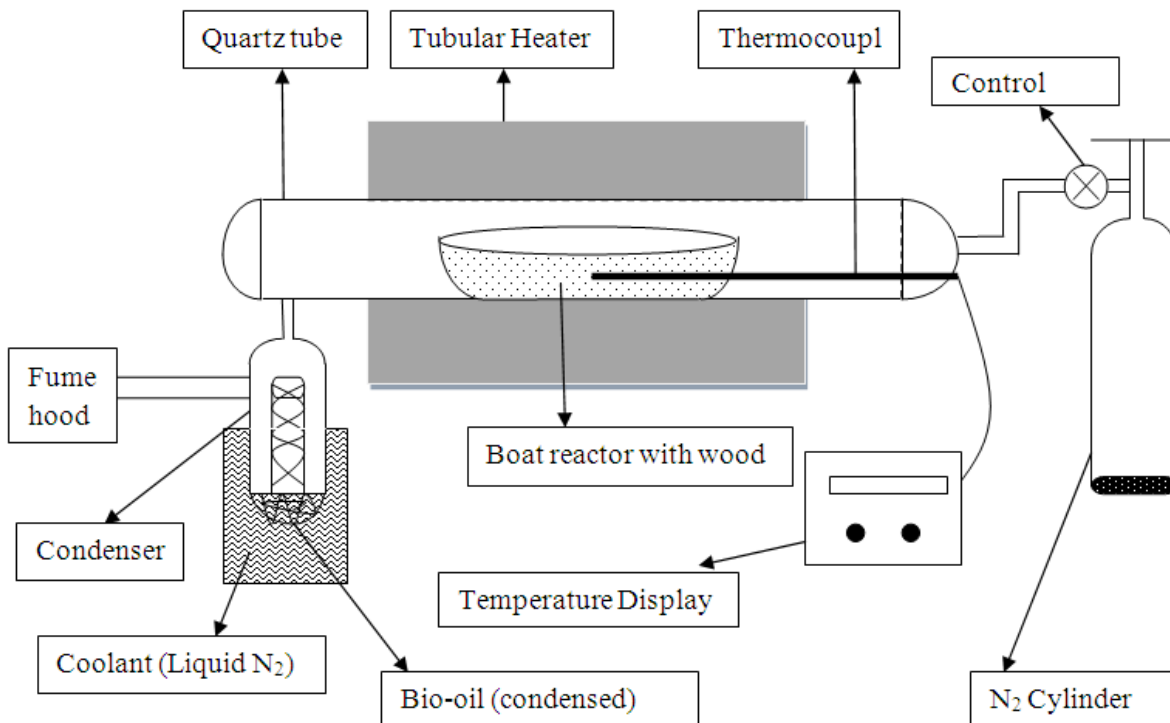
Figure 4.3: Schematic of tubular pyrolysis reactor

The length, width and depth of the boat container are 10, 5 and 3 cm respectively. The thickness of the glass is around 0.5 cm, the length of the quartz tube is around 80 cm, with the central portion of the quartz tube spanning 40 cm covered by the tubular furnace. The diameter of the quartz tube is around 5 cm.

4.2 Experimental Run

4.2.1 Objective

The objective of these experiments are to produce high quality bio-oil in a small scale reactor to study the effect of various selected catalysts on the quality of bio-oil and the percentage of char

produced and to investigate the influence of process parameters and catalytic conditions on chemical composition of the pyrolysis oils.

4.2.2 Raw material

The wood sample selected for the experiments in the tubular reactor is loblolly pine due to its abundant supply in the southeast. The particle size distribution obtained by Alex Williams (Muzzy et al., 2010) in our group is presented in Table 4.1.

For any particle the aspect ratio (AR), length (L) and width (W) are given by the relationship in Equation 4.1,

$$AR = \frac{L}{W} \tag{4.1}$$

It will be assumed, based upon qualitative observations, that the particle shape will either tend towards elliptical or rectangular with the reality being that the shape is somewhere in between. Parallelogram shapes with internal angles deviating far from 90º would be unexpected and have not been qualitatively observed. The distinction between elliptical and rectangular in shape will be made based upon particle perimeter and theoretical perimeter based upon aspect ratio.

A perimeter approximation for a perfect ellipse is given by Equation 4.2 with the aspect ratio substitution made in Equation 4.3.

$$P \approx 2\pi \sqrt{\frac{L^2 + W^2}{2}} \tag{4.2}$$

$$P \approx 2\pi \sqrt{\frac{L^2}{2} + \frac{L^2}{2AR^2}} \tag{4.3}$$

The perimeter of a rectangle is given by Equation 4.4 with the aspect ratio substitution made in Equation 4.5.

$$P = 2L + 2W \tag{4.4}$$

$$P = \frac{(AR+1)(2L)}{AR} \qquad\qquad (4.5)$$

Taking the average aspect ratio of $AR=1.8$ and average length of $L = 0.32$mm the theoretical rectangular perimeter is $P_{rect}= 1.00$mm and theoretical elliptical perimeter is $P_{ellipse}= 1.64$mm. The measured average perimeter was $P_{ave}= 0.94$mm indicating that the particle shape is much closer to rectangular than elliptical.

Table 4.1: Particle size distribution results and statistics (Muzzy et al., 2010)

Image #	Area %	# Particles	Ave A_p [mm^2]	Ave L_p [mm]	Ave P_p [mm]	Ave AR
1	8.77	137	0.0763	0.35	1.06	1.79
2	7.58	132	0.06957	0.36	1.04	1.82
3	6.99	183	0.04829	0.29	0.86	1.74
4	8.14	155	0.05874	0.31	0.91	1.81
5	4.44	134	0.03906	0.26	0.76	1.84
6	7.43	135	0.05719	0.32	0.93	1.87
7	4.15	120	0.04236	0.29	0.81	1.88
8	4.14	112	0.0473	0.31	0.88	1.98
9	10.84	208	0.06325	0.32	0.91	1.86
10	8.84	137	0.0801	0.37	1.06	1.82
11	16.29	392	0.04727	0.27	0.8	1.71
12	7.22	170	0.04974	0.28	0.82	1.74
13	7.01	136	0.05959	0.29	0.89	1.67
14	12.05	208	0.06317	0.33	0.96	1.86
15	14.79	228	0.07784	0.37	1.1	1.8
16	10.76	229	0.05439	0.33	0.94	1.88
17	9.51	161	0.06922	0.37	1.04	1.95
18	10.01	180	0.06481	0.35	1.01	1.8
19	4.84	92	0.05832	0.31	0.89	1.75
20	9.76	201	0.05583	0.28	0.83	1.73
21	10.37	197	0.05825	0.31	0.91	1.76
22	15.65	295	0.06131	0.32	0.95	1.81

Table 4.1 continued						
Image #	Area %	# Particles	Ave A_p [mm^2]	Ave L_p [mm]	Ave P_p [mm]	Ave AR
23	18.67	295	0.07558	0.34	1.02	1.74
24	14.59	252	0.07051	0.34	1.01	1.78
25	10.13	205	0.05766	0.33	0.94	1.86
26	15.94	244	0.07708	0.36	1.06	1.76
27	18.42	307	0.06987	0.31	0.94	1.66
28	18.69	305	0.07111	0.33	0.98	1.76
29	12.94	210	0.07312	0.35	1.03	1.77
Mean	10.65	199	0.06196	0.32	0.94	1.80
STDev	4.41	71	0.01122	0.03	0.090	0.074
%STDEV	41.4%	35.6%	18.1%	9.6%	9.6%	4.1%

4.2.3 Procedure

Procedure for a typical experimental run is described below:

- A known amount of catalyst is taken and dissolved in water. This is mixed with ground pine to allow the catalyst to soak into the wood. Once the water is soaked into the wood, it is dried at 75^{0}C for four hours (until there is no reduction in the mass of the wood sample) to reduce the moisture content in the ground pine to less than 10% inside an oven.

- The quartz tube is placed on the support stand and the height of the stand is adjusted to the level of tubular furnace. The condensers are fixed to the other end of the quartz tube. These condensers are placed inside an insulated container where liquid nitrogen will be poured (coolant for condensing oil) in step 6.

- The temperature of the tubular furnace is set to the required temperature. The temperature of the tubular furnace is set at a higher temperature than the reaction temperature (see

section 4.3 for further details). Once the tubular furnace has attained the required temperature, the ground pine sample is taken from the oven. This is done to minimize the moisture absorption by the pine.

- A known quantity of sample is measured and placed into the boat container. The thermocouple is carefully inserted into the slot provided in the boat to avoid any sample spill. The boat is slowly inserted into the quartz tube without spilling any sample into the tube. The boat is positioned such that it matches approximately with the center of the tubular heater.

- Once the sample is placed in the tube, all the joints are closed tightly with O-rings to ensure that there are no air gaps. Any gap in the system can lead to leakage of pyrolysis gases and represent a hazard. Then, the flow rate of nitrogen is set to a required value and allowed to run for a minute to purge out atmospheric gases.

- Then liquid nitrogen is carefully poured into the insulated condenser using gloves.

- The tubular furnace is carefully positioned around the quartz tube. It is important to ensure that the walls of the quartz tube are not in contact with the tubular furnace. Once the heater is positioned, switch on the timer and measure the temperature of the wood as a function of time. These reading are noted down at every thirty seconds for approximately twenty minutes. After fifteen minutes, it is noticed that the rate of increase in temperature of the wood is small and there is no visible release of pyrolysis vapors. At the end of twenty minutes, the temperature of wood reaches a steady value.

- Switch off the heater, remove the heater from the quartz tube and allow the sample to cool to room temperature. It is important not to switch off the nitrogen flow as it may

create a vacuum inside the quartz tube leading to entry of moisture and atmospheric gases into the system through leaks.

- Once the system reaches room temperature, switch off the nitrogen flow and immediately remove the char sample from the quartz tube. Measure the weight of the char and transfer it to a container.

- Remove the condensers carefully and close them tightly with caps to prevent any escape of gas into it. Also, seal the quartz tube tightly to prevent entry of air into the system.

- Liquid collected in the condenser and on the walls of the glass tube is washed with acetone and collected in a glass container. This sample is placed in a roto-vap to evaporate the acetone. The oil remaining in the roto-vap is collected for analysis.

4.3 Temperature Calibration

4.3.1 Thermocouple

Reaction temperature plays a crucial role in determining the products of pyrolysis. Hence, it is important to measure accurately the temperature of the wood. The tubular furnace was set at 450^0C, temperature at which pyrolysis reaction was supposed to occur. The temperature of the sample in the boat was assumed to be same as the temperature of the tubular furnace. Later, it was predicted that the flow of nitrogen gas through the system and the presence of thick glass might offer resistance to heat transfer and the temperature of tubular furnace might not represent the actual temperature of the sample in the boat. Hence, it was decided to incorporate a thermocouple into the wood sample to measure the actual temperature of the wood. Figure 4.4 represents the temperature measured by a thick thermocouple (refer to Table 4.7) when placed on the surface of the wood. It is observed that the actual temperature of the wood is offset from tubular furnace temperature by a huge margin even after 30 minutes of run time. Hence, the

45

initial set of runs (performed at the tubular furnace temperature set at 450^0C) was performed at temperatures different from furnace temperature.

The next step of the experimentation was to establish a tubular furnace temperature so that the temperature of the wood inside the boat would be close to 450^0C. A series of runs were performed and the results are presented in Figure 4.5. From Figure 4.5, we can infer that the temperature of the wood, when the tubular pyrolysis temperature is set at 620^0C, reaches a steady state value of 450^0C. Also, the rate of increase of temperature, as observed in Figure 4.6, dips at around 200 seconds (for sample containing pine at tubular furnace temperature set at 620^0C). The wood temperature at 200 second is around 350^0C, a temperature where significant pyrolysis reaction starts to occur. This indicates that, pyrolysis being an endothermic reaction, absorbs heat from the ambient atmosphere, reducing the rate of heating. For other cases (Figure 4.6), a dip in the curve was not observed, indicating a low rate of pyrolysis reaction.

Note that there are two types of thermocouples used in the experiment namely, thick and thin thermocouples. The specifications of the thermocouples are given in Table 4.7. Also, the temperature profile of the wood sample is studied using thermocouples at different positions. Figure 4.12 explains the schematic of thermocouples in different positions. This schematic will be frequently noted in this chapter.
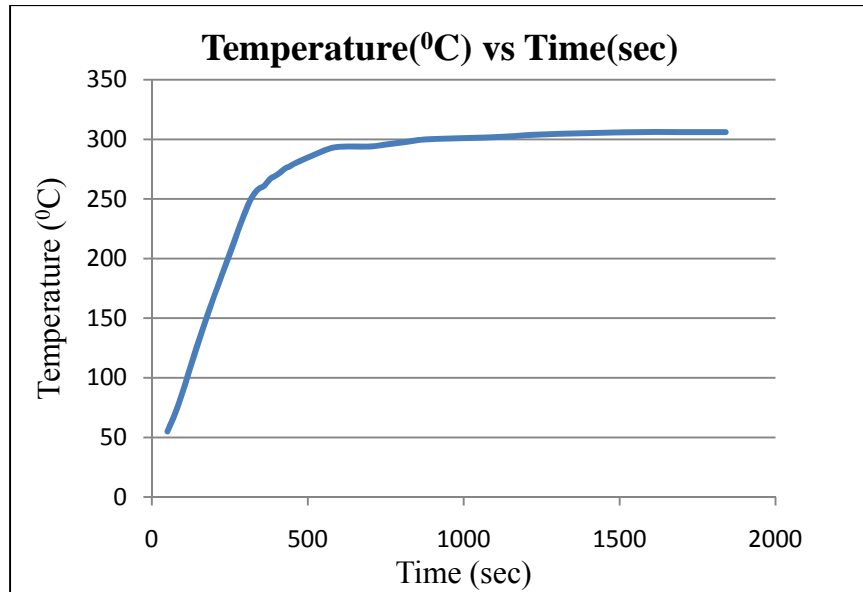
Figure 4.4: Wood temperature profile measured by a thick thermocouple for tubular furnace at 450 ^{0}C
(refer to Figure 4.12, Schematic 3, Table 4.7 for specifications)
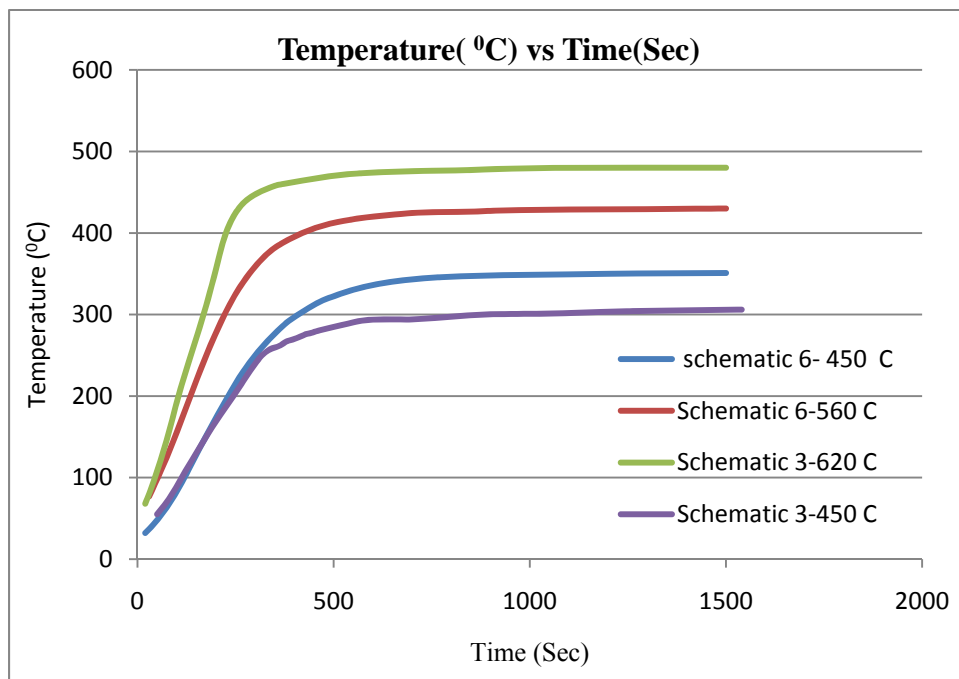
Figure 4.5: Wood temperature profile measured by a thick thermocouple for tubular furnace at different experimental conditions
(refer to Figure 4.12, for schematics, Table 4.7 for specification)
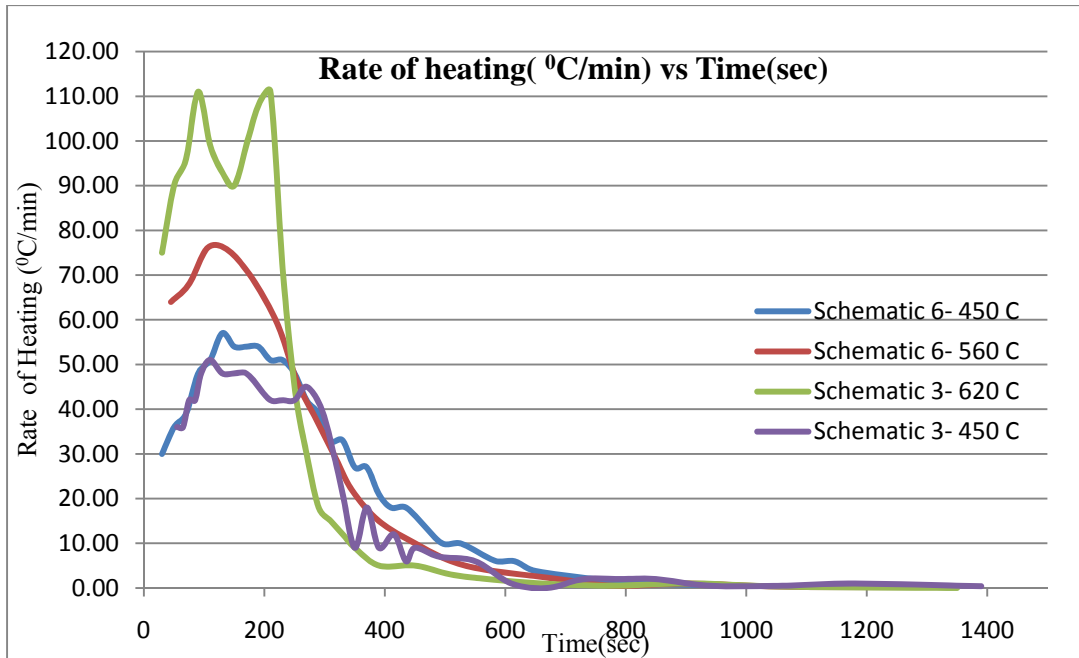
Figure 4.6: Rate of heating (^{0}C\min) vs. time in a boat container using thick thermocouple under different conditions

(refer to Figure 4.12, for schematics, Table 4.7 for specification)

It was predicted that the thick thermocouple (see Table 4.7) might not be the actual temperature of the surface of wood. This is due to the fact that, the lead of thermocouple has a greater surface area and is placed on the surface of the wood. Hence, there might be a possibility that the temperature indicated by the thermocouple is due to radiative heating or the ambient environment but not the actual temperature of the wood. Hence, the boat container was modified to insert the thermocouple into the middle of the boat. Results obtained comparing these thermocouples are presented in Figure 4.7. In both the experiments, the temperature of the tubular furnace was set at 620^0C and the thermocouple was placed in the middle of the ground pine (schematic 3, Figure 4.12). We observe (from Figure 4.7) that, except for faster dynamics in terms of temperature measurement, there is not much difference in terms of actual temperature.

48

Temperature (^{0}C) Vs Time(sec)
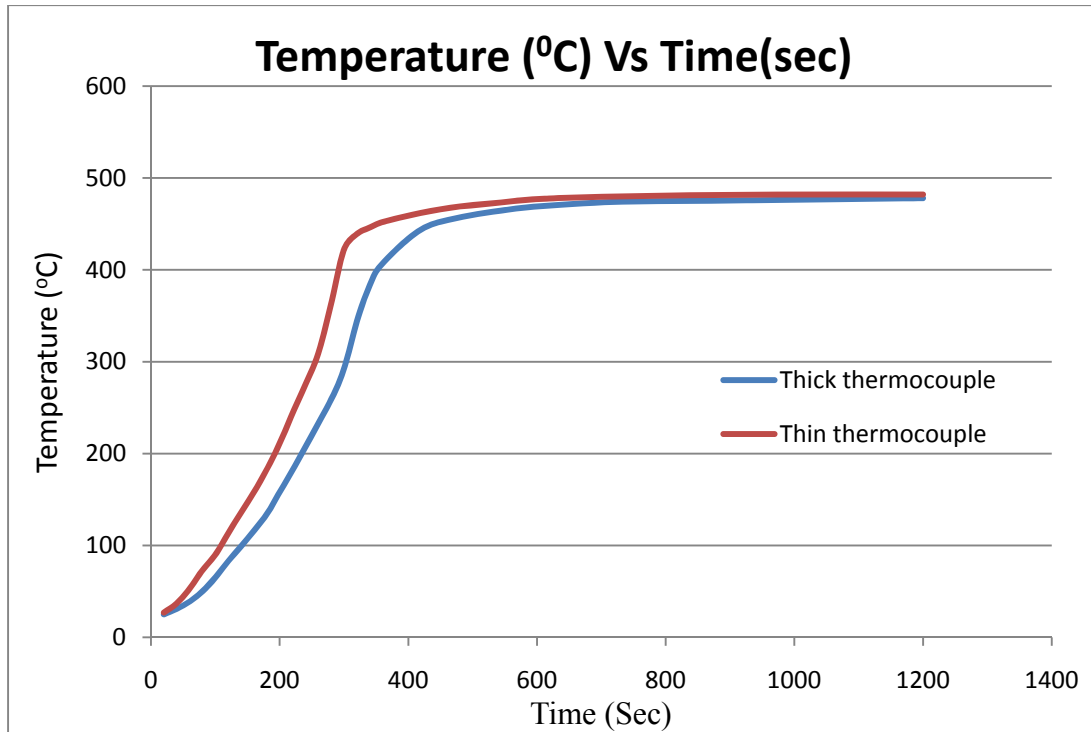
Figure 4. 7: Temperature profile for thick and thin thermocouples
(see Table 4.7 for specifications)

We are primarily concerned about the actual temperature of the wood sample during the pyrolysis reaction. From Figure 4.7, we can infer that the pyrolysis reaction occurs between 200 and 400 seconds where the temperature of the wood sample increases from 200^0C to 450^0C. The difference in temperature between the thin thermocouple and thick thermocouple increase from 50^0C to 100^0C between 200 to 300 seconds and drops down from 100^0C to 20^0C between 300 to 400 seconds. This is due to the fact that pyrolysis reaction occurs between the above specified temperature boundary and thin thermocouple captures the temperature difference faster compared to the thick thermocouple. However, we are in the pyrolysis reaction zone between 200 to 400 seconds according to the measurements of the thin or thick thermocouple. Hence, the usage of either thin or thick thermocouple does not significantly impact the measurement of actual temperature to an extent that the measured temperature is considerably different from the

49

pyrolysis temperature. Therefore, both the thermocouple can be used interchangeably and the offset in actual measured temperature can be corrected based on Figure 4.7.

4.3.2 Effect of external factors on temperature calibration by thermocouple

In section 4.3.1, it was established that the actual temperature of the wood sample is different from the tubular furnace temperature. In this section, effects of different parameters like the thickness of the wood, flow rate of nitrogen and radiation by the tubular furnace on the thermocouple measurement are studied. Since, it is established that there is no difference between the thin and thick thermocouple in terms of temperature calibration except for faster dynamics, the thick thermocouple is used in the experiments for convenience. Experimental conditions are given in Table 4.2.

Table 4.2: Experimental conditions for measuring temperature under different conditions

External Temperature of Thermostat	620^0C
Time of experiment (min)	20
Sample	Untreated wood
Flow rate of Nitrogen (L/min)	2

4.3.2.1 Effect of flow rate of nitrogen

When the thermocouple is placed on the surface of the wood, it is predicted that flow rate of a nitrogen over the thermocouple might lead to cooling of the thermocouple, leading to display of a different output temperature. Hence the temperature profile of the thermocouple is studied for four different scenarios presented below and the results obtained are shown in Figure 4.8.

- Thermocouple placed on the surface of the wood when the boat is completely filled (Schematic 1, Figure 4.12)

- Thermocouple placed on the surface of the wood when the boat is half filled with pine (Schematic 4, Figure 4.12)

- Thermocouple inserted in between the wood when the boat is completely filled (Schematic 3, Figure 4.12)

- Thermocouple placed at the bottom of the wood when the boat is completely filled (Schematic 2, Figure 4.12)

From Figure 4.8, we can infer the following:

- The temperature profile of schematic 3 up to 500 seconds is different from the profiles for schematic 1 and 4. This is according to expectations because the thermocouple in schematic 3 is not subjected to radiation unlike schematic 4 and 1. Also the flow rate of nitrogen cannot cause any cooling for schematic 3. Therefore, the temperature profile of schematic 3 is not influenced by heating due to radiation or cooling due to nitrogen flow. After 500 seconds, the temperature of the wood reaches a higher temperature and the thermocouple in schematic 3 is not subjected to cooling by nitrogen gas unlike schematic 1 and 4. Hence, the temperature profile of schematic 3 reaches a higher steady state value of temperature (by 10^0C approximately) compared to schematics 1 and 4.

- Comparing schematic 1 and schematic 2, both of them are equally subjected to radiative heating but the primary difference between them is the cooling of nitrogen. Schematic 1 is subjected to cooling by nitrogen where as schematic 2 is not. Hence, the temperature profile of schematic 1 is slightly below schematic 2 throughout the experiment. Note that due to practical difficulties, the thin thermocouple is used in schematic 2 whereas thick

51

thermocouple is used in schematic 1. Accounting for faster dynamics by the thin thermocouple (see Figure 4.7, Table 4.7), the temperature difference between schematic 1 and schematic 2 in the range of pyrolysis temperature (250-450^{0}C) is approximately 15°C. Hence, the flow rate of nitrogen lead to cooling of the sample on the surface but it is not significant.

- Comparing schematics 1 and 4, we see that both the scenarios are subjected to radiative heating. Two differences that primarily exist between schematics 1 and 4 are the thickness of the wood and the flow rate of nitrogen. The temperature profile for schematic 4 is slightly greater than schematic 1 (between 200-350 seconds) indicating that the flow profile of the nitrogen is over the surface of the boat reactor and does not dip into the boat when the boat is half filled. Also, schematic 1 and 4 reach same steady state temperature indicating that they are equally cooled by the nitrogen gas.
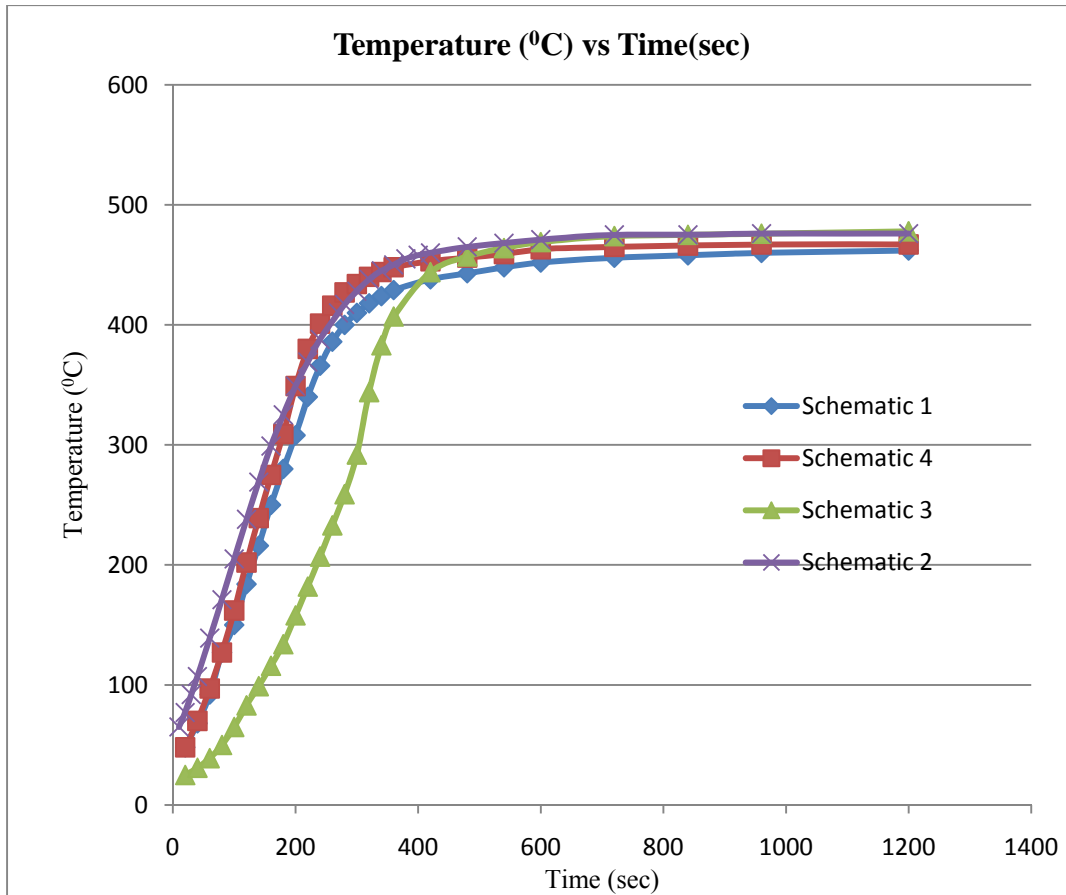
Figure 4.8: Effect of flow rate of Nitrogen and wood thickness on temperature calibration
(refer to Figure 4.12, for schematics)

4.3.2.2 Effect of radiation from tubular furnace

From the above experiments, the flow profile of nitrogen gas over the boat reactor and effect on nitrogen gas on cooling of the thermocouple are established. However, the effect of radiation and presence of wood is not clearly established. Hence, further experimentation was carried on for a few move scenarios explained below and the results are presented in Figure 4.9.

- Thermocouple placed in the middle of a boat without any sample (Schematic 6, Figure 4.12)

53

- Thermocouple placed in the middle of a boat and the boat is covered with aluminum foil (Schematic 5, Figure 4.12).
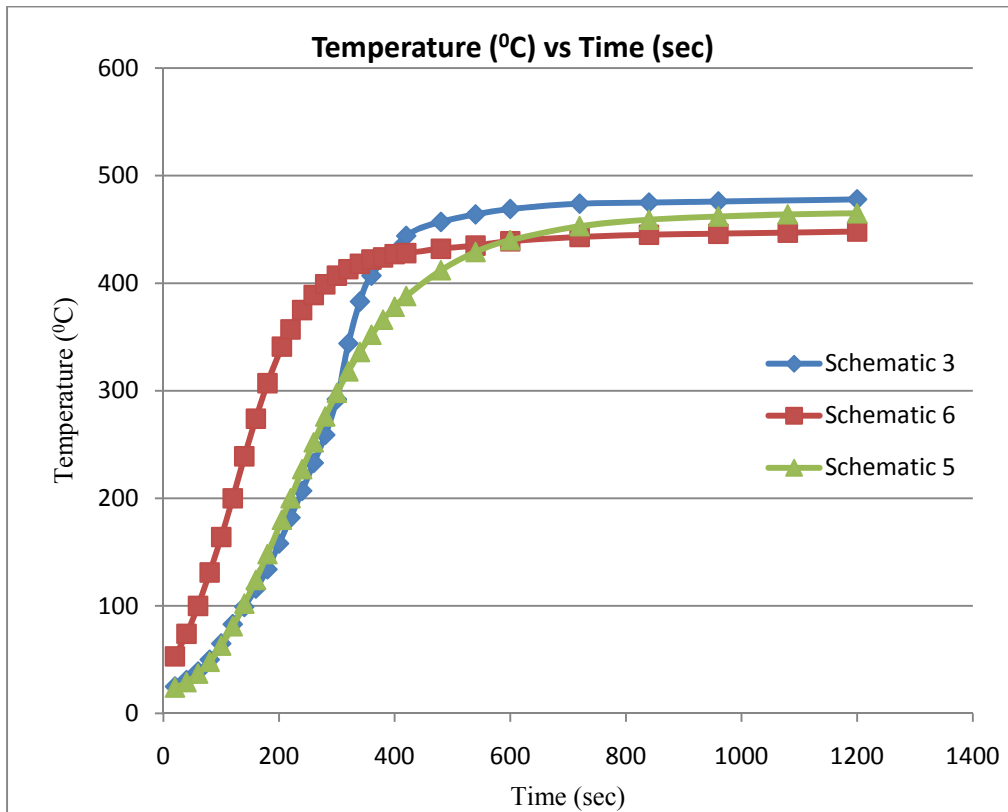
Figure 4.9: Temperature profile of the thermocouple to investigate the effect of radiation on temperature calibration
(refer to Figure 4.12, for schematics)

From Figure 4.9, we can infer the following:

- Comparing schematic 6 and schematic 5, we can infer that the heating effect due to radiation has a significant impact on the temperature profile. There is no radiation effect in schematic 5 as the boat is covered entirely with aluminum foil. In schematic 6, the boat is exposed completely and there is no sample. Hence the temperature profile between 0-

500 seconds is significantly higher for schematic 6. The primary region of interest in the experiment is between 200 and 400 seconds where actual pyrolysis reaction is in progress. The temperature difference schematic 5 and 6 decreases from 140^0C to 120^0C between 200-400 seconds. After 500 seconds, when the system started reaching steady state temperature, thermocouple exposed completely (schematic 6) is cooled by the flow of nitrogen but this is not the case for schematic 5. Hence, we observe that steady state temperature of schematic 5 is slightly greater than schematic 6. Hence radiation is the dominating factor which leads to significant heating of the woody biomass and can offset the measured temperature of the thermocouple measurement when placed on the surface the wood by a huge margin.

- Comparing schematic 3 and 5, both of them are not subjected to heating by radiation or cooling by flow of nitrogen. The only difference being presence of wood in former and air in later case. The temperature profile in the initial heating phase (0-350 seconds) is almost the same for both the cases. After 350 seconds, wood having a higher thermal conductivity than air, schematic 3 has a higher temperature profile compared to schematic 5. For example, the temperature difference between schematic 3 and schematic 5 at 350 seconds (when the pyrolysis reaction is in progress) is approximately 50^0C. Hence, the presence of wood is making a significant impact on the temperature measurement by the thermocouple after the initial heating phase.

From the above set of experiments the following conclusions can be drawn about the use of thick or thin thermocouples, the thickness of the wood, the effect of radiation and cooling due to flow of the nitrogen gas independently.

- The difference in temperature between the thin thermocouple and thick thermocouple increases from 50^0C to 100^0C between 200 to 300 seconds and drops down from 100^0C to 20^0C between 300 to 400 seconds. This is due to the fact that the pyrolysis reaction occurs between the above specified temperature boundary and the thin thermocouple captures the temperature difference faster compared to the thick thermocouple due to faster response. However, we are in the pyrolysis reaction zone between 200 to 400 seconds according to the measurement of the thin or thick thermocouple. Hence, the use of either a thin or thick thermocouple does not significantly impact the measurement of actual temperature of the wood to an extent that the measured temperature is considerably different from the pyrolysis temperature. The temperature recorded for thin thermocouple can be converted to thick thermocouple based on the calibration done in Figure 4.7

- The presence of wood leads to a different temperature measured by the thermocouple. During pyrolysis reaction, wood having higher thermal conductivity than air, the temperature difference between schematic 3 and schematic 5 is around 50^0C.

- Accounting for faster dynamics by the thin thermocouple, the temperature difference between schematic 1 and schematic 2 in the range of pyrolysis temperature $(250-450^0C)$ is approximately 15^oC. Hence, the flow rate of nitrogen does not lead to significant cooling of the sample on the surface.

- For reaction times between 200 and 400 seconds, where actual pyrolysis reaction is in progress, the temperature difference due to radiation is approximately 130^0C. Hence radiation is the dominant mode of heat transfer which leads to significant heating of the woody biomass and can offset the measured temperature of the thermocouple measurement by a huge margin when placed on the surface the wood.

Therefore, thermocouple has to be placed inside the wood (schematic 3) so that the effects of radiation are not significant. Hence, schematic 3 is the position of the thermocouple for the experiments done in section 4.4 and the temperature measured is close to the temperature of the wood.
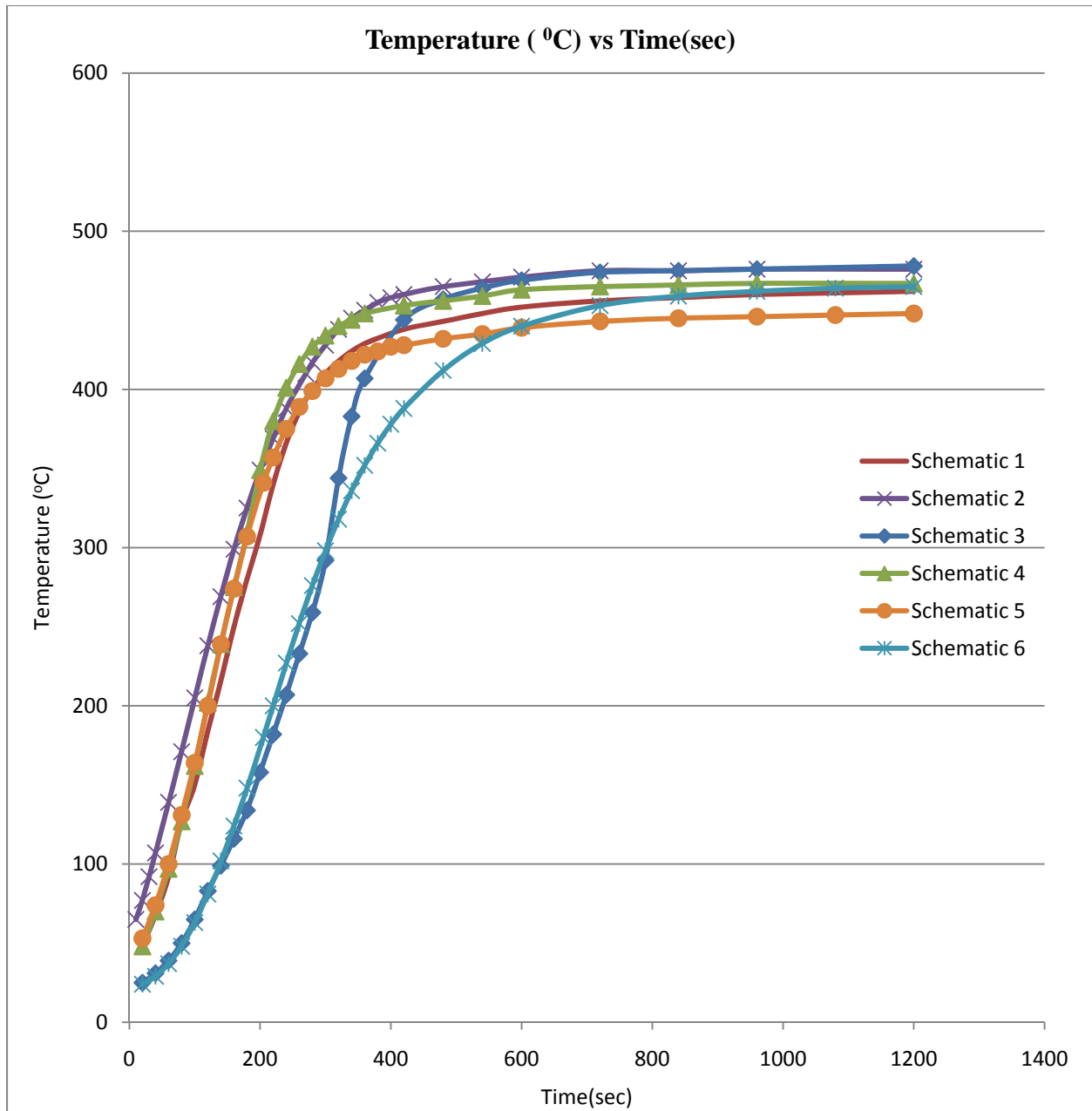
Figure 4.10: Temperature profile under different scenarios
(refer to Figure 4.12, for schematics)

Results obtained in Figure 4.8 and 4.9 are combined and presented in Figure 4.10. Note that the results are presented separately for clarity. From Figure 4.10 (inferences from Figure 4.8 and 4.9), we conclude that radiation from tubular furnace is the primary factor that can significantly offset the reading of thermocouple when exposed to radiation. This is clearly evident from Figure 4.10, temperature profiles of schematics 3 and 5 are completely different from other cases due to lack of radiation heating of the thermocouples in these two cases.

4.4 Experimental Results

4.4.1 Tubular pyrolysis reactor run

Loblolly pine impregnated with few catalysts was subjected to pyrolysis in a tubular reactor; char and bio-oil were collected and analyzed further. From previous micro-reactor studies performed by Alex Williams and Kasi David in our group (Muzzy et. al., 2009) carbonate salts appeared most promising with regard to producing bio-oil at a faster rate with potentially less oxygen. In order to obtain more oil for characterization, the same catalyst series was run in the tubular pyrolysis reactor. The results obtained are presented in Table 4.3.

Table 4. 3: Percentage of char obtained from Tubular reactor

Catalyst	Reaction Time (min)	Temperature of tubular furnace (^{0}C)	Flow rate of N_2 (lit/min)	gr. of cat./gr. of wood	% char (including catalyst)	Wt. of wood (gr)
No catalyst - undried wood	15	400	0.5	none	28.23	8.00
No catalyst - dried wood	20	450	0.5	none	26.22	12.28
Li_2CO_3 - dried wood	20	450	0.5	0.025	32.67	9.83
Na_2CO_3 - dried wood	20	450	0.5	0.025	32.49	7
Na_2CO_3 - dried wood (run 2)	20	450	0.5	0.025	33.00	10.25
K_2CO_3 - dried wood	20	450	0.5	0.025	34.70	10.00
Cs_2CO_3 - dried wood	20	450	0.5	0.025	36.48	10.23

The oil yields are not reported because the quartz tube had to be washed with acetone to recover oil condensed on it. Then the oil and acetone were roto-vaped to remove the acetone. Some light compounds in the oil probably evaporated with the acetone. These samples have been sent for elemental analysis to Galbraith Laboratories and the results are presented in Table 4.4.

From Table 4.3, we can infer the following:

- Additions of catalyst to wood increases the percentage of char but the quality of oil in terms of oxygen content is yet to be determined.

- As we increase the molecular weight of cations (from Lithium to Cesium), percentage of char is increasing. Experiments are done on the basis of the same weight ratio (weight of catalyst/weight of wood). In other words, the moles of catalyst used are decreasing progressing down the periodic table. Hence, the runs need to be repeated on a constant catalyst molar basis rather than a constant weight percentage.

- Two runs using Na_2CO_3 as catalyst led to almost same percentage of char for different weights of wood sample. This provides support for the hypothesis that the percentage of char is not affected by the weight of the sample.

Table 4.4: Elemental analysis of the bio-oil received from Galbraith laboratories for different samples

Sample	C	H	N	O	Water %
Untreated tube furnace –non dried	60.89	5.92	< 0.5%	33.47	21.50
Untreated tube furnace-dried	58.90	6.43	< 0.5%	33.84	10.77
Na_2CO_3 tube furnace	61.16	7.4	< 0.5%	30.59	24.62

Note that the temperature value in the Table 4.3 is the temperature of the tubular furnace and not the actual temperature of the wood. These runs were performed before the thick thermocouple was inserted inside the tubular reactor to measure the actual temperature of the wood. (See Figure 4.5 for actual temperature profile)

The elemental analysis is on a dried basis. There appears to be a moderate reduction in oxygen content when the sodium carbonate catalyst is present. The bio-oils from the tube furnace were subjected to a roto-vap; hence, their moisture contents are lower relative to the bio-oil obtained from micro reactor by Alex Williams and Kasi David (Muzzy et. al., 2010). Additional analysis on bio-oil (C-NMR, GC-MS, GPC, PH, Density, P-NMR, TG-MS) was performed by Kasi David. (Muzzy et. al., 2010).

In the above experiment, the oil collected from the tube furnace is subjected to a roto-vap to remove the acetone. Hence, it is anticipated that lower molecular weight fractions of bio-oil might have been evaporated. Therefore, a new set of experiments was performed with three major modifications. The modifications are as follows:

1.) A thermocouple was inserted into the boat container to measure the actual temperature of the wood and the temperature of the tubular furnace is set at 620^0C so that the actual temperature of the wood is close to the desired temperature of pyrolysis. (See Figure 4.5).

2.) Oil condensed inside the condenser was directly collected without washing with acetone. Oil stuck to the walls of the tubular reactor is washed with acetone, subjected to roto-vap and collected separately. The main aim of this approach was to check if there are any differences between the oil analysed from both the samples. Although, it is anticipated that the lower molecular weight fractions evaporate initially and are condensed inside the condenser whereas the higher molecular weight fractions are condensed on the walls of the condenser.

3.) The same moles of catalyst are added rather than the same weight of catalyst.

The results obtained are tabulated in Table 4.5

Table 4.5: Percentage of char obtained from Tubular pyrolysis reactor using different catalysts

Catalyst	Reaction Time (min)	Temperature of tubular furnace(^{0}C)	Flow rate of N2(lit/min)	Moles of catalyst/gr. of wood	% char	wt of wood(gr.)
No catalyst-dried wood (Run1)	20	620	1	none	21.53	11.75
No catalyst-dried wood (Run2)	20	620	1	none	21.44	11.52
Na$_2$CO$_3$- dried wood (Run1)	20	620	1	2.375×10^{-4}	27.67	8.24
Na$_2$CO$_3$- dried wood (Run2)	20	620	1	2.375×10^{-4}	27.84	8.37
Na$_2$CO$_3$- dried wood (Run3)	7	620	1	2.375×10^{-4}	28.89	8.47
K$_2$CO$_3$-dried wood(Run-1)	20	620	1	2.375×10^{-4}	28.33	8.26
K$_2$CO$_3$-dried wood(Run-2)	20	620	1	2.375×10^{-4}	28.57	7.42
Li$_2$CO$_3$- dried wood (Run 1)	20	620	1	2.375×10^{-4}	27.52	5.96
Li$_2$CO$_3$- dried wood (Run 2)	20	620	1	2.375×10^{-4}	27.61	6.52
NaOH- dried wood (Run 1)	20	620	1	2.375×10^{-4}	26.14	8.3
NaOH- dried wood (Run 2)	20	450	1	2.375×10^{-4}	26.50	8.34

From Table 4.5 we can infer the following:

- The percentage of char is almost the same for all the catalysts when they are in same molar ratio basis (moles of cat./ gr. of wood)

- The percentage of char is not dependent on the weight of wood sample pyrolyzed.

- The usage of catalyst increases the percentage of char formed compared to no catalyst addition. Although, preliminary elemental analysis (see Table 4.4) shows that it reduces the percentage of oxygen content in the oil.

- The time-temperature profiles of the samples in the boat were recorded for both the runs of all the catalysts to test the consistency of the results. Initially, between 0-150 seconds, the percentage deviation was around 10% but between 200-400 seconds where the pyrolysis reaction occurs, the percentage deviation was less than 1%. The graph shown in Figure 4.11 (for lithium carbonate) and the percentage of char obtained in Table 4.5 indicate that the runs are replicable

- Run 3 using Na_2CO_3 as catalyst resulted in almost the same percentage of char as runs 1 and 2. This indicates that the pyrolysis is completed at the end of 7 minutes as there is no further reduction in percentage of char. This can also be verified from Figure 4.5 where the temperature of the boat at the end of 7 minutes is around 450^0C indicating the completion of pyrolysis reaction. Although, this can only be confirmed after comparing the quality of oil obtained from Run 1 and Run3.

Additional analysis of the bio-oil (C-NMR, GC-MS, GPC, PH, Density, P-NMR, TG-MS) was performed by Kasi David. (Muzzy et al., 2010).
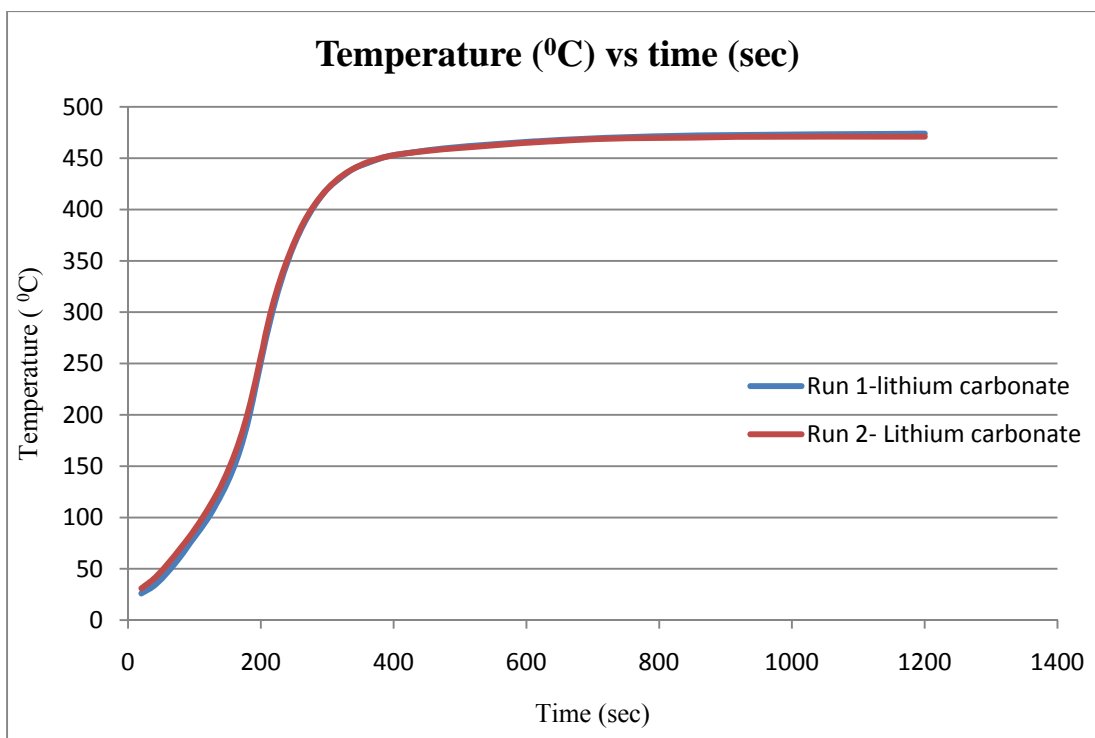
Figure 4.11: Temperature versus time measured by a thick thermocouple in the wood sample using a furnace temperature setting of 620 ^{0}C

(see Table 4.7)

Results of elemental analysis of these oil samples obtained from Galbraith laboratory is presented in Table 4.6. These samples are selected in such a manner to capture any variation in the results caused due to sampling of oils. From Table 4.6, combined Na_2CO_3 1 and 2 implies that the oil from the condenser for both the runs (1 and 2) is combined and two samples are analyzed respectively from the combination. K_2CO_3 1 implies that the oil from the condenser from run 1 is analyzed. Samples analyzed from pyrolysis of wood with K_2CO_3 show a discrepancy in the percentage of water. This wide variation is due to the fact that oil in the condenser is mostly a representative of lighter weight fractions of bio-oil as it boils at lower temperature. The oil collected from the condenser separated into two immiscible phases when left stationary for some time. Hence, sample from condenser is a mixture of water and light

weight fractions that are immiscible with water. Hence, sampling of these oils may result in different results depending on which phase the sample is being taken from. Therefore, these samples are not representative of the entire spectrum of oil composition. Hence, it is suggested to wash the sample with a solvent (preferably THF) to obtain a homogenous sample. This sample is subjected to roto-vap and the resulting oil is analyzed for different product compositions (including the distillate collected from the roto-vap). Also, the percentage of water is high compared to results from Table 4.5 because the oil is not subjected to roto-vap. Therefore, the procedure of directly collecting the sample from condenser without washing with acetone has been discarded due to its high variability in results.

Table 4.6: Elemental analysis of the bio-oil received from Galbraith laboratories

Sample	C %	H%	N%	O%	Water content %
No Catalyst	52.72	6.38	<0.5%	30.69	40.90
Combined Na_2CO_3 1	68.13	7.29	<0.5%	29.72	64.07
Combined Na_2CO_3 2	44.99	8.39	<0.5%	39.35	57.10
K_2CO_3 1	48.33	7.67	<0.5%	29.86	70.72
K_2CO_3 2	44.32	7.02	<0.5%	26.56	24.98
Li_2CO_3 1	49.86	6.58	2.17	29.67	60.77
NaOH 1	48.66	7.24	1.78	37.79	62.27

There are several problems encountered in performing the experiments in the tubular pyrolysis reactor. They are as follows:

- Increasing the flow rate of nitrogen above 2 l/min could potentially reduce the residence time of the oil in the tube and increase the quality of the oil. Increasing the residence time, leads to faster condensation of oil at the entrance of the condenser leading to clogging of the condenser. The vapor then forcefully escapes from small vents in the set

up leading to no useful result. Hence, we have a constraint on the flow rate of the nitrogen due to the size of the condenser.

- The quartz tube needs to be regularly cleaned as there is deposit of char on the surface of the tube and it might affect the quality of the oil by its own catalytic action.

- We have a problem in measuring the yield of the oil because oil sticks to the wall of the glass tube apart from collecting in the condenser. We cannot collect this oil without washing with acetone. Secondly the pure oil obtained from acetone after this evaporation step is not an accurate measurement of oil yield as some amount of light weight fraction oil is expected to be lost along with acetone.

4.5 Summary and Conclusions

- The difference in temperature between the thin thermocouple and thick thermocouple increase from 50^0C to 100^0C between 200 to 300 seconds and drops down from 100^0C to 20^0C between 300 to 400 seconds. Hence, the use of either thin or thick thermocouple does not significantly impact the measurement of actual temperature of the wood to an extent that the measured temperature is considerably different from the pyrolysis temperature.

- The flow rate of nitrogen does not lead to significant cooling of the sample on the surface. The temperature difference between schematic 1 and schematic 2 in the range of pyrolysis temperature ($250-450^0C$) is approximately 15^oC.

- Radiation is the dominant mode of heat transfer which leads to significant heating of the woody biomass and can offset the measured temperature of the thermocouple measurement by huge margin when the thermocouple is placed on the surface the wood. During pyrolysis, when the thermocouple is placed on the surface of the wood, the

66

temperature measured by the thermocouple is 35% more than the actual temperature of the wood.

- The best position of the thermocouple to minimize external effects like cooling due to the flow of nitrogen gas and radiation heating is presented in schematic 3.

- Addition of catalyst to wood is increasing the percentage of char (when added in same mole basis) and the percentage of char is not affected by the weight of the wood sample. Percentage of char has increased from 21% to 28% when the wood sample was impregnated with different catalysts based on same mole ratio.

- The percentage of char is almost same for all the catalysts when they are added in same molar ratio basis (moles of cat./ gr. of wood). Approximately 28% of char was obtained for different catalysts when same mole ratio of catalyst to wood is added

4.6 Thermocouple specification and schematics
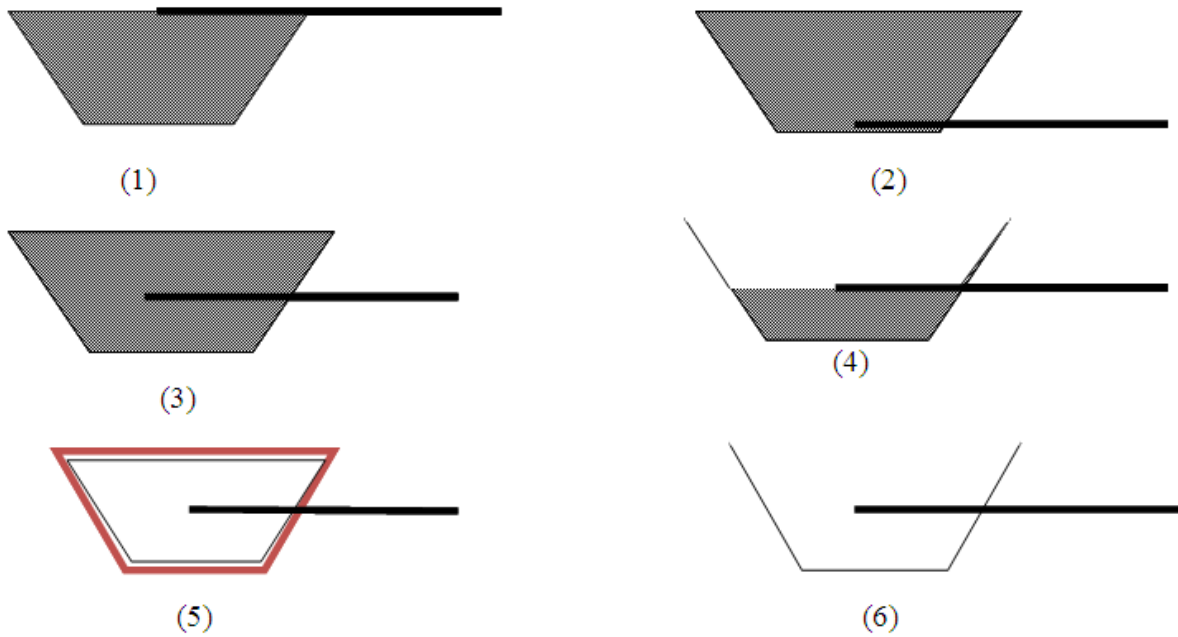
Figure 4.12: Schematic of the different positions of the thermocouple

(1)Thermocouple placed on the surface of the wood, fully filled boat, (2)Thermocouple placed at the bottom of the wood, fully filled boat, (3) Thermocouple placed in the middle of the wood, fully filled boat, (4) Thermocouple placed on the surface of the wood, half filled boat, (5) Boat wrapped by an aluminum foil, no wood sample, thermocouple placed in the middle of the boat, (6) No wood sample, thermocouple placed in the middle of the boat

Table 4.7: Specifications of the thick and thin thermocouple

Thermocouple	Thermocouple Type	Sheath Material	Sheath Diameter (inch)	Thermocouple Junction	Sheath Length (inch)
Thick (Old)	K	Inconel	1/4	Exposed	24
Thin (New)	K	Inconel	1/16	Exposed	24

CHAPTER 5

REACTOR KINETICS AND MASS BALANCE MODEL

5.1 Residence Time Distribution (RTD) model

This chapter describes a model for predicting the product distribution of pine pyrolysis in an auger reactor as a function of residence time and temperature. The auger reactor is modeled as a single screw extruder with a residence time distribution (RTD) based on operating conditions. It is known that at different temperatures, different components of wood, namely cellulose, hemicelluloses and lignin, pyrolyze to give various products. The product distribution of the pyrolysis of pine is highly dependent upon the residence time of a biomass particle in the reactor at that temperature. Hence, an auger reactor is divided into three zones having different temperatures respectively to facilitate the collection of cellulose, hemicelluloses and lignin pyrolysis products for a given RTD. The model developed by Yeh et al, 1999, is used to describe the RTD of each zone. This model can be used for different operating conditions, materials and extruders and can estimate RTD from operating conditions. Therefore, it is very helpful for process designing and control if the RTD can be predicted for operating conditions. This model consists of a plug flow reactor (PFR) in series with a continuous stirred tank reactor (CSTR) with a fraction of flow held up in a stagnant dead volume. Two operating parameters, namely screw speed and feed rate, are the major factors in determining the RTD in this model. The flow pattern in an auger reactor, with a total volume V, consists of PFR in series with CSTR with a stagnant dead volume. The feed enters the PFR with a volume fraction of P as shown in Figure 5.1, and then flows into the CSTR with a volume fraction of (1-d)*(1-P). There exists a stagnant dead volume having a volume fraction of d*(1-P), where d is the fraction of dead volume in CSTR

(Yeh et al., 1999). The residence time distribution of the material in an auger reactor can be modeled using above described model. Two parameters namely, the mean residence time and the fraction of volume in PFR can be varied to match the given RTD curve. The assumption of stagnant dead volume simplifies the analysis of RTD. Effects of temperature and moisture of the material are not included in the model and is assumed that it may not affect the RTD.
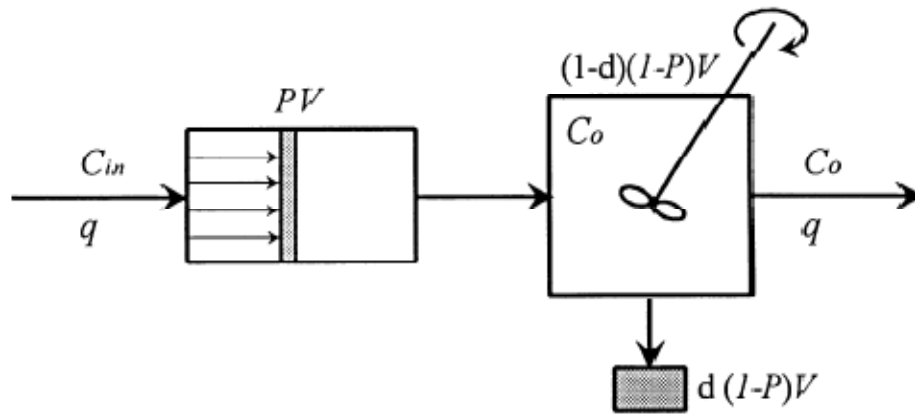
Figure 5. 1: Flow diagram of the PFR in series to a CSTR with a stagnant dead volume
(Yeh et al., 1999)

The residence time distribution E (t), curve obtained for the above described model is presented below:

$$E(t) = \left(\frac{u(t)}{(1-d)(1-P)t_d} \right) \left[e^{\frac{-(t-Pt_d)}{(1-d)(1-P)t_d}} \right]$$
(5.1)

$$u(t) = 0, t \le Pt_d$$
$$u(t) = 1, t > Pt_d$$
(5.2)

The value of P is determined by the operating conditions, materials and extruder parameters. For the operating conditions tested in the literature, P increased with the feed rate, but decreased as the screw speed increased. At high screw speed and low feed rate, the extruder tended to have a

P smaller than 0.5. The value of d varied between 0.044 and 0.164. An average of 0.108 for d

obtained from literature is chosen for the model. (Yeh et al., 1999)

In general, mean residence time (t_d) and parameter P are a function of screw speed (S_s), feed rate

(F_r) of the reactant and configuration of the screw. For example, the regressed equation for a

forward element screw configuration relation RTD parameters to screw speed and feed rate using

polished rice as feed material is given in equation 5.3-5.4 (Yeh et al., 1999). Note the units of

feed rate is Kg/hr, screw speed is rpm and mean residence time is seconds.

$$t_d = 1159.77 - 133.68F_r - 3.07S_s + 0.17F_r*S_s + 5.35F_r^2 \tag{5.3}$$

$$P = 0.7752685 - 0.0021974F_r - 0.0052142S_s + 0.00002787F_r*S_s \tag{5.4}$$

5.2 Kinetic Model

The kinetic model proposed by Shafizadeh.et.al (1977) is used in the model to describe the

kinetics of wood pyrolysis. The mechanism is based on lumping the different molecular products

into three product groups: gas, oil, and char. Thus, the wood decomposition is described by three

parallel reactions (reactions **1, 2,** and **3),** called the primary reactions. Secondary reactions of oil

decomposing to gas and char again are not considered in our model. A schematic of the reaction

mechanism is given below:
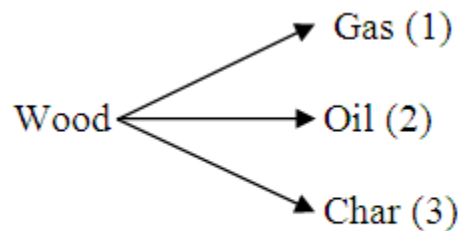
Figure 5.2: Model of wood pyrolysis kinetics suggested by Shafizadeh et al. (1977)

Assuming that each primary reaction is first order, the formation or disappearance rate of each component is given below. Note that these relations are expressed in terms of mass rather than moles of each component. Hence it is convenient to express these equations in terms of weight fractions

$$\frac{dw_w}{dt} = -(k_1 + k_2 + k_3)w_w(t)$$

$$\frac{dw_G(t)}{dt} = k_1 w_w(t)$$

$$\frac{dw_T(t)}{dt} = k_2 w_w(t)$$

$$\frac{dw_C(t)}{dt} = k_3 w_w(t)$$

(5.5-5.8)

Initial conditions used in the above differential equations are

$w_w(0) = 1, w_G(0) = w_T(0) = w_C(0) = 0$, where w_G, w_T, w_C, w_w are weight fractions of gas, oil, char and wood respectively. The frequency factors and activation energies obtained by Thurner.et.al (1981) are used in the model and presented below.

Table 5. 1: Activation energy and frequency factor by Thurner et al. (1981)

Reaction rate constant	Frequency factor (sec^{-1})	Activation energy(KJ/mol)
K_1	$1.43*10^4$	88.6
K_2	$4.13*10^6$	112.7
K_3	$7.38*10^5$	106.5

The auger reactor consists of 3 different zones at different temperatures. RTD and the reaction kinetics described above are used in the model. A schematic of zone wise pyrolysis in the auger reactor is presented below:
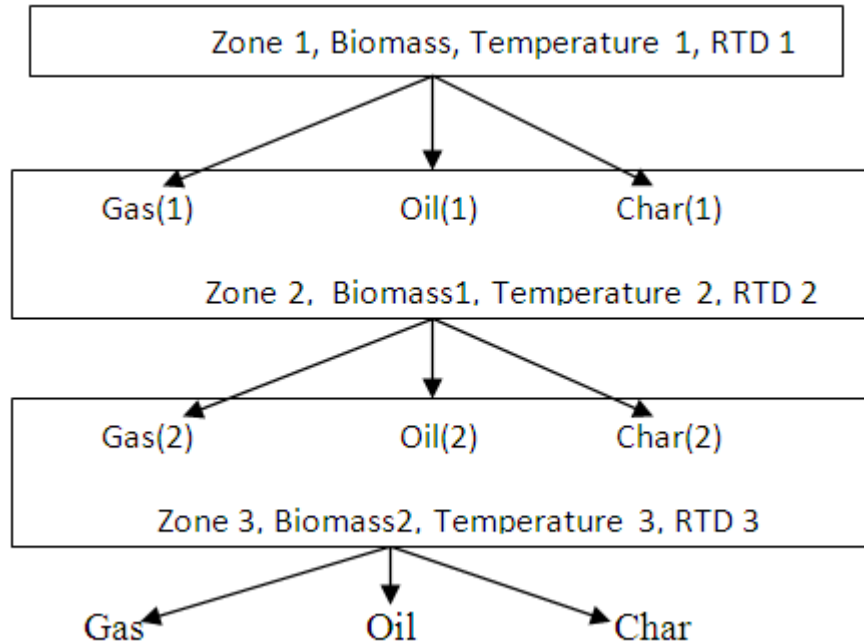
Figure5. 3: Schematic of Zone wise pyrolysis in the auger reactor

5.3 Assumptions

Following are the list of assumptions made in the reactor modeling:

- Kinetic parameters obtained from literature are isothermal data points. It is assumed that these parameters do not change significantly while analyzing the zone temperature sensitivity of oil yield.

- All three zones in the auger reactor are independent. This implies that there is no back mixing of reactants or products in the auger feed. Reactants that exit a particular zone do not reenter the same zone.

- RTD curve of all the zones is assumed to be the same because the viscosity of the biomass mixture does not significantly change in the given temperature regime.

- Mean residence time is heuristically taken as approximately one tenth of the total reaction time so that secondary reactions are prevented which reduce the quality of oil

- In most cases the fraction of dead volume in the RTD is around 11% (Yeh et.al, 1999)

5.4 Objective of the reactor model

A schematic of the functioning of the reactor model (for any zone, i) is given below (Fig. 5.4). All the input parameters like zone temperature and RTD parameters are defined in the main program. The main program calls a particular zone, i, and these values are passed to the zone function. The zone function then transfers these values initially obtained from the main program to the RTD and kinetic modules respectively. These modules return back the value of RTD and yields of products respectively at that given condition to the zone module. This zone module returns the output yields at the end of zone i to the main program. These output yields at the end of zone i are used as an input for zone i+1 and the same procedure is iterated. At the end of zone 3, the main program displays the output yields of products as a function of RTD parameters.
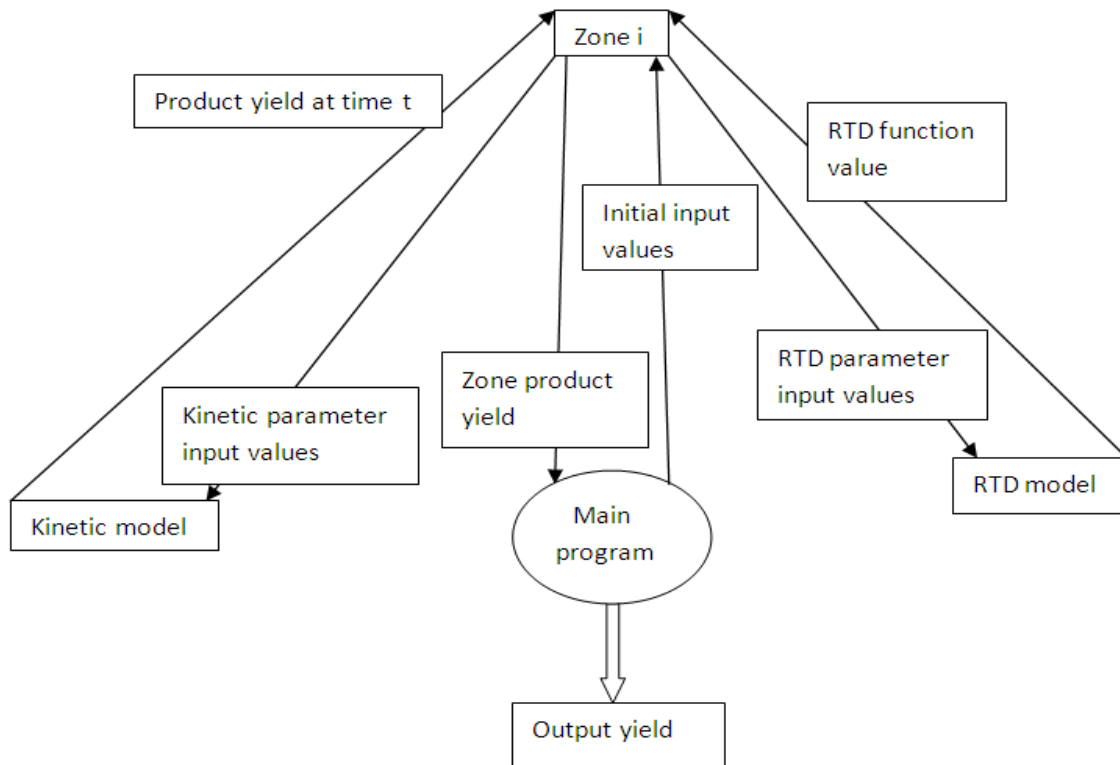
Figure 5.4: Schematic of functioning of reactor model

The objectives of the reactor model are as follows:

- Study the effect of RTD parameters on the production of oil

- Analyze the sensitivity of zone temperatures on oil production for a given RTD

- Analyze the sensitivity of calculated values of the kinetic parameters from a given yield curve with respect to variations in RTD parameters

- Small variations in RTD parameters lead to variations in calculated values of kinetic parameters for a given yield curve. When these values of kinetic parameters are used in the model, it may lead to variations in predicting yields of products. These variations may be significant and will be analyzed in the model

5.4.1 Effect of RTD on product distribution of biomass pyrolysis

Schematic of zone wise pyrolysis reactor explains the functioning of pyrolysis reactor. This is a continuous process and ground pine is fed to the reactor at the rate of 1000 kg/hr. Products are collected at the end of zone 3. The effect of parameters like P and the mean residence time (t_d) on the amount of bio oil produced for given kinetic parameters are presented below.

Table 5.2: Typical operating conditions

Feed rate of biomass(Kg/hr)	1000
Temperature zone 1(K)	523
Temperature zone 2(K)	623
Temperature zone 3(K)	723
Total reactor run time(min)	15
Range of t_d in each zone(sec)	5-30
dead volume fraction for each zone(d)	0.108
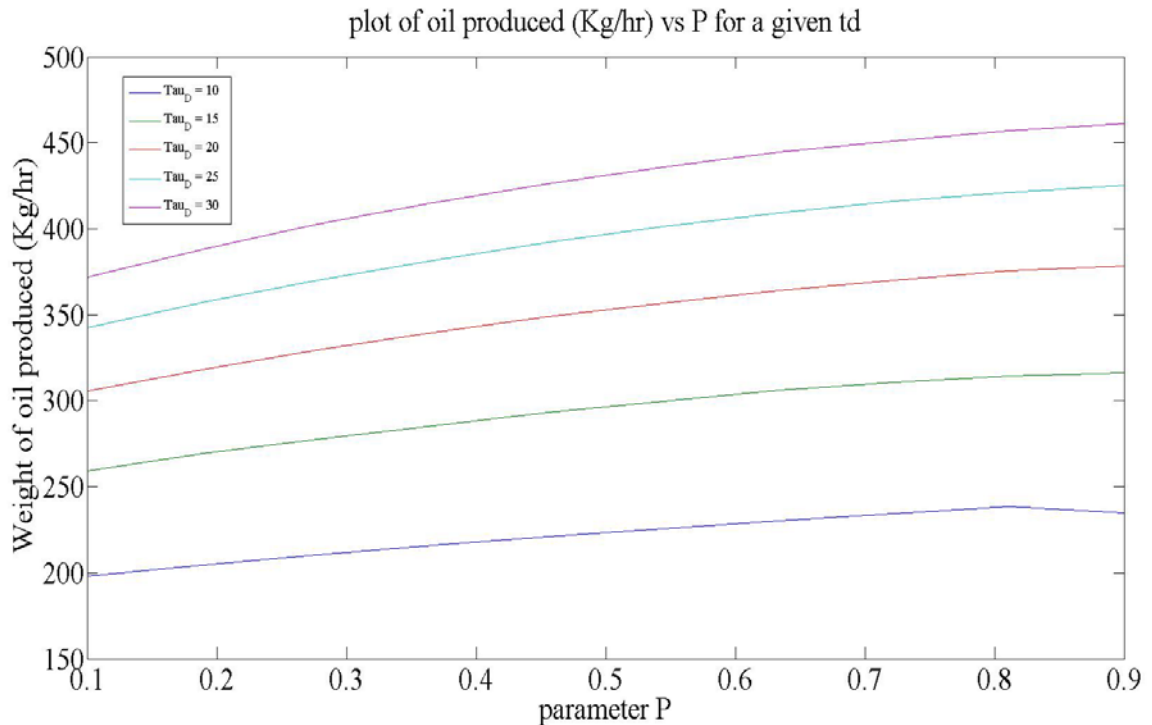
Figure 5.5 Oil produced (Kg/hr) vs. P for a given t_d (Kinetic parameters by Thurner et al.,1981)

From Figure 5.5 we can infer the following:

- The quantity of oil produced in general increases with parameter P for any given value of t_d.

- The amount of oil produced increases with the mean residence time for a given value of P. Although, the amount of oil produced increases with the mean residence time for a given value of P, the percentage increase in oil produced for a given value of P decreases with an increase in the value of t_d. For example, comparing $t_d = 10$ and $t_d=15$, at a value of P=0.2, the percentage increase in oil production is approximately 30%. Comparing $t_d = 25$ and $t_d=30$, at a value of P=0.2, the percentage increase in oil production is approximately 10%.

- The percentage increase in the production of oil as the value of P varies from 0.1 to 0.9 increases with the value of t_d. The percentage increase in oil is varying from 6% for t_d equal to 10 to approximately 16% for value of t_d equal to 30. This implies that plug flow behavior of RTD model would maximize the yield of oil.

- The maximum amount of oil produced at a given temperature and given kinetics (of Shafizadeh.et.al, 1977) is 45% for P=0.9, t_d=30 seconds (Kinetic rate constants by Thurner et al., 1981)

- Note that the secondary reactions are not taken into consideration in the above calculations. Hence, increasing the t_d value can cause secondary reactions which can affect both quantity and quality of oil produced.

The quantity of oil produced also depends significantly on the reaction kinetics of pyrolysis. Kinetics of pyrolysis depends on the experimental set up. The kinetic parameters for oak

pyrolysis by Thurner.et.al (1981) are based on experiments done in a boat pyrolysis reactor. Kinetic parameters obtained from Wagenaar et al. (1994) in a TGA sample pan are given below. Using these kinetic parameters under the same experimental conditions can lead to different results (see Figure 5.6)

Table 5.3: Activation energy and frequency factors by Wagenaar et al. (1994)

Reaction rate constant	Frequency factor(sec^{-1})	Activation energy(KJ/mol)
K_1	$1.11*10^{11}$	177
K_2	$9.28*10^9$	149
K_3	$3.05*10^7$	125

From Figure 5.6 we can infer the following:

- The amount of oil produced varied significantly by changing the experimental set up. The maximum amount of oil produced increased from 55% to 75% for P equal to 0.9 and t_d equal to 30.

- Although, the amount of oil produced increases with mean residence time for a given value of P, the percentage increase in oil output for a given value of P decreases with an increase in the value of t_d. For example, comparing $t_d = 10$ and $t_d=15$, at value of P=0.2, the percentage of increase in oil production is approximately 12%. Comparing $t_d = 25$ and $t_d=30$, at a value of P=0.2, the percentage increase in oil production is approximately 2%.

- The percentage increase in the production of oil as the value of P varies from 0.1 to 0.9 decreases with an increase in the value of t_d, contrary to Figure 5.5. The percentage increase in oil output is varying from 18% for t_d equal to 10 to approximately 5.6% for t_d equal to 30.

78

- Finally, the rate of increase of oil production is increasing at a faster rate for values of P less than 0.5 and tapering at a faster rate for values of P greater than 0.5 compared to Figure 5.5.
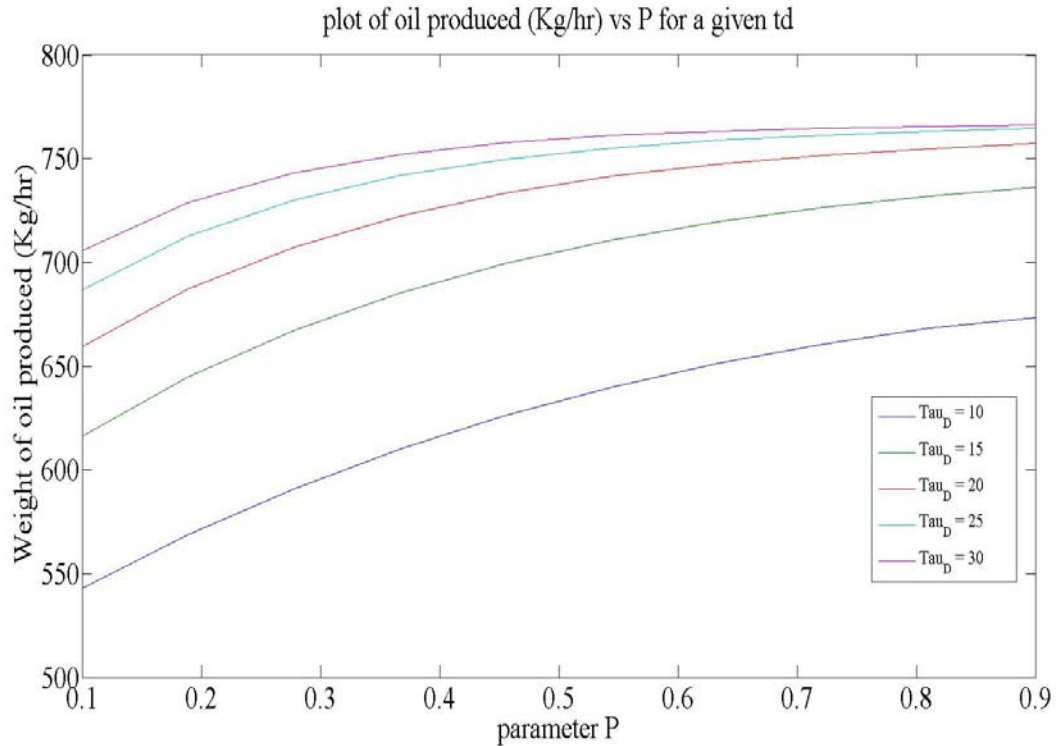
Figure 5.6: Oil produced (Kg/hr) vs. P for a given t_d for kinetic parameters by Wagenaar et al. (1994)

Hence, we can conclude that kinetics play a very crucial role in determining the output of oil and the kinetics of pine pyrolysis in an auger based reactor is very important in predicting the output yields of products for a given RTD.

If the fraction of dead volume in RTD is increased from 0.108 to 0.508, all other experimental conditions remaining the same, a reduction in oil production quantity is observed (Figure 5.7) for low values of P compared to Figure 5.5. For high values of P (0.85-0.9), the quantity of oil produced is comparable to Figure 5.5 for any given value of t_d. Secondly, the percentage increase

in the production of oil as the value of P varies from 0.1 to 0.9 for a given value of t_d is significantly more compared to Figure 5.5. For example, the percentage increase in oil is approximately 57% for t_d equal to 10 and 50% for value of t_d equal to 30. These results are in accordance with expectations because increasing the value of P increases the fraction of the PFR's volume reducing the significance of the dead volume and the CSTR. Hence, ideally we have reactions taking place in the PFR.
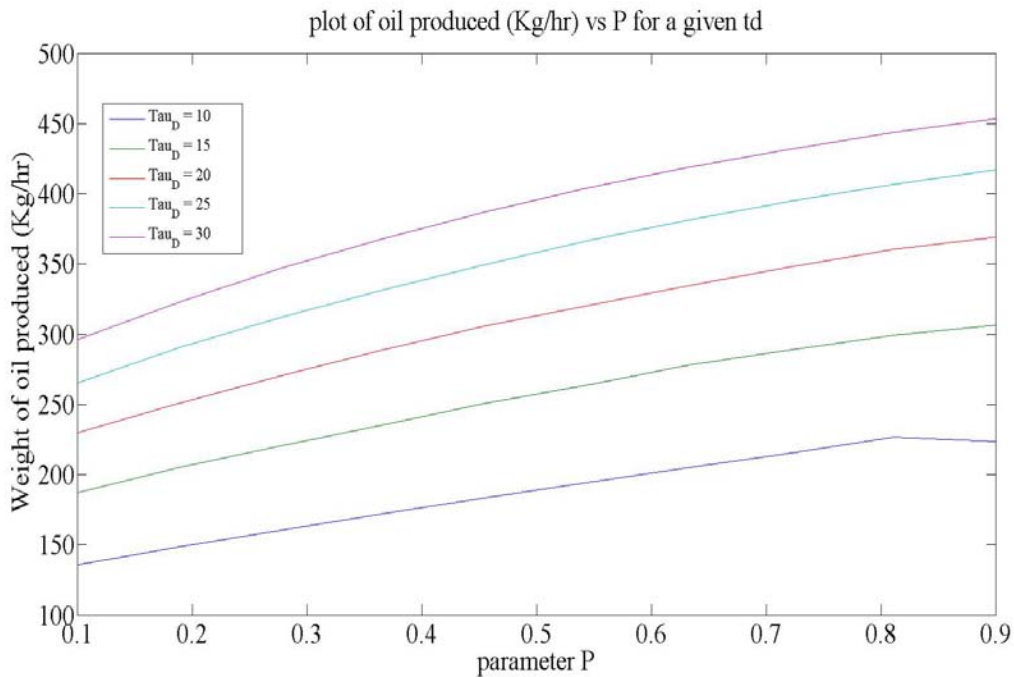
Figure 5.7: Oil produced (Kg/hr) vs. P for a given t_d for d = 0.508
(Kinetic parameters by Thurner et al.,1981)

5.4.2 Effect of zone temperature on production of oil

The zones of the auger reactor are maintained at different temperatures as mentioned earlier. Varying the temperature of these zones can change the rate of pyrolysis leading to different product composition. Hence, the sensitivity of zone temperatures on the product distributions for different RTD's is analyzed.

80

Table 5.4: Experimental conditions for Temperature variations in Zone 3

Feed rate of biomass(Kg/hr)	1000
Temperature zone 1(K)	523
Temperature zone 2(K)	623
Temperature zone 3(K)	703-743
Reactor run time(min)	15
t_d in each zone(sec)	30
dead volume fraction(d)	0.108
P	0.3
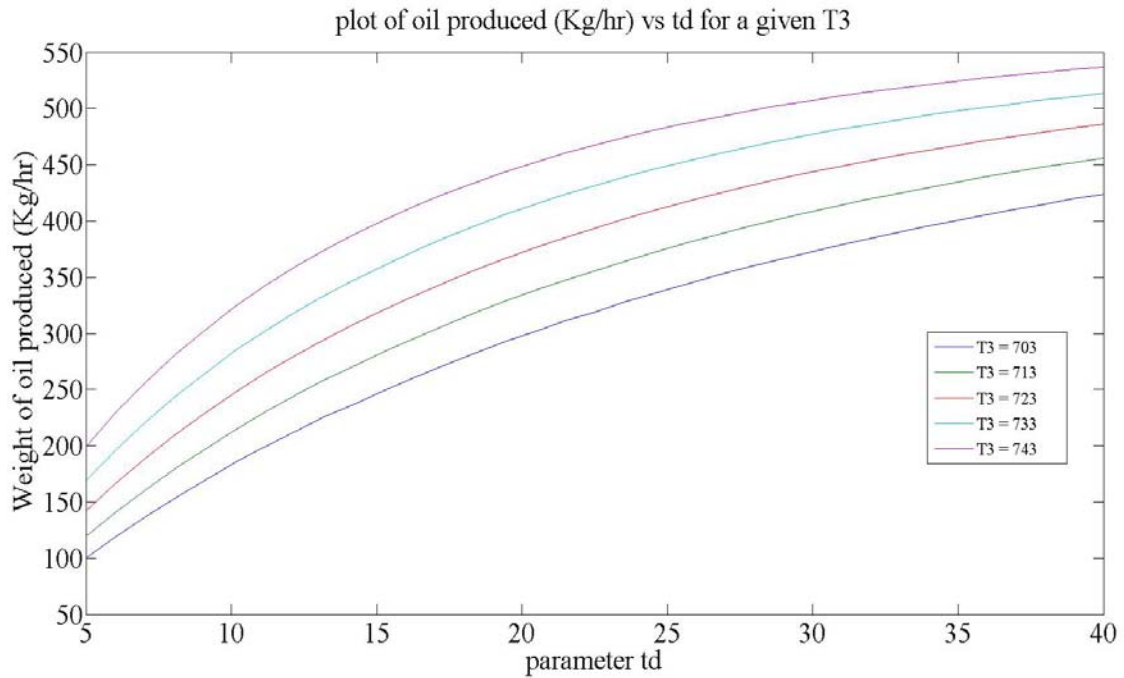
Figure 5.8: Oil produced (Kg/hr) vs t_d for a given value of zone 3 temperature (T3)

(Kinetic parameters by Thurner et al.,1981)

From the above figure, we can infer the following:

- The yield of oil increases with temperature for a given residence time. Also, the increase of oil yield as we move from one temperature to another temperature for a given residence time varies significantly.

- For any given temperature, increasing the residence time increases the yield of the oil.

- The percentage increase in the yield of oil as the value of t_d varies from 5 to 30 decreases with the value of increasing T3. For example, the percentage increase in oil is varying from 167% for a value of T3 equal to 743 K to approximately 330% for T3 equal to 703K. Hence, we can infer that the temperature of zone 3 can significantly affect the yield of the oil.

- The maximum oil yield of approximately 50% is achieved for a t_d value of 30 seconds and temperature of zone 3 at 743 K.

In Figure 5.8 the volume fraction of the PFR in the RTD is 0.3. Increasing the volume fraction of the PFR to a value of 0.8, keeping all other parameters the same surprisingly resulted in a graph (Figure 5.9) similar to Figure 5.8. The yield of oil is slightly more (5%) compared to Figure 5.8.
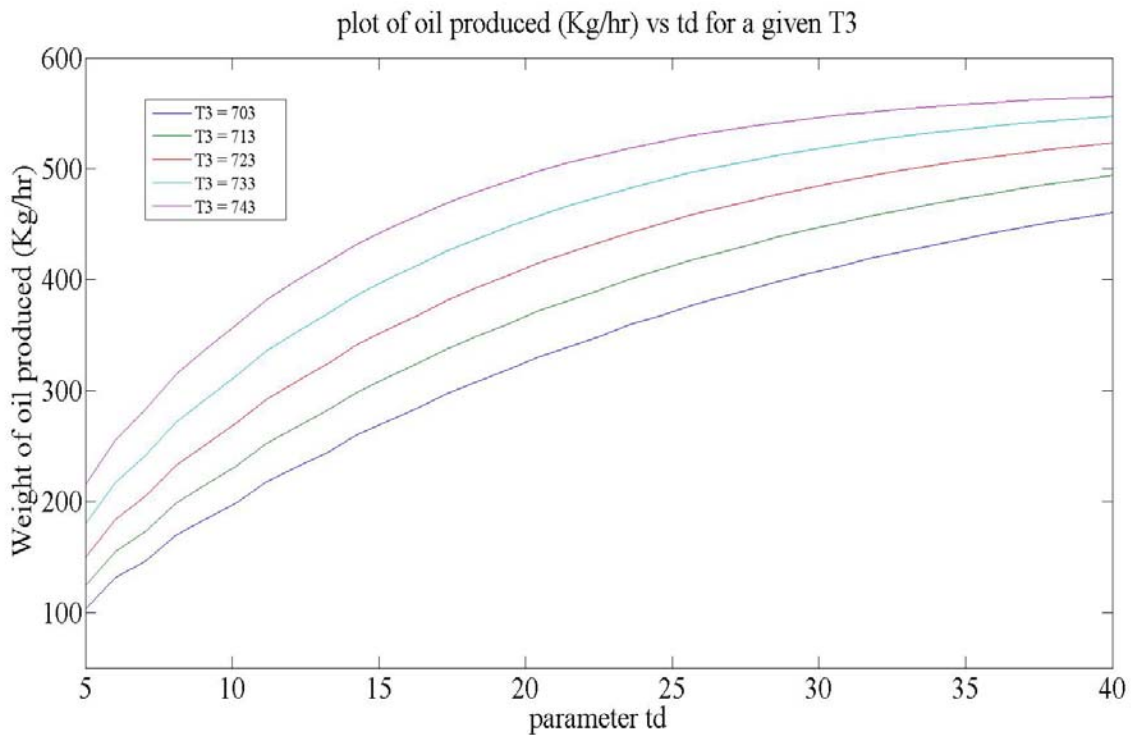
Figure 5.9: Oil yield vs t_d (sec) for a given T_3(P=0.8) (Kinetic parameters from Table 5.1)
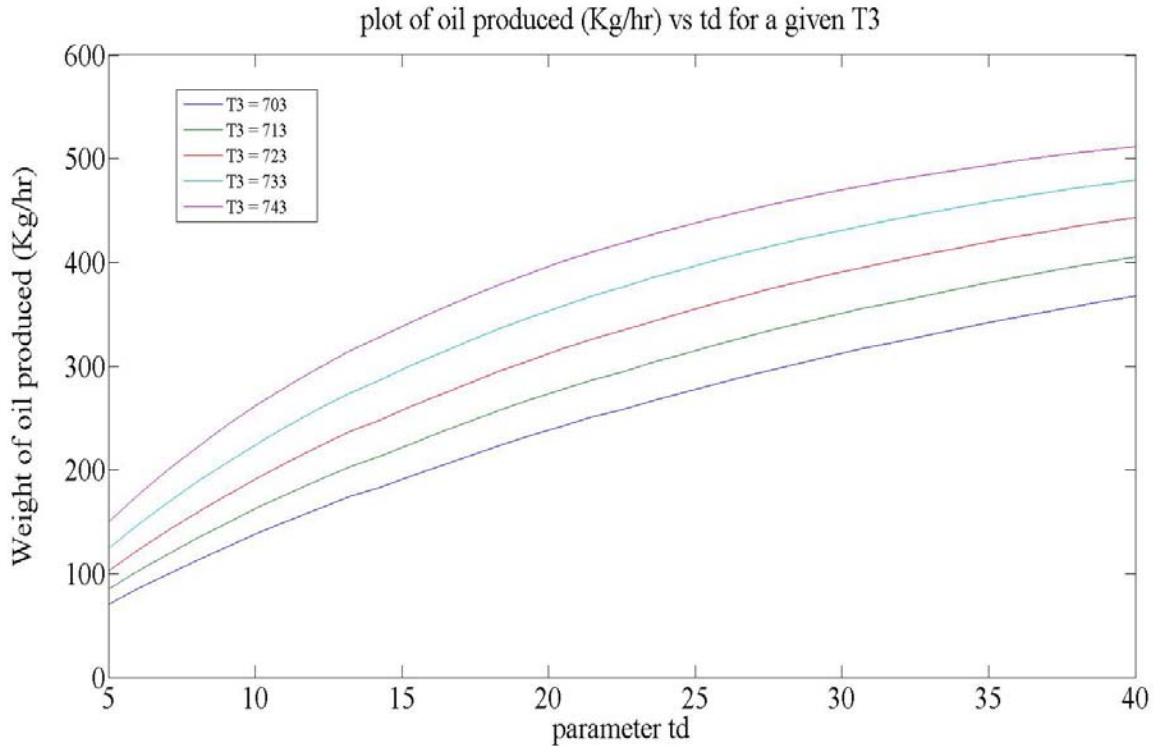
Figure 5.10: Oil produced (Kg/hr) vs. t_d (sec) for a given T3 (P=0.3, d=0.508)
(Kinetic parameters by Thurner et al.,1981)

Considering the dead volume fraction to be 0.508 and the volume fraction of the PFR (P) to be 0.3, a decrease in the yield of oil was observed. This is due to the reduction in total volume of the reactor available for reaction to occur (Figure 5.10). The trend of the curves is comparable to the previous graphs.

Kinetic parameters can significantly affect the trend and value of oil yield. Using the kinetic parameters from Table 5.3 and experimental conditions from Table 5.4, the sensitivity of oil yield with respect to temperature of zone 3 was analyzed (Figure 5.11).
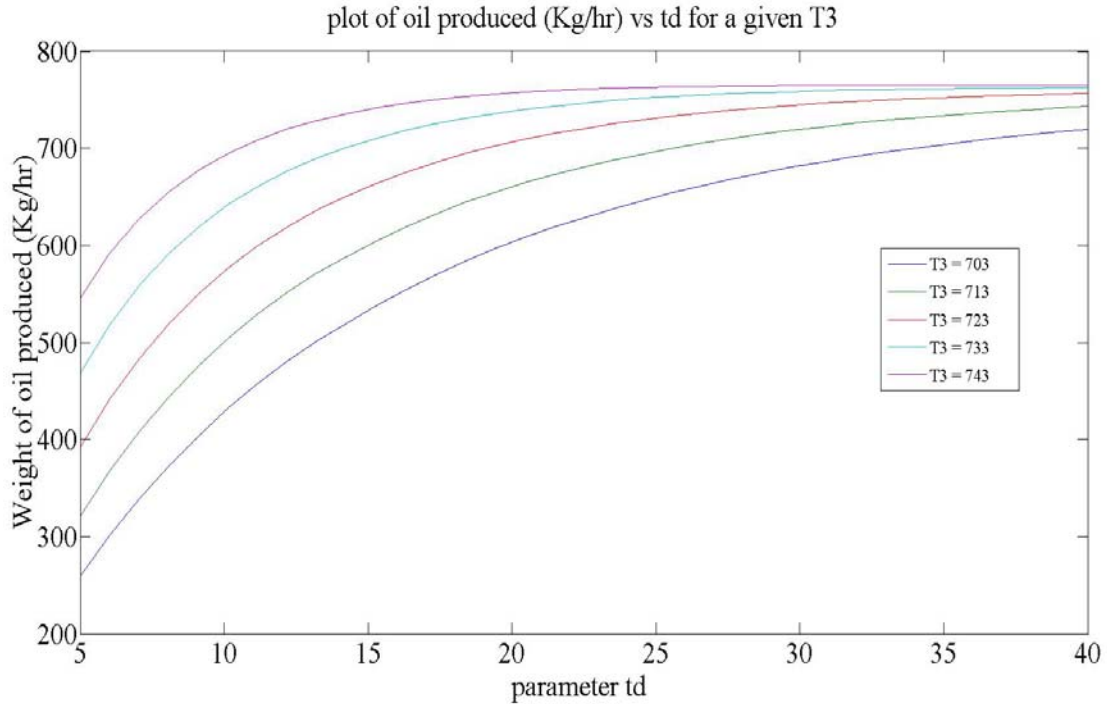
Figure 5.11: Yield of oil (Kg/hr) vs. td for a given T3. (Kinetic parameters from Table 5.3)

The trend of oil yield from Figure 5.11 is different compared to Figure 5.10 in the following ways:

- The oil yield increases until t_d equals 15 for all values of T3 and then tapers to a constant value

- The maximum yield of oil is around 70% unlike 50% from Figure 5.10.

- The percentage increase in oil yield for a given value of t_d between consecutive T3 curves is decreasing (along the direction of increasing T3).

- The percentage increase in the yield of oil as the value of t_d varies from 5 to 30 for a given T3 is less compared to Figure 5.10.

Hence, the kinetic parameters (depending on the experimental set up) can play a significant role in the determining the yield of oil.

The effect on oil yield of varying the temperature of zone 2, keeping temperatures of zones 1 and 3 constant, is presented below. Kinetic parameters by Thruner.et.al (1981) are considered in the calculation.

Table 5.5: Experimental conditions for Temperature variations in Zone 2

Feed rate of biomass(Kg/hr)	1000
Temperature zone 1(K)	523
Temperature zone 2(K)	603-643
Temperature zone 3(K)	723
Reactor run time(min)	15
td max in each zone(sec)	30
dead volume fraction(d)	0.108
P	0.3
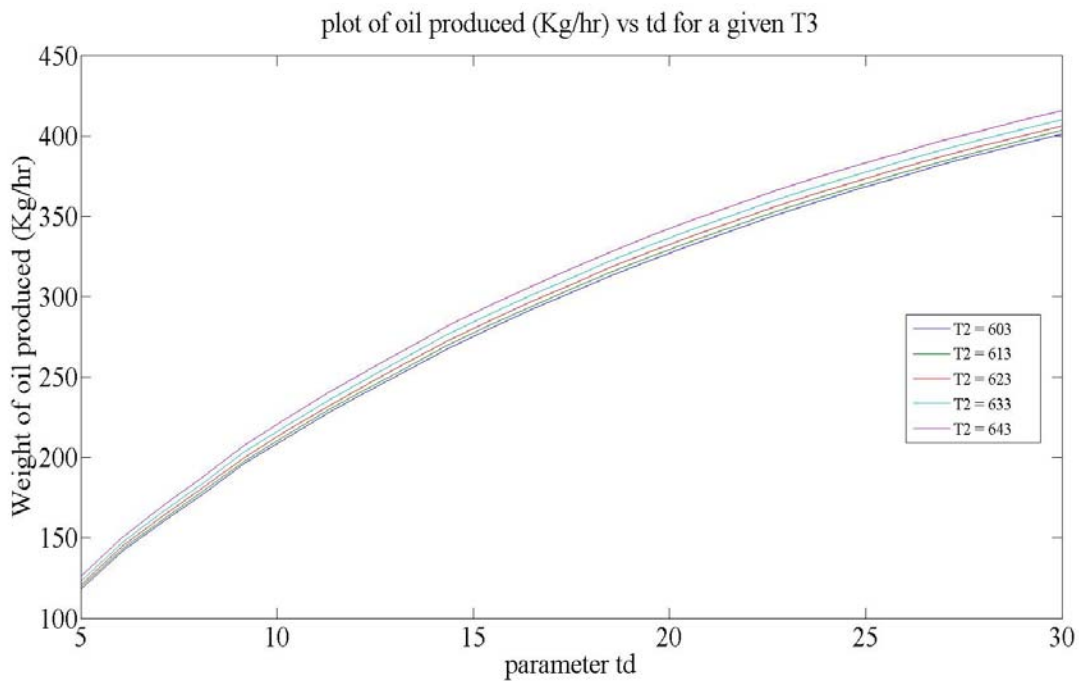
Figure 5.12: Yield of oil (Kg/hr) vs t_d (sec) for a given T2

From the above graph, we can infer that the oil yield at the end of zone 3 is not sensitive to the temperature variations in zone 2. Although, increasing t_d for a given value of T2 is increasing the yield of oil.

The effect on oil yield of varying the temperature of zone 1, keeping temperatures of zones 2 and 3 constant, is presented below. Kinetic parameters by Thruner.et.al (1981) are considered in the calculation.

Table 5.6: Experimental conditions for Temperature variations in Zone 1

Feed rate of biomass(Kg/hr)	1000
Temperature zone 1(K)	503-603
Temperature zone 2(K)	623
Temperature zone 3(K)	723
Reactor run time(min)	15
td max in each zone(sec)	30
dead volume fraction(d)	0.108
P	0.3
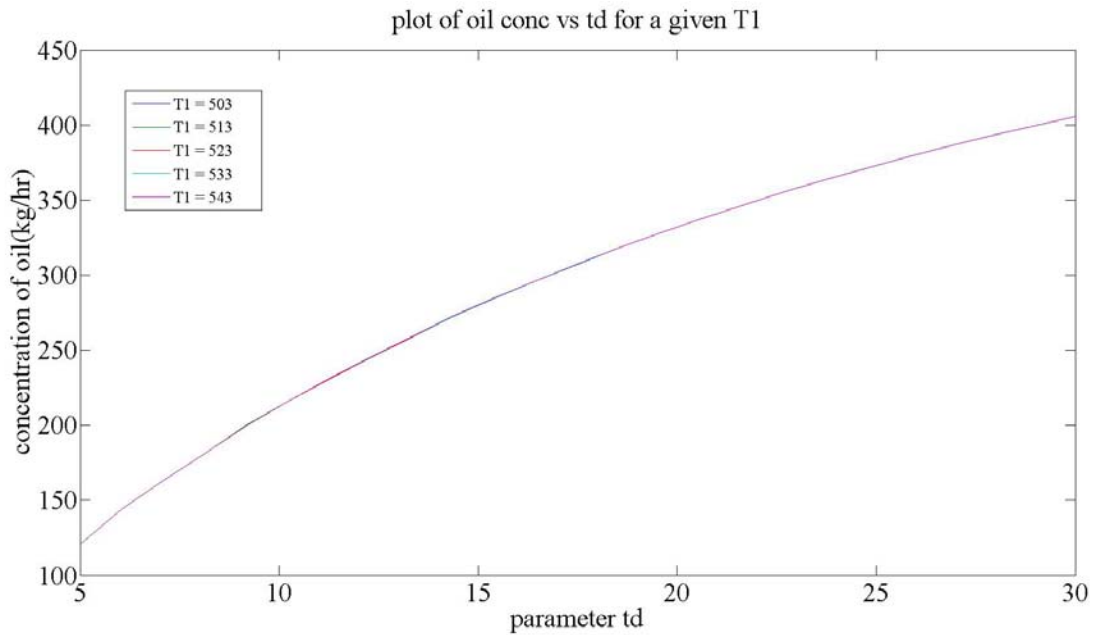
Figure 5.13: Yield of oil (Kg/hr) vs. t_d (sec) for a given T1

86

From the above graph, we can infer that the oil yield at the end of zone 3 is not sensitive to the temperature variations in zone 1. All the oil yield curves overlap into one single line without any distinction. Although, increasing t_d for a given value of T1 is increasing the yield of oil.

5.4.3 Kinetic parameter fit

In section 5.4.1, the yield of products at the end of zone 3 for a given temperature, kinetic rate constants and RTD parameters (P and t_d) was calculated. In this section, a reverse approach is followed. For given yields of products at the end of zone 3 and given zone temperatures; RTD parameters (P and t_d) are varied normally within a given variance and the frequency factors (A_i's) for the three products (gas, oil and char) are calculated. Note that the energies of activation (Ea_i's) of all the three components are assumed to be the same as the values from Thurner et al. (1981). In other words, performing an experiment in the auger reactor will result in data points consisting of reactant yields at a given temperature, RTD parameters within the range of experimental error. These are used as input values to calculate the kinetic parameters of wood pyrolysis. If a similar set of values of the kinetic parameters for a given operating conditions are obtained, as were first fed into the model, it can be inferred that the kinetic parameters are not very sensitive to the operating conditions. On the contrary, if significantly different frequency factors are found for operating conditions within experimental error, then these kinetic parameters are sensitive to the operating conditions. Any minor change or disturbance in operating conditions may result in prediction of completely different kinetic parameters. A flow chart of a Matlab program to implement the parameter estimation is given below (Figure. 5.14).
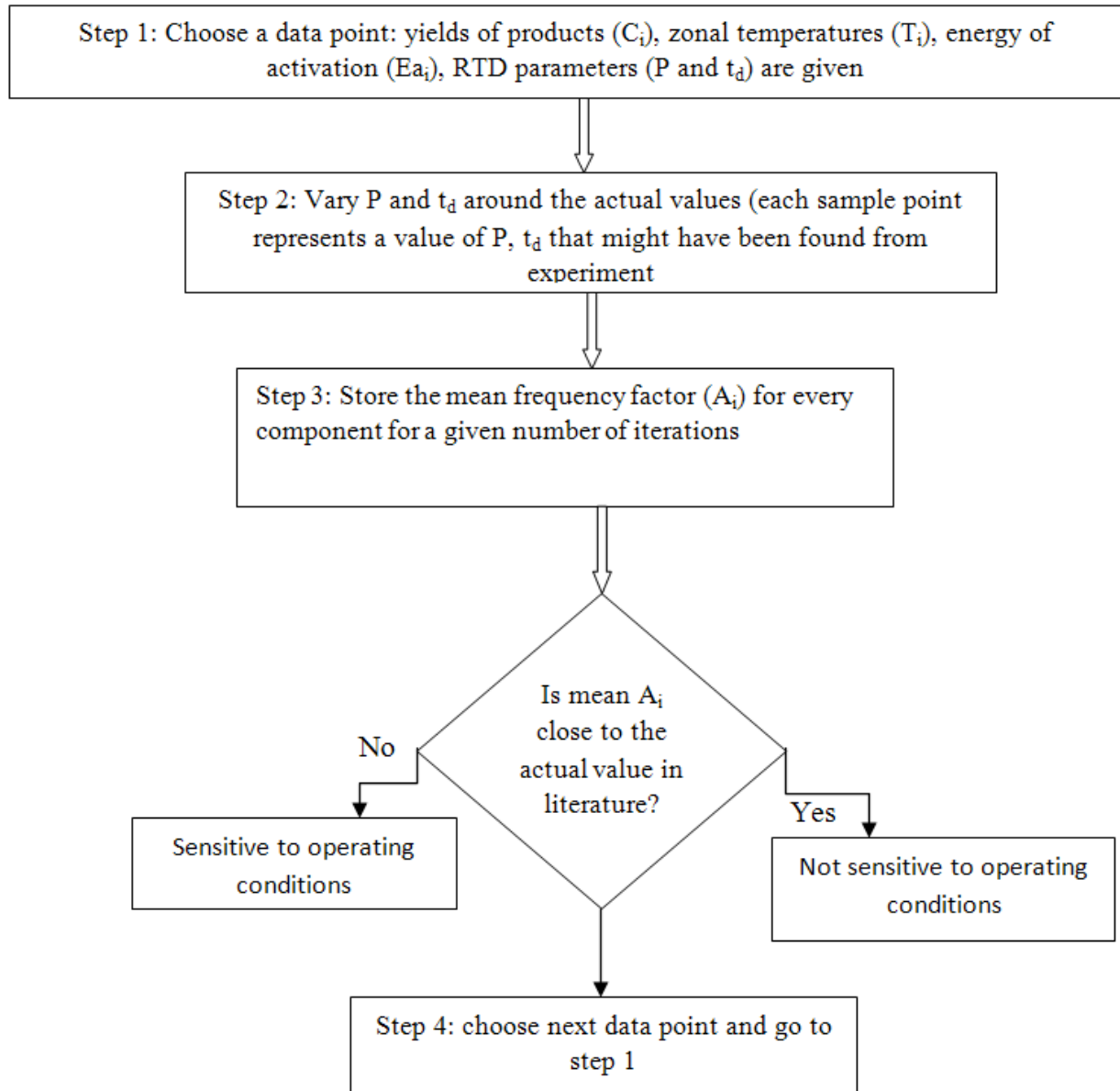
Figure 5.14: Flow chart for calculation of parameter fit (Ai's)

Experimental conditions used in this run are given in Table 5.7. Energies of activation (Ea$_i$'s) of the three products are assumed to be the same in the given temperature range (Table 5.1). Note that the unit of frequency factors is sec^{-1}.

Table 5.7: Operating conditions of kinetic parameter fit

Feed rate of biomass(Kg/hr)	1000
Temperature zone 1(K)	523
Temperature zone 2(K)	623
Temperature zone 3(K)	723
Reactor run time(min)	15
t_d(mean residence time)(sec)	5-30
Fraction of dead volume fraction (in CSTR) for each zone(d)	0.108
P	0.3-0.7
Number of Iterations at each data point	1000
Standard deviation in td and P (%)	10

Table 5.8 summarizes the mean and standard deviation of the pre-exponential factors (A_i's) obtained from the above run.

Table 5.8: Mean and standard deviation of pre-exponential factor

Pre-exponential factor (sec^{-1})	Mean	% Standard deviation	Actual value (A_i)
A1	1.44E+04	0.74	1.43E+04
A2	4.14E+06	0.60	4.13E+06
A3	7.40E+05	0.62	7.38E+05

Hence, for a given kinetic scheme of pyrolysis reaction, calculated values of kinetic parameters are not sensitive to the experimental conditions. Any small error in experimental conditions may not significantly change the calculated values of the kinetic parameters.

5.4.4 Sensitivity of product yields due to variations in kinetic parameters

Given that there is some variance in calculation of pre-exponential factors, the next step is to check whether these small variations in A_i cause large variations in output yield of oil. The values of the pre-exponential factors given in Table 5.8 are used as upper and lower bounds for

the pre-exponential factors. A flow chart of a Matlab program to implement the same is given

below (Figure. 5.15). Note that the experimental conditions used in this run are the same as

Table 5.7.
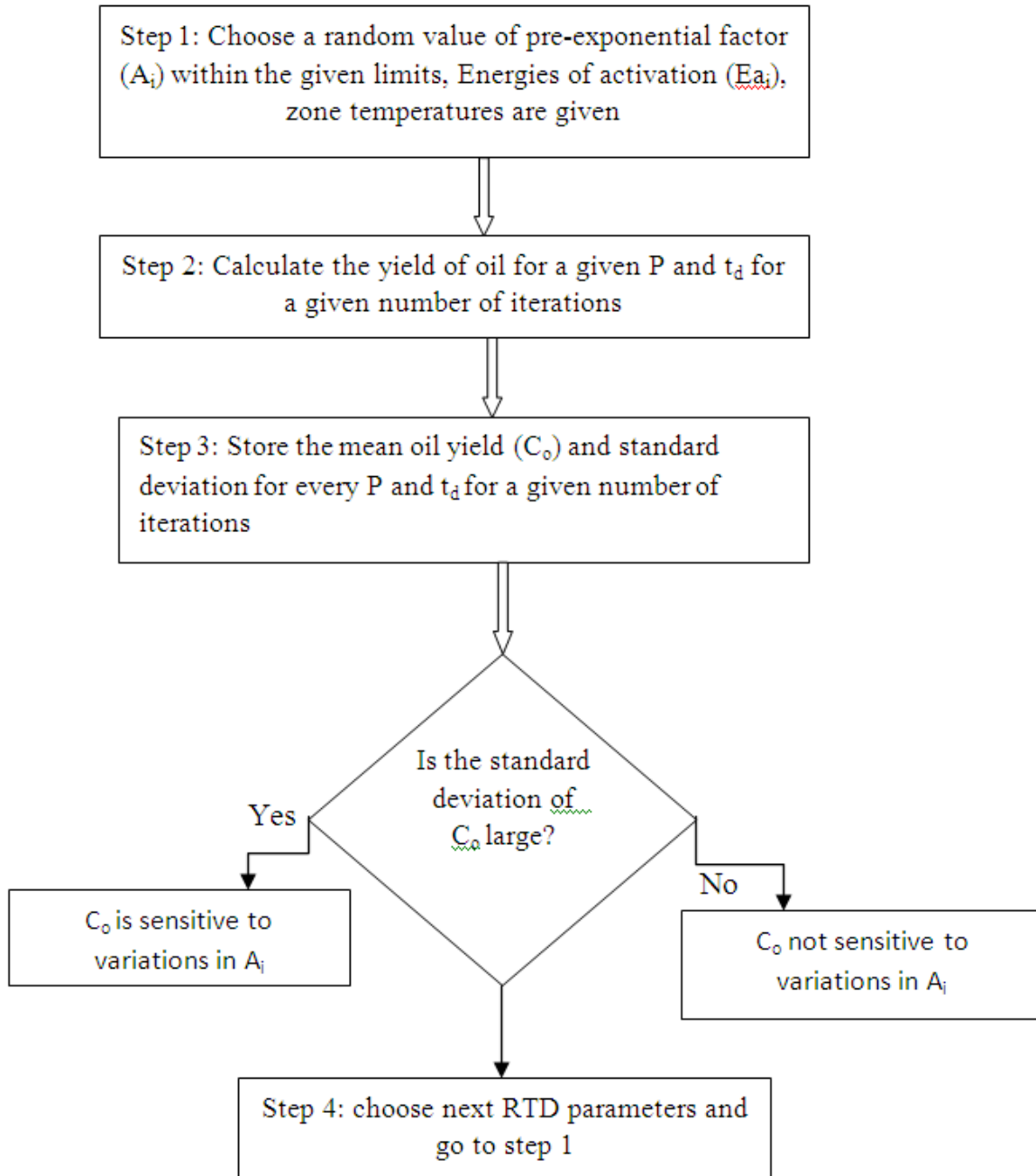
Figure 5.15: Flow chart for calculation of mean yield of oil
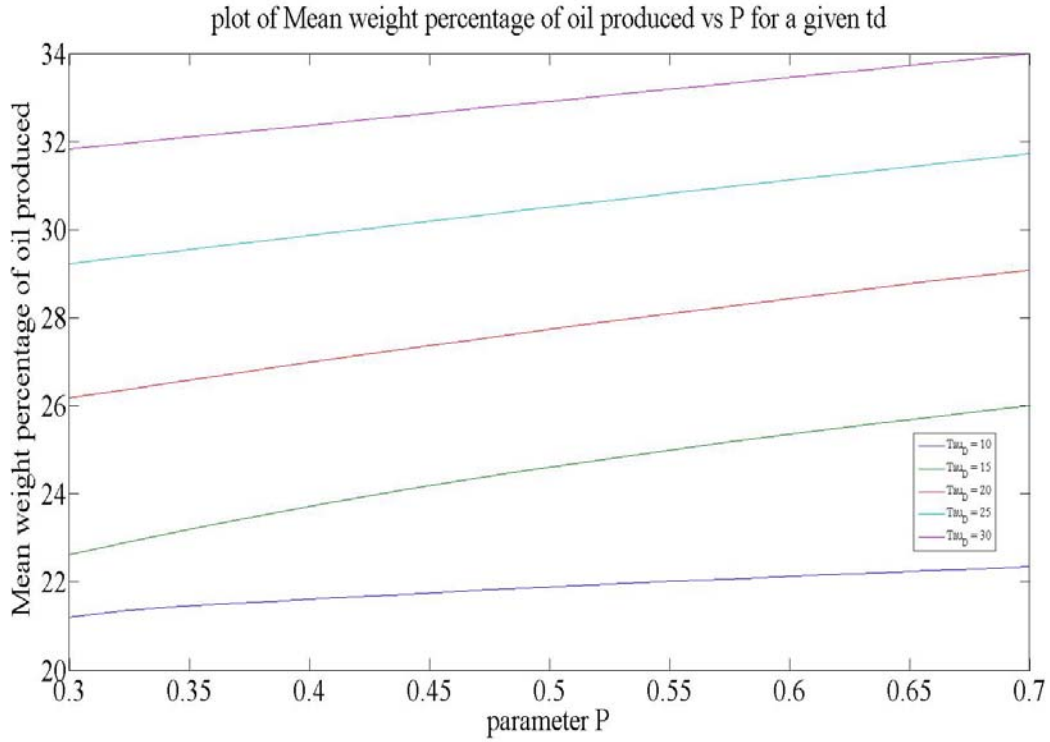
Figure 5.16: Mean weight percentage of oil produced vs. P for a given t_d (sec)
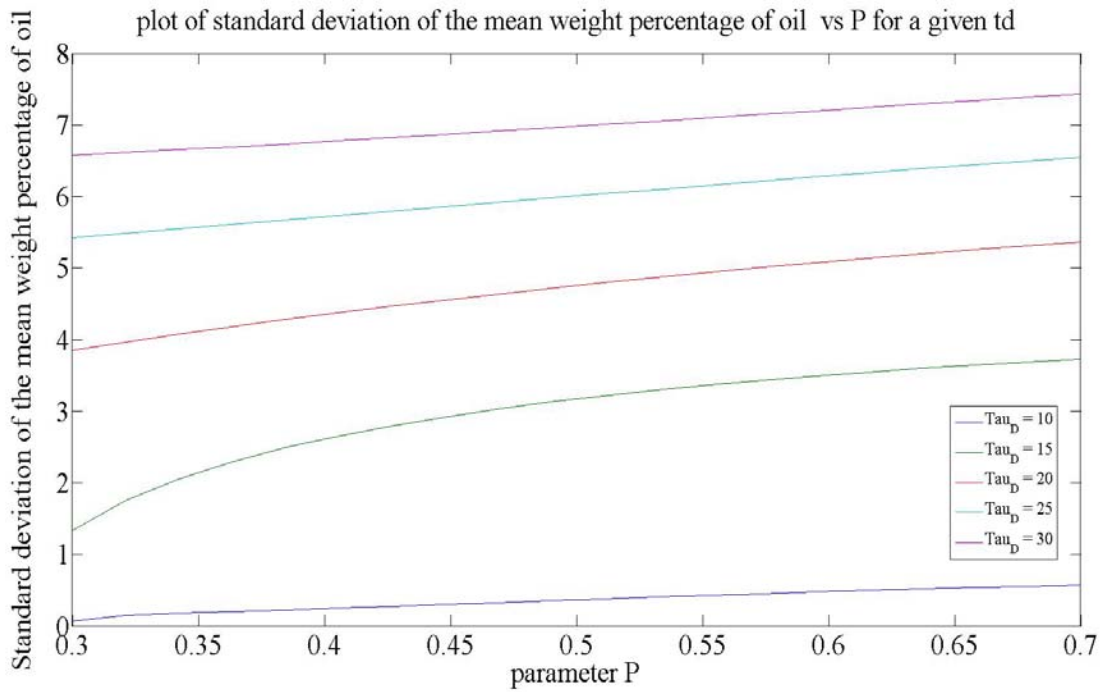
Figure 5.17: Standard deviation of the mean weight % of oil vs. P for a given t_d (sec)

91

The trend observed in Figure 5.16 is similar to Figure 5.5. The standard deviation at low values of t_d (10-20) is not very significant for the entire range of parameter P. One the contrary, at higher values of t_d (30) significant deviation in the yield of oil is observed for the entire range of parameter P (Figure 5.17). Note that the weight percentage of oil in Figures 5.16 and 5.17 are based on the percentage of biomass in the reaction.

Hence, it can be concluded that errors in the calculation of RTD parameters P and t_d do not significantly influence the calculated values of the pre-exponential factors (A_i). The error in calculating the pre-exponential factors due to errors in measurement of the RTD parameters does not significantly change the calculated value of output oil yield at low values of t_d. At higher values of t_d, the variations in pre-exponential factors are expected to vary the output oil yield significantly.

5.5 Calculation of Arrhenius constants from yield curve

The main aim of this section is to calculate the Arrhenius constants namely, frequency factors (A_i) and energies of activation (E_a) from the given data points. Yield of products at the end of the zone is obtained as a function of RTD parameters and different zone temperatures. Kinetic rate constants can be derived from this plot. A plot of kinetic rate constant with respect to inverse of zone temperature will give us Arrhenius constants; the slope of the line is proportional to E_a and the intercept is proportional to A (Eqn. 5.9-5.11). The flow chart representing the schematic for calculation of the Arrhenius constants is given in Figure 5.18. In this section, a single zone instead of 3 different zones is used to evaluate Arrhenius parameters. Experimental conditions used in this section are given in Table 5.9.

$\ln(k_i) = (-E_a/R)*(1/T) + \ln(A_i)$ (5.9)

$\text{Slope} = (-E_a/R)$ (5.10)

$\text{Intercept} = \ln(A_i)$ (5.11)

Table 5.9: Experimental conditions for calculations of Arrhenius parameters

Feed rate of Biomass (Kg/hr)	100
P	0.3
t_d(mean residence time) (sec)	5-30
d (fraction of dead volume)	0.108
T (Zone temperature) (K)	623-773
Variance in t_d (%)	10
Number of iterations	2
Number of different temperature points	4
Number of different t_d values	2

The total number of runs mentioned is Table 5.9 is close to the actual number of runs conducted in an experiment. Hence, any variation in calculations of RTD parameters which may result in different Arrhenius constants from actual experiments is taken into account. The results obtained from this model is given in Table 5.10
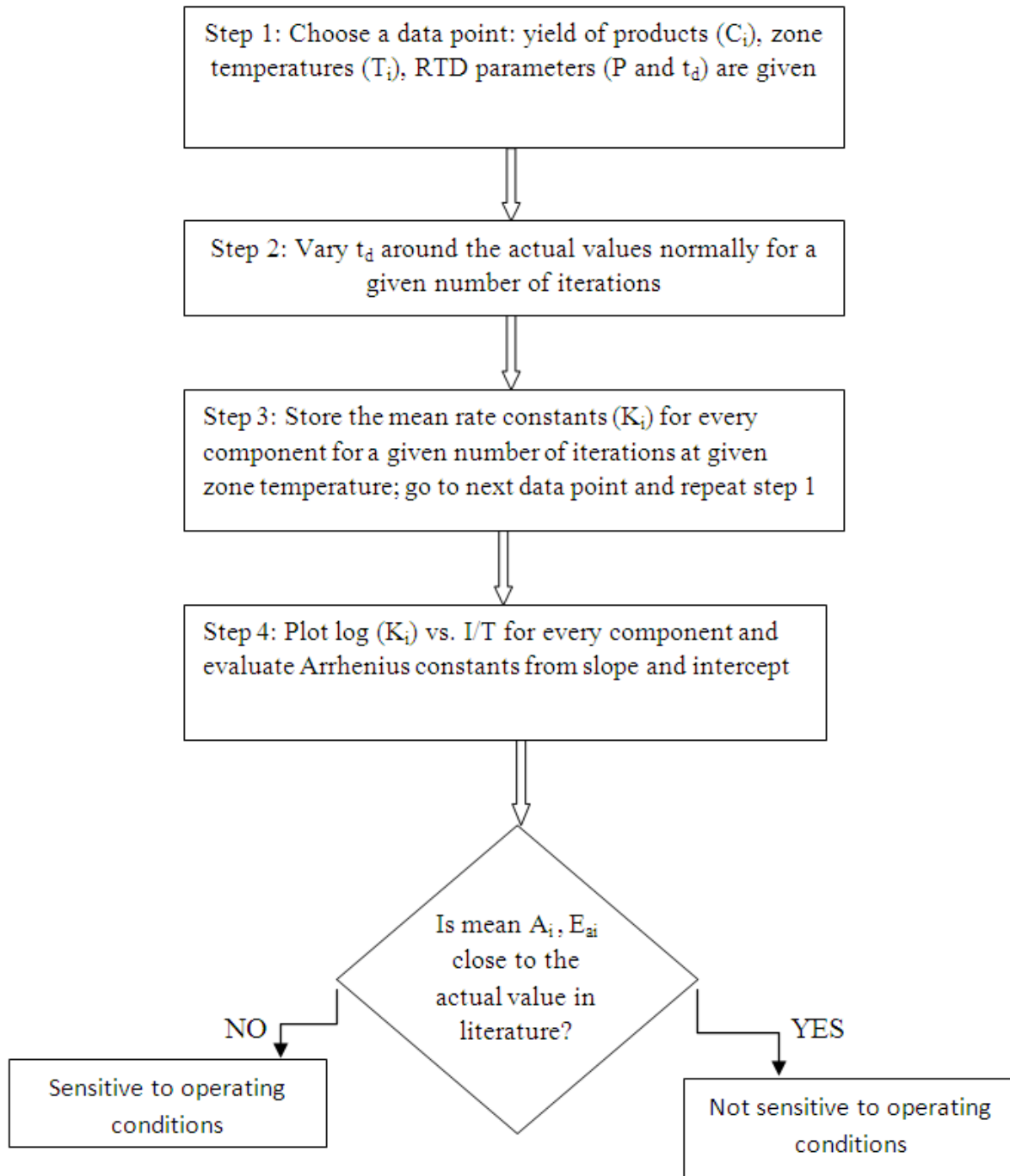
Figure 5.18: Flow sheet for calculation of Arrhenius parameters

Table 5.10: Values of Arrhenius parameters obtained from a graphical fit

Component	A (sec^{-1}) (actual value)	A (sec^{-1}) (graph value)	% error	E_a(J/mol) (actual value)	E_a(J/mol) (Graph value)	% Error
Gas	14300	8400	41.26	85650	88600	3.44
Oil	4125000	2430000	41.09	109750	112700	2.69
Char	737700	434000	41.17	103550	106500	2.85

From Table 5.10, we can infer that the percentage error in the values of the energies of activation obtained graphically is quite low compared to the percentage error in frequency factor. It is observed that the ratio of percentage error of frequency factors is almost the same. This implies that the amount of products formed do not change as the ratio of frequency factors obtained from graphical and actual values is the same (product formation is governed by 3 independent parallel reactions). Graphically, the straight line fit obtained from lnK vs. (1/T) plot has the same slope but is shifted by some distance. Secondly, it is observed the value of the sum of the kinetic rate constants for a different set of runs is almost the same (In other words, the amount of biomass reacted is the same). Hence, it can be concluded that experimental error in calculation of RTD parameters can induce error in calculation of Arrhenius constant but these values are able to predict the yield of products accurately. In other words, if the sum of the kinetic rate constants and ratio of kinetic rate constants remain the same with respect to actual value in the literature, different values of Arrhenius constants still yield the same result and are suitable for use.

5.6 Summary and conclusions of reactor model

- The quantity of oil produced in general increases with parameter P for any given value of t_d

- The quantity of oil produced increases with t_d for a given value of P

- The kinetic parameters (depending on experimental set up) play a crucial role in determining the yield of oil

- Variations in temperature of zone 3 play a crucial role in varying the output yield of oil whereas variations in temperatures of zones 2 and 1 do not significantly impact output oil yield

- For a given kinetic scheme for the pyrolysis reactions, calculated values of the kinetic parameters are not sensitive to experimental conditions

- Errors in calculation of the pre-exponential factors caused by errors in measurement of RTD parameters does not significantly change the calculated value of output oil yield at low values of t_d

- Experimental error in calculation of the RTD parameters can induce error in calculation of the Arrhenius constants but these values can still predict the yield of products accurately

5.7 List of symbols and abbreviations

Symbol	Abbreviation	Units	Typical value
P	Fraction of volume in plug flow reactor	-	0.3-0.7
d	Fraction of volume in dead zone	-	0.108
F_r	Feed rate of the reactant	Kg/hr	1000
S_s	Screw speed	rpm	90
K	Kinetic rate constant	sec^{-1}	Refer to table 5.1
A	Frequency factor	sec^{-1}	Refer to table 5.1
Ea	Energy of activation	J/mol	Refer to Table 5.1
t_d	mean residence time	sec	5-30
t	time	sec	900 (unless specified)
T	Temperature	K	523-773
R	Gas constant	J/mol/K	8.314
w_i	weight fraction of component i	-	-

CHAPTER 6

ENERGY BALANCE

6.1 Energy flow chart

This chapter develops an energy balance and quantifies the energy flux on a macroscopic scale in an auger based pyrolysis reactor. A flow chart describing the flow of energy in a pyrolysis reactor is presented in Figure 6.1.
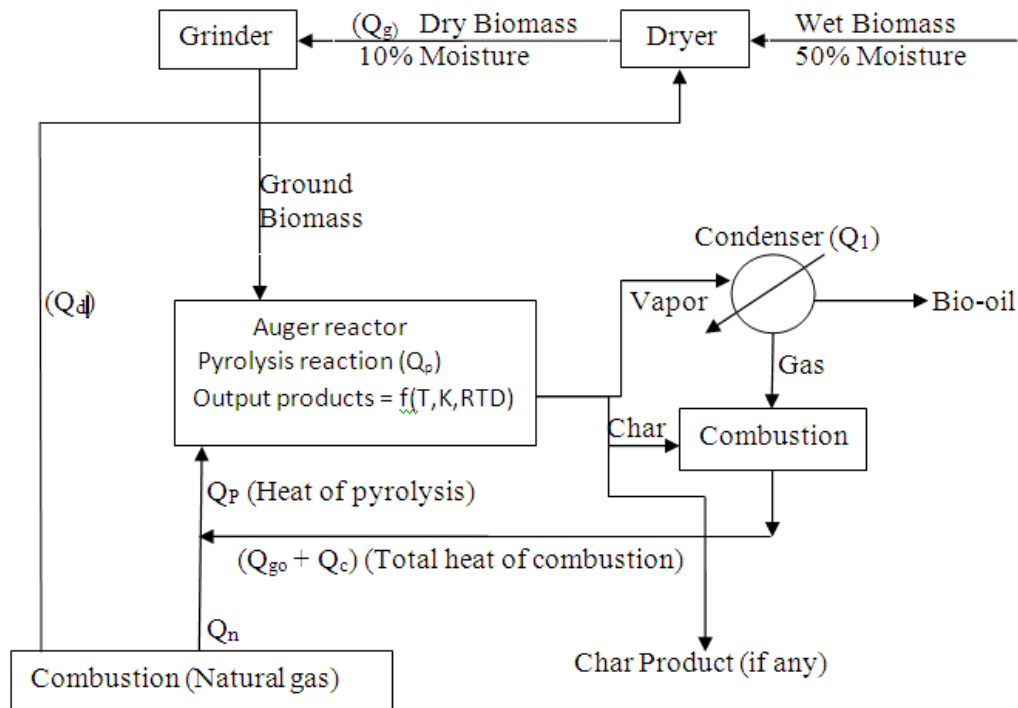
Figure 6.1: Energy balance around auger reactor

Wet woody biomass is fed to the dryer as chips to reduce the moisture content from 50% to 10%. Moisture percentage plays a significant role in determining the quality of bio-oil. Hence, it is important to reduce the moisture percentage to 10% before feeding the auger reactor. Q_d is the amount of heat required to dry the biomass to 10% moisture. Dried woody biomass is now

ground in a ball mill to reduce the particle size of the wood. Q_g is the amount of energy required to grind the dried woody biomass to the required particle size. Ground and dried woody biomass is now fed into an auger reactor. As described in Chapter 5, output yield of products is a function zone temperatures (T), reaction kinetics (K) and residence time distribution (RTD) of reactant. The heat of pyrolysis (Q_P) is an endothermic reaction and energy from an external source is required for the reaction to proceed. Energy from external sources like combustion of natural gas (Q_n) can be used to augment the energy required for the pyrolysis reaction. Vapor from pyrolysis of biomass is a mixture of condensable and non-condensable gases. Vapor is passed through a condenser where the vapor phase is cooled from the reactor exit temperature to room temperature. Water (25^oC) is used as a medium of cooling in condenser. Gas (non-condensable vapor) obtained from pyrolysis is subjected to combustion and the energy (Q_g) obtained can be used to provide the heat required for pyrolysis reaction. Char obtained from pyrolysis of woody biomass can be partially subjected to combustion to provide energy for the pyrolysis reaction. The remaining char can be used as a fertilizer as it is rich in nutrients. Energy from external sources like combustion of natural gas can be used for drying the woody biomass. All the calculations are based on feed rate of 83.3 tons/hr (2000 tons/day) of woody biomass. The energy required for each process is calculated in section 6.2. Note that the energy requirements for different unit operations calculated in the next section is based on pine being treated as the source of woody biomass, these values can change for a different woody biomass. Hence, pine and woody biomass are interchangeably used in the next section.

6.2 Energy calculations

6.2.1 Dryer

Biomass has to be heated from 25°C to 75°C to reduce the moisture content in the biomass from 50% of the initial wood chips to less than 10% of the final ground biomass. As explained earlier, excess moisture in biomass can trigger secondary reactions and lead to unwanted products, affecting the quality of bio-oil obtained. Specific heat capacity of biomass at 298 K is 1.2 KJ/kg/K (Van de Velden et al, 2010). It is assumed that the heat capacity in the given temperature range does not change significantly. Properties of water are taken from literature (Perry and Green Handbook, 1997).

The heat required (Q_d) to dry 83.3 tons/hr of biomass is given by the equation below:

$$Q_d = m_1*C_p*\Delta T + m_2*C_{pw}*\Delta T + L*m_3 \tag{6.1}$$

ΔT = 50 K (Difference between initial and final wood temperature)

m_1 = 83.3*(0.5) tons/hr (feed rate of biomass)

m_2 = 83.3*(0.5) = 41.65 tons/hr (amount of water in the biomass)

m_3 = 83.3*(0.5) – 4.64 = 37.01 tons/hr (mass of water evaporated at 75°C)

C_{pw} = 4.1806 KJ/Kg/C (average specific heat of water)

L = 2322.8 KJ/Kg (heat of vaporization of water at 75°C)

C_p = 1.2 KJ/Kg/K (Heat capacity of biomass)

Thus, energy required to dry biomass (83.3 tons/hr to 10% moisture) (Q_d) = **97,200 MJ/hr**

Note that dryers have a poor heat transfer efficiency of 20% and this will be considered in the dryer utility calculations in Chapter 7. Also, 4.64 tons/hr is m_3 calculation refers to final amount of water in the wood biomass that accounts to 10% of the total weight.

6.2.2 Grinder

Dried biomass is now subjected to grinding to reduce the particle size of the biomass. Smaller particle size of ground pine enhances the heat transfer and enables fast pyrolysis in the auger reactor. From Table 3.1 in Chapter 3 we can infer that more than 90% of the particles are less than 425μm diameter. The Biot number (Bi) is the ratio of internal resistance to heat penetration to external resistance to heat transfer. Mathematically, Bi is expressed as follows:

$$Bi = (rh/K_p) \qquad\qquad (6.2)$$

r = radius of the spherical particle

K_p= thermal conductivity of wood

h = external heat transfer coefficient in an auger reactor

The heat transfer coefficient depends on the gas-solid contacting mode. It ranges from

10 W/m^2/K for a static bed, to 50-100 W/m^2/K in a fixed bed with forced circulation (TGA) and several hundreds of W/m^2/K for bubbling and circulating fluidized beds(Van de Velden et al, 2010). The value of the heat transfer coefficient in an auger reactor is expected to be between the TGA and circulating fluidized bed values due to its heat transfer characteristics. Heat transfer in an auger reactor is not as good as in a circulating fluidized bed but is certainly better than a TGA. Hence, the heat transfer coefficient in an auger based reactor is between 300-500W/m^2/K. The thermal conductivity (K_p) of pine is 0.12 W/m/K. For a pine particle of diameter 450μm at 773K, the values of the Biot number are as follows:

h = 300 W/m^2/K   Bi = 225*10^{-6}*300/0.12 = 0.57

h = 400 W/m^2/K   Bi = 225*10^{-6}*400/0.12 = 0.75

h = 500 W/m^2/K   Bi = 225*10^{-6}*500/0.12 = 0.94

The Biot number is less than 1 in all the cases, implying that the external resistance associated with convection heat transfer largely dominates. Hence, there will not be any major temperature gradients between the surface and core of the pine particle. Hence, the entire particle reacts the same way producing the same pyrolysis products at a given zone temperature.

Abdullah et.al (2009) performed grinding of dried biomass in a ball mill. According to them, it is estimated that the biomass grinding requires an electricity consumption of 37.5kWh/t and more than 75% (volume percentage) of the particles have diameters less than 450μm at the end of 15 minutes. Hence energy required to grind (Q_g) dried pine to a particle size less than 450μm is given below:

Q_g= 37.5*(3.6)*[(83.3)*(0.50) + 4.63] = **6250 MJ/hr**

Note that 3.6 is the conversion factor of KWh to MegaJoules

6.2.3 Condenser

Pyrolysis of pine will yield vapor and char as products. The vapor produced is then passed through a condenser to cool the vapor to collect bio-oil and separate the bio-oil from non-condensable gases. The energy required to cool the vapor phase from reactor exit temperature to room temperature is given below:

$$Q_c = (m_1 * C_{po} * \Delta T) + (m_2 * H_{vb}) \tag{6.3}$$

where

m_1 = mass of vapor (gr)

m_2 = mass of bio-oil (gr)

C_{po}= specific heat capacity of vapor (J/gr/K)

ΔT = Difference between exit reactor and room temperature (K)

H_{vb} = latent heat of vaporization of bio-oil (J/gr)

Diebold et.al (1999) stated that the composition of bio-oils results from a complex interrelationship of many factors. They are presented as follows:

- The biomass species used as feedstock (organic and inorganic compositions, including dirt and moisture).

- Organic nitrogen or protein content of the feedstock.

- The heat transfer rate and final char temperature during pyrolysis.

- The extent of vapor dilution in the reactor.

- The time and temperature history of the vapors in the reactor.

- The time and temperature history of the vapors in the heated transfer lines from the pyrolysis reactor through the char removal equipment to the quench zone.

- Whether the vapors pass through accumulated char (i.e., in hot-gas char filtration between back flushing operations).

- The efficiency of the char recovery system to separate the char from the bio-oil vapors before condensation.

- The efficiency of the condensation equipment to recover the volatile components from the noncondensable gas stream, e.g., water and low molecular weight esters, ethers, acetals, alcohols, and aldehydes.

- Whether the condensates have been filtered to remove suspended char fines.

- The water content of the bio-oil.

- The extent of contamination of the bio-oil during storage by corrosion or leaching of the containers.

- Exposure to air during storage.

- The length of storage time.

- The storage temperature.

Bio-oil is therefore a complex mixture of hundreds of chemical components (refer to appendix B) and can vary based on the above mentioned factors. It would therefore be extremely difficult to calculate the specific heat capacity and latent heat of bio-oil. Diebold et. al(1999) tabulated the composition of 89 organic components of bio-oil along with their upper and lower weight percentages. They are presented in Table 6.1. This table along with a group contribution method can be used to calculate the specific heat capacity and latent heat of bio-oil.

Table 6.1: Lower and upper bounds of organic components in bio-oil (Diebold, 1999)

Component	Relaxed Lb (wt%)	Relaxed Ub (wt%)	Component	Relaxed Lb (wt%)	Relaxed Ub (wt%)
Formic	0.38	12.13	Angelicalactone	0.13	1.60
Acetic	0.63	16.00	Levoglucosan	0.50	1.87
Propanoic	0.13	2.40	Glucose	0.50	1.73
Hydroxyacetic	0.13	1.20	Fructose	0.88	3.87
Butanoic	0.13	0.67	D-Xylose	0.13	1.87
Pentanoic	0.13	1.07	D-Arobinose	0.13	0.13
4-oxypentanioc	0.13	0.53	Cellobiosan	0.75	4.27
Hexanoic	0.13	0.40	1,6 Anhrdroglucofuranose	3.88	4.13
Benzoic	0.25	0.40	2-Methoxy Phenol	0.13	1.47
Heptanoic	0.38	0.40	4-Methyl Guaiacol	0.13	2.53
Methanol	0.50	3.20	Ethyl Guaiacol	0.13	0.80
Ethanol	0.75	1.87	Eugenol	0.13	3.07
Ethylene Glycol	0.88	2.67	Isoeugenol	0.13	9.60
Acetone	3.50	3.73	4-Propylguaiacol	0.13	0.53
2-Butanone	0.38	1.20	Acetoguiacone	1.00	1.07
2,3-Pentenedione	0.25	0.53	Prpioguiacone	1.00	1.07
3Me2cyclopenten2ollone	0.13	2.53	2,6-DiOMe Phenol	0.88	6.40
2-Et-cyclopentanone	0.25	0.40	Methyl Syringol	0.13	0.40
Dimethylcyclopentanone	0.38	0.40	4-Ethyl Syringol	0.25	0.27
Trimethylcyclopentenone	0.13	0.67	Propyl Syringol	0.13	2.00
Trimethylcyclopentanone	0.25	0.53	Syringaldehyde	0.13	2.00
Formaldehyde	0.13	4.40	4-Propenyl Syringol	0.13	0.40
Acetaldehyde	0.13	11.33	4-OH-3,5-DiOMe Phenol Ethanone	0.13	0.40
2-Propenal	0.75	1.20	Furan	0.13	0.40
2-Methyl-2-butenal	0.13	0.67	2-Methyl Furan	0.13	0.27
Pentanal	0.63	0.67	2-Furanone	0.13	1.47

Table 6.1(continued): Lower and upper bounds of organic components in bio-oil (Diebold, 1999)

Component	Relaxed Lb (wt%)	Relaxed Ub (wt%)	Component	Relaxed Lb (wt%)	Relaxed Ub (wt%)
Ethanedial	1.13	6.13	Furfural	0.13	1.47
Phenol	0.13	5.07	3-Methyl-2(3h) Furanone	0.13	0.13
2-Methyl Phenol	0.13	0.80	Furfural alcohol	0.13	6.93
3-Methyl Phenol	0.13	0.53	Furoic Acid	0.50	0.53
4-Methyl Phenol	0.13	0.67	5-Methyfurfural	0.13	0.80
2,3 Dimethyl Phenol	0.13	0.67	5-OH-Methyl-2-Furfural	0.38	2.93
2,4 Dimethyl Phenol	0.13	0.40	Hydroxyacetaldehyde	1.13	17.33
2,5 Dimethyl Phenol	0.25	0.53	Acetol	0.88	9.87
2,6 Dimethyl Phenol	0.13	0.53	Acetal	0.13	0.27
2-Ethylphenol	0.13	1.73	Acetyloxy-2-propanone	0.13	1.07
2,4,6 TriMe Phenol	0.38	0.40	2-OH-3-Me-2-cyclopentene-1-one	0.13	0.67
1,2 DiOH Benzene	0.13	0.93	Methyl Cyclopenolone	0.13	2.53
1,3 DiOH Benzene	0.13	0.40	1-Acetyloxy-2-Propanone	0.13	1.07
1,4 DiOH Benzene	0.13	2.53	2-Methy-3-hydroxy-2-pyrone	0.25	0.53
4-Methoxy Catechol	0.75	0.80	2-Methoxy-4-metylanisole	0.13	0.53
1,2,3 Trio-OH-Benzene	0.75	0.80	4-OH-3 methoxybenzaldehyde	0.13	1.47
Methyl Formate	0.13	1.20	Dimethylcyclopentene	0.88	0.93
Butyrolactone	0.13	1.20	Lignin	31.25	40.00
Valerolactone	0.25	0.27			

6.2.3.1 Specific Heat capacity of bio- oil

The bio-oil and gases from the auger reactor need to be cooled to the room temperature by the condenser to separate oil from gas. For this to be calculated, the specific heat capacities for all the 89 components in the bio-oil organics, together with those for the five components in the gases, need to be known. However, many of the components do not have the specific heat capacity data available in the literature for them. In the case that there is no literature data available, the estimation method in Perry's Chemical Engineer's Handbook (Perry and Green, 1997) was used to calculate the heat capacity, which is an estimation method based on the contribution from different types of atoms as stated by the equation below.

$$Cp0 = a1 + a2C + a3H + a4O + a5N + a6S + a7F + a8Cl + a9I + a10Br + a11Si + a12Al +$$

$$a13B + a14P + a15E \tag{6.4}$$

where, *Cp0* = ideal gas heat capacity, J/mol K

a1 – a15 = parameters

C, H, O, N = number of carbon, hydrogen, oxygen, and nitrogen atoms in the molecule

S, F, Cl, I, Br = number of sulfur, fluorine, chlorine, iodine, bromine atoms in the molecule, respectively

Si, Al, B, P = number of silicon, aluminum, boron, phosphorus atoms in the molecule, respectively

E = number of atoms in the molecule excluding the 13 atom types listed above

So based on this method and also some literature data, the specific heat capacities of the 93 components in the bio-oil and gases were calculated by Ling Zhang (2004) and listed in Table 6.2.

From Table 6.1, it is understood that the composition of organic components in bio-oil is bounded between the upper and lower bound. Hence, a matlab code was written to randomly assign weight percentages to bio-oil components within the bounds and then, mean specific heat capacity and the standard deviation is calculated for a given number of iterations. If the standard deviation of specific heat capacity is too high, the mean heat capacity of bio-oil is significantly affected by the bio- oil composition of individual components. Hence, there is a need for better characterization of bio-oil for every experimental procedure. On the other side, a smaller standard deviation relaxes the above mentioned constraint. A flow chart describing the matlab code is given in Figure 6.2.

Table 6.2: Specific heat of components in bio-oil/gases (Ling Zhang, 2004)

Component	Cp (J/mol/°C)	Component	Cp (J/mol/°C)
Formic [*]	83.8	Glucose	425.9
Acetic [*]	134.4	Fructose	425.9
Propanoic	188.3	D-Xylose	353.5
Hydroxyacetic	156.7	D-Arobinose	353.5
Butanoic	240.3	Cellobiosan	758.7
Pentanoic	292.3	1,6 Anhrdroglucofuranose	375.1
4-oxypentanioc	282.3	2-Methoxy Phenol	305.1
Hexanoic	344.3	4-Methyl Guaiacol	357.1
Benzoic	274.7	Ethyl Guaiacol	409.1
Heptanoic	396.3	Eugenol	430.7
Methanol [*]	89.8	Isoeugenol	430.7
Ethanol	146.3	4-Propylguaiacol	461.1
Ethylene Glycol	166.7	Acetoguiacone	399.1
Acetone [*]	164.4	Prpioguiacone	451.1
2-Butanone	219.9	2,6-DiOMe Phenol	377.5
2,3-Pentenedione	261.9	Methyl Syringol	429.5
3Mc2cyclopcntcn2ollonc	283.5	4-Ethyl Syringol	481.5
2-Et-cyclopentanone	345.5	Propyl Syringol	533.5
Dimethylcyclopentanone	345.5	Syringaldehyde	419.5
Trimethylcyclopentenone	367.1	4-Propenyl Syringol	503.1
Trimethylcyclopentanone	397.5	4-OH-3,5-DiOMe Phenol Ethanone	471.5
Formaldehyde [*]	62.2	Furan	159.1
Acetaldehyde [*]	125.8	2-Methyl Furan	211.1
2-Propenal	137.5	2-Furanone	179.5
2-Methyl-2-butenal	241.5	Furfural	201.1
Pentanal	271.9	3-Methyl-2(3h) Furanone	231.5
Ethanedial	105.9	Furfural alcohol	231.5
Phenol [*]	233.1	Furoic Acid	221.5

Table 6.2 (continued): Specific heat of components in bio-oil/gases (Ling Zhang, 2004)

Component	Cp (J/mol/°C)	Component	Cp (J/mol/°C)
2-Methyl Phenol	284.7	5-Methyfurfural	253.1
3-Methyl Phenol	284.7	5-OH-Methyl-2-Furfural	273.5
4-Methyl Phenol	284.7	Hydroxyacetaldehyde	136.3
2,3 Dimethyl Phenol	336.7	Acetol	188.3
2,4 Dimethyl Phenol	336.7	Acetal	374.7
2,5 Dimethyl Phenol	336.7	Acetyloxy-2-propanone	282.3
2,6 Dimethyl Phenol	336.7	2-OH-3-Me-2-cyclopentene-1-one	283.5
2-Ethylphenol	336.7	Methyl Cyclopenolone	283.5
2,4,6 TriMe Phenol	388.7	1-Acetyloxy-2-Propanone	282.3
1,2 DiOH Benzene	253.1	2-Methy-3-hydroxy-2-pyrone	273.5
1,3 DiOH Benzene	253.1	2-Methoxy-4-metylanisole	409.1
1,4 DiOH Benzene	253.1	4-OH-3 methoxybenzaldehyde	347.1
4-Methoxy Catechol	325.5	Dimethylcyclopentene	325.1
1,2,3 Trio-OH-Benzene	273.5	Lignin	340.7
Methyl Formate	136.3	CO [*]	29.8
Butyrolactone	209.9	CH4 [*]	70.1
Valerolactone	261.9	CO2 [*]	82.1
Angelicalactone	231.5	H2 [*]	27.2
Levoglucosan	375.1	H2O [*]	34.2

* Data from literature (Dean, 1987; Yaws, 1997)
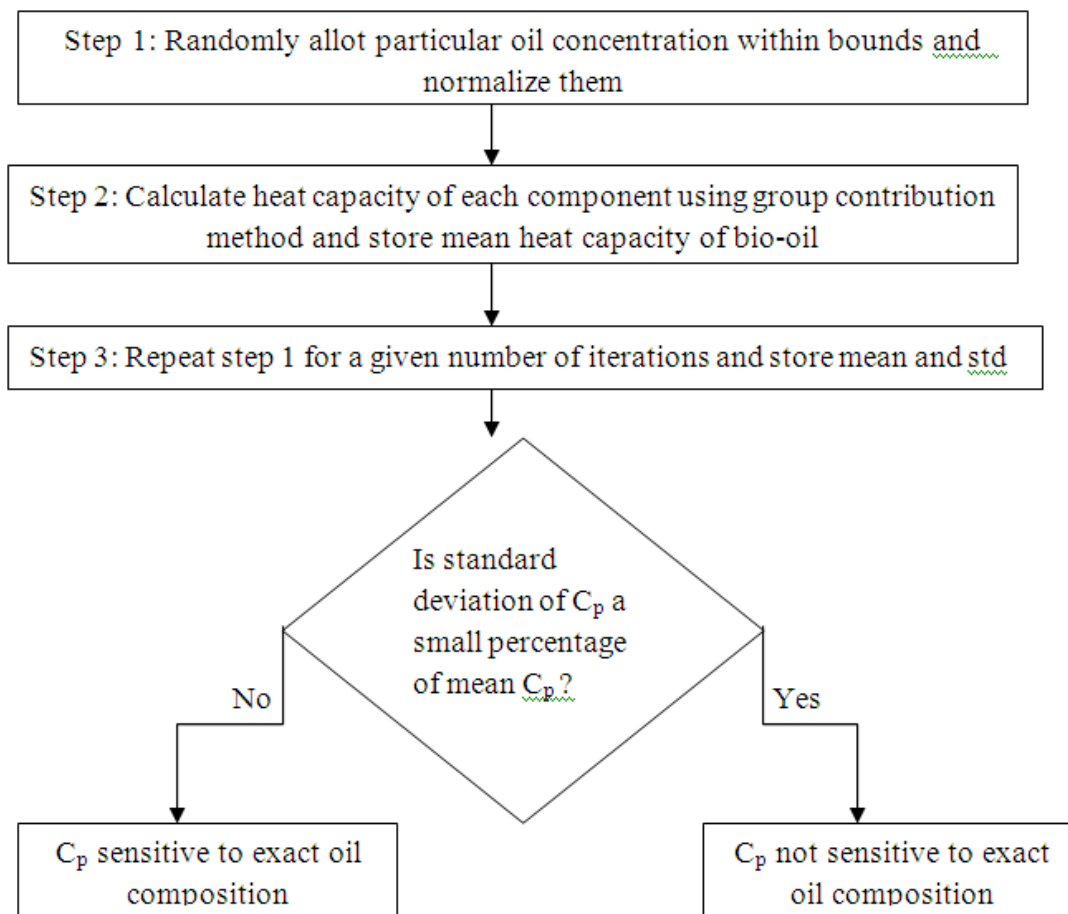
Figure 6.2: Flow chart to estimate the mean value of specific heat capacity of bio- oil and its standard deviation

Results obtained using the flow chart mentioned above are presented in Table 6.3. From Table 6.3, we can infer that the mean specific heat capacity of bio-oil is not sensitive to the exact composition of organic components in bio-oil. Any variation in composition of organic components of bio- oil within the bounds does not significantly change the mean heat capacity of bio- oil.

Table 6.3: Mean and standard deviation value of specific heat capacity of bio-oil

Total number of iterations	1000000
Mean specific heat capacity of bio-oil (J/gr/K)	2.4346
Standard deviation of specific heat capacity of bio-oil (%)	0.8297

6.2.3.2 Latent Heat of vaporization of bio-oil

The latent heat of vaporization for any given organic compound can be calculated using the Riedel equation (Reid et al., 1977)(6.5).

$$\Delta H_{vb} = 1.093 * T_c * R * \left[T_{br} * \frac{(\ln P_c - 1)}{(0.930 - T_{br})} \right] \qquad (6.5)$$

Where; ΔH_{vb} = Latent heat of vaporization of component (J/gr)

T_c = Critical temperature (K)

P_c = Critical pressure (atm)

$T_{br} = T_b/T_c$, T_b is the boiling point temperature (K) at atmospheric pressure

R = 8.314 J/mol/K

The critical temperature and pressure for a compound can be estimated using the group contribution technique by Lydersen (6.6-6.7) (Reid et. al, 1977). This estimation method employs structural contributions to estimate T_c and P_c. The units employed are kelvin and atmosphere respectively. The Δ quantities are evaluated by summing contributions of various atoms or groups of atoms (appendix B). To employ this method, only the normal boiling point T_b and the molecular weight M are needed.

$T_c = T_b*(0.567 + \sum \Delta_T - (\sum \Delta_T)^2)^{-1}$ \qquad (6.6)

$P_c = M*(0.34 + \sum \Delta_p)^{-2}$ \qquad (6.7)

The normal boiling point can be estimated from group the contribution method by Joback (Reid et al., 1977) (Equation 6.8). The $\sum$ quantities are evaluated by summing contributions of various functional groups in the compound (appendix B)

$$T_b = 198 + \sum G_i \tag{6.8}$$

So, based on this method, the sample latent heats of vaporization of the 93 components in the bio-oil and gases were calculated and listed in Table 6.4.

From Table 6.1, it is understood that the composition of organic components in bio-oil is bounded between the upper and lower bound. Hence, a Matlab^R code is written to randomly assign weight percentages to bio-oil components within the bounds and then, mean latent heat of vaporization and standard deviation are calculated for a given number of iterations. If the standard deviation of the mean latent heat of vaporization is too high, then the mean latent heat of vaporization of the bio-oil is significantly affected by the bio-oil composition of individual components. Hence, there is a need for better characterization of bio-oil for every experimental procedure. On the other side, a small standard deviation relaxes the above mentioned constraint. A flow chart describing the matlab code is given in Figure 6.3.

Table 6.4: Latent heat of vaporization of organic components in bio-oil

Component	HV(J/gr)	Component	HV(J/gr)
Formic acid	900.7	2-Methyl Phenol	456
Acetic	719.4	3-Methyl Phenol	456
Propanoic acid	629.2	4-Methyl Phenol	456
Hydroxyacetic acid	936.9	2,3 Dimethyl Phenol	429
Butanoic acid	543.6	2,4 Dimethyl Phenol	429
Pentanoic	496.9	2,5 Dimethyl Phenol	429
4-oxypentanoic	558.7	2,6 Dimethyl Phenol	429
Hexanoic	464	2-Ethyl Phenol	424.7
Benzoic	488.6	2,4,6 TriMe Phenol	410
Heptanoic	440.2	1,2 DiOH Benzene	583.8
Methanol[**]	1156.8 (1100)	1,3 DiOH Benzene	583.8
Ethanol[**]	848.7 (846)	1,4 DiOH Benzene	583.8
Ethylene Glycol	1086.5	4-Methoxy Catechol	517.5
Acetone	521.5	1,2,3 Trio-OH- Benzene	680.9
2-Butanone	450.8	Methyl Formate	523.6
2,3-Pentenedioine	436.8	Butyrolactone	490.2
3Me2cyclopenten2ollone	532.5	Valerolactone	449.1
2-Et-cyclopentanone	382.5	Furfural	408.7
Dimethlycyclopentanone	374.7	3-Methyl-2(3h) Furanone	443.5
Trimethylcyclopentenone	356.6	Furfural alcohol	571.2
Trimethylcyclopentanone	349.9	Furoic acid	525.1
Formaldehyde[**]	850.2 (776.67)	5-Methyl furfural	405.8
Acetaldehyde	626.7	5-OH-Methyl-2-Furfural	488.4
2-Propenal	531.8	Hydroxyacetaldehyde	821.4
2-Methly-2-Butenal	392.9	Acetol	707.1
Pentanal	377.7	Acetal	277.4
Angelicalactone	550.5	Acetyloxy-2-propanone	416.5
Levoglucosan	832.2	2-OH-3-Me-2-cyclopentene-1-one	519.9
Glucose	1117.8	Methyl Cyclopentolone	463
Fructose	1145	1-Acetyloxy-2-propanone	367.6
D-Xylose	1169.1	2-Methyl-3-hydroxy-2pyrone	395.4
D-Arobinose	1169.1	2-Methoxy-4-methylanisole	324.5
Cellobiosan	493.7	4-OH-3methoxybenzaldehyde	412.6
1,6 Anhydroglucofuranose	528.8	Dimethlycyclopentene	335.2
2-Methoxy phenol	329.9	Liginin	612.9

Table 6.4: Latent heat of vaporization of organic components in bio-oil (continued)

4-Methly Guaiacol	312.7	Propyl Syringol	299.5
Ethyl Guaiacol	307.4	Syringaldehyde	321.4
Eugenol	289.2	4-propenyl Syringol	278.5
Isoeugenol	289.6	4-OH-3,5-DiOMe Phenol ethanone	314.8
4-Propylguaiacol	304.6	Furan	461.1
Acetoguiacone	329.5	2-Methyl Furan	411.5
Propioguiacone	321.2	2-Furanone	471.4
2,6- DiOMe Phenol	313.4	Ethanedial	614.6
Methyl Syringol	308.6	Phenol	481.1
4- Ethyl syringol	303.1		

[**] Data in parenthesis is the actual value from the literature (Dean, 1987; Yaws, 1997)
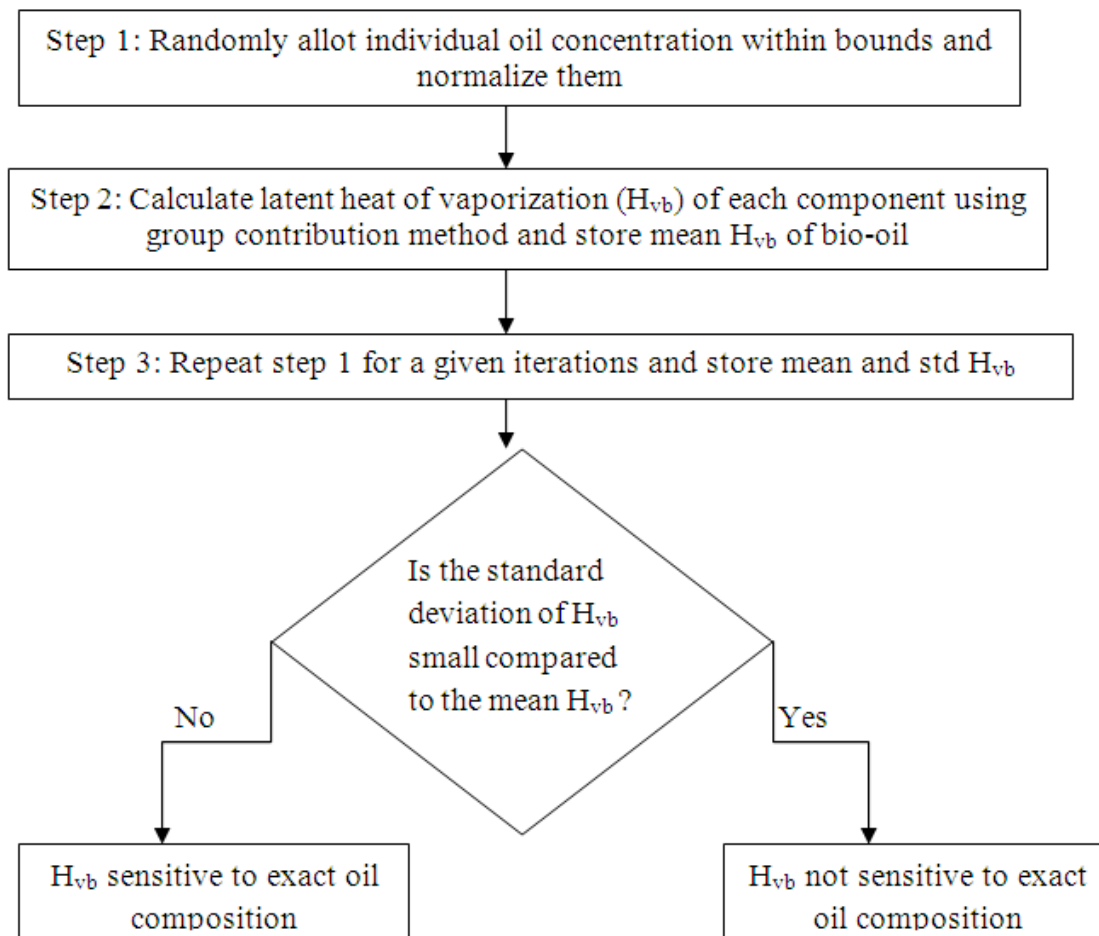
Figure 6.3: Flow chart to estimate the mean value of the latent heat of vaporization of bio-oil and its standard deviation

Results obtained using the flow charts above are presented in Table 6.5. From Table 6.5, we can infer that the mean latent heat of vaporization of bio-oil is not sensitive to the exact composition of organic components in the bio-oil. Any variation in composition of organic components of bio-oil within the bounds does not significantly change the mean latent heat of vaporization of the bio-oil.

Table 6.5: Mean and standard deviation of latent heat of vaporization (H_{vo}) of bio-oil

Total number of iterations	1000000
Mean H_{vb} of bio-oil (J/gr)	609.9312
Standard deviation of H_{vo} of bio-oil (%)	2.2237

6.2.4 Combustion

6.2.4.1 Heat of combustion of gases

The composition of the gases was obtained from Liu and his colleagues (Liu, et. al., 1999). The gas composition is listed in Table 6.6. This composition is in mole percentage of the total non-condensable gases, not including the bio-oil organics or water. When the gases and bio-oils were lumped together, they were assumed to be ideally mixed. Note that the higher heating values of combustion of gases are considered in the calculation.

Table 6.6: Composition and heat of combustion of gaseous components

Gas component	mole %	Heat of Combustion (KJ/mol)
CO	60.29	283
CO_2	6.4	0
CH_4	31.67	889
H_2	1.63	286

Hence, the average heat of combustion (calculated from Table 6.6) = **18270 KJ/Kg.**

6.2.4.2 Heat of combustion of char and natural gas

Lower heating value of char is obtained from experimental work done by Alex Williams (Muzzy et. al., 2009).

Heat of combustion of char = **26.4 MJ/Kg**

Note that the structural characteristic of char is similar to low carbon content coal (asphalt). Hence, the mean specific heat capacity of char can be approximated by asphalt (Perry and Green, 1997).

Specific heat capacity of char = 1.956 J/gr/^{0}C

Natural gas consists primarily of methane (95% by volume) and the heat of combustion (higher heating value) of natural gas is 54 MJ/Kg.

6.2.5 Heat of pyrolysis

Enthalpy of pyrolysis for white pine was determined using a pilot scale pyrolysis system (Daugaard et.al, 2003). The analytical method uses an energy balance on a pyrolytic reactor. The energy required is measured at a fast pyrolysis reactor temperature near 500°C using nitrogen as an inert fluidizing agent. The typical moisture content of biomass used in the pyrolytic reactor is between 8.0% to 12.0% of water on a dry basis. In the above experiment, pine was fed at room temperature (25°C) and products were collected at the reactor exit temperature. Char is in solid state and vapor is in gaseous state at reactor exit temperature of 500^{0}C. Hence, the heat of pyrolysis includes the heat required to raise the products from room temperature to reactor exit temperature.

Heat of pyrolysis of pine on dry basis (Daugaard et.al, 2003) = 1**.64*10^3 MJ/ton**

6.3 Energy distribution

From section 6.2, energy input and output values for different unit operations are calculated. In this section, the distribution of energy between different unit operations as a function of operating parameters of an auger reactor will be discussed. Operating conditions for the

pyrolysis reactor used in these calculations are presented in Table 6.7. Note that the kinetic parameter values given by Thurner et.al (1981) are used in the calculations.

Table 6.7: Operating conditions for the pyrolysis reactor for energy distribution between different unit operations

Feed rate of biomass(Tons/hr)	83.3
Temperature zone 1(K)	523
Temperature zone 2(K)	623
Temperature zone 3(K)	723
Reactor run time(min)	15
td range in each zone(sec)	10-30
Dead volume fraction for each zone(d)	0.108
P range	0.3-0.7

6.3.1 Energy from char and gas combustion to be used for pyrolysis reaction

Char and gas obtained from pyrolysis of pine from an auger reactor can be subjected to combustion. Energy obtained from combustion can be used to supplement the energy required for pyrolysis of pine. If energy from combustion of gas and char exceeds the energy required for pyrolysis in an auger reactor, then char is subjected to combustion partially and the remaining amount of char can be sold as a product. If energy obtained from combustion of gas and char does not meet the energy required for pyrolysis, natural gas can be subjected to combustion to meet the additional energy requirement. Note that the heat transfer efficiency of the heat exchanger to transfer energy from the combustion reactions to pine pyrolysis is assumed to be around 70% and is considered in the above calculations. In other words, if heat of pyrolysis is 70 units, there is a requirement of 100 units of energy from combustion reaction to meet the energy requirement.

119

In the energy calculations, energy from total combustion of char and gas exceeds the energy required for pyrolysis. Hence, some amount of char is not subjected to combustion and can be sold as a product. Figure 6.4 describes amount of char that can be sold as a product as a function of RTD after gas and char (partially) are subjected to combustion to meet pyrolysis energy requirements.
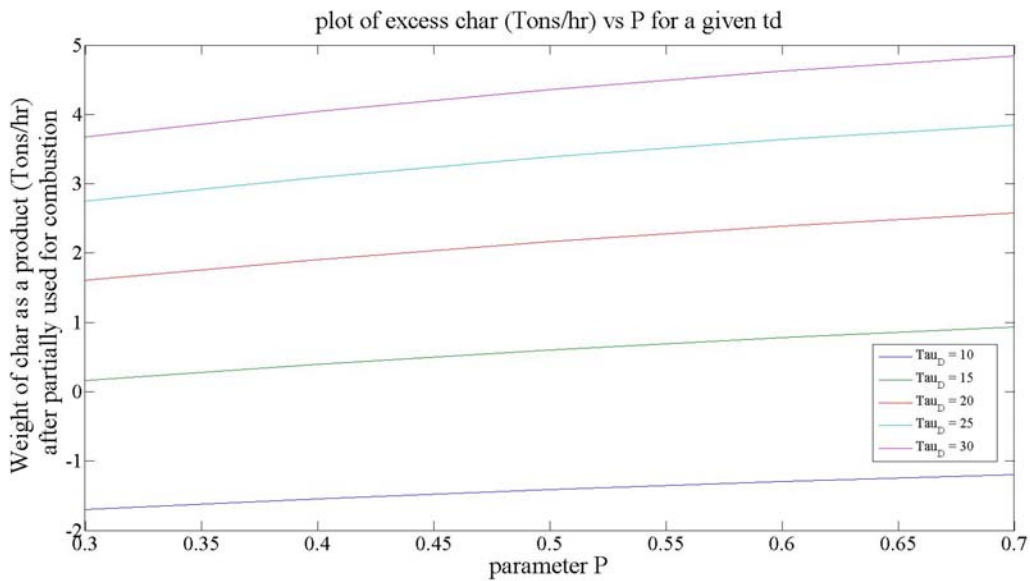
Figure 6.4: Amount of char that can be sold as a product (Tons/hr) after meeting pyrolysis energy requirement

From Figure 6.4, we can infer that irrespective of the operating conditions of the auger reactor, char can always be sold as a product after partially used to supplement energy for pine pyrolysis for mean residence time greater than 15 seconds. Secondly, amount of char (as a product) produced increases as the mean residence time (td) increases for any given value of P. This result is in accordance with the trend obtained in chapter 5. We have observed that, all three products yields increase as the mean residence time is increased (at a different rate). Hence, more energy is obtained from combustion of char and gas, leading to more char not used for combustion.

6.3.2 Energy required for pyrolysis of biomass

The energy required for pyrolysis of a ton of woody biomass is reported in section 6.2.5. Hence, the total energy required for pyrolysis of 41.65 tons/hr of dry biomass is as follows:

Net energy required for pyrolysis of pine $= 83.3*0.5*1.64*10^3$ MJ/ton $= 68,306$ MJ/hr

6.3.3 Energy required to cool bio-oil

As discussed in section 6.2, bio-oil is collected after the vapor is subjected to condensation. Mean specific heat capacity and mean latent heat values are calculated in section 6.2.

Figure 6.5 calculates the amount of heat energy per ton of oil produced to be removed to cool the bio-oil from the reactor exit temperature to room temperature (according to equation 6.3).
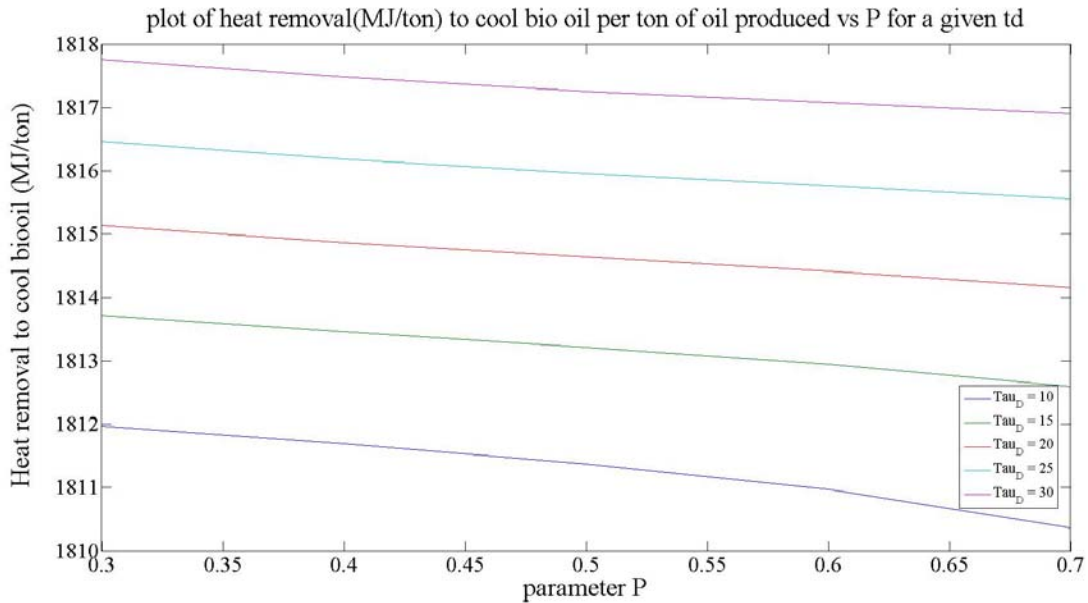
Figure 6.5: Heat energy removal (MJ/ton) to cool bio-oil to room temperature

From the above figure, we can observe that the amount of heat energy to be removed from bio-oil lies between 1810 and 1818 MJ/ton for any given operating conditions. Hence, the amount of

121

heat energy required per ton of oil produced to cool the oil from the reactor exit temperature to room temperature does not change significantly with operating conditions.

6.4 Summary and conclusions

The energy required to dry biomass is 91,100 MJ/hr and the energy to grind biomass is 6750 MJ/hr (based on 83.3tons/hr feed rate of biomass).

Energy from the total combustion of char and gas exceeds the energy required for pyrolysis. Hence, some amount of char is not subjected to combustion and can be sold as a product (for mean residence time greater than 15 seconds and any value of parameter P).

The mean specific heat capacity and the mean latent heat of vaporization of bio-oil are not sensitive to the exact composition of organic components in the bio-oil. Any variation in composition of organic components of the bio-oil within the bounds does not significantly change the mean heat capacity and the mean latent heat of vaporization of the bio-oil (Table 6.3 and Table 6.5).

The cooling duty required (per ton of oil produced) to cool the oil from the reactor exit temperature to room temperature does not change significantly with operating conditions. Variation of the calculated value of cooling duty per ton of oil produced (from Figure 6.4) is within 0.2 %.

In chapter 7, sizing of unit operations and economics of bio-oil production will be considered.

6.5 List of symbols and abbreviations

Symbol	Abbreviation	Units	Typical value
P	Fraction of volume in Plug flow reactor	-	0.3-0.7
d	Fraction of volume in dead zone	-	0.108
Bi	Biot number	-	Less than 1
r	Radius of particle	μm	300-450
K_p	Thermal conductivity of wood	W/m/K	0.12
h	External heat transfer coefficient in an Auger reactor	$W/m^2/K$	300-500
L	Latent heat of vaporization of water at 75^0C	KJ/Kg	2322.8
C_{pw}	specific heat capacity of water at 50^0C	J/gr/K	4.1806
C_{po}	specific heat capacity of vapor	J/gr/K	Refer to Table-6.3
H_{vb}	latent heat of vaporization of bio-oil	J/gr	Refer to Table-6.5
Q_d	Energy required to dry biomass	J/hr	60×10^6
Q_g	Energy required to grind biomass	J/hr	33.75×10^6
Q_p	Energy required to pyrolyze biomass	J/Kg	1.64×10^6
Q_{go}	Heat of combustion of gas	J/gr	18273
Q_c	Heat of combustion of char	J/gr	26400
Q_l	Heat required to cool bio-oil	J/gr	Refer to fig 6.5
T_c	Critical temperature	K	-
P_c	Critical pressure	atm	-
td	mean residence time	sec	10-30
t	time	sec	900 (unless specified)
T	Temperature	Kelvin	523-773
R	Gas constant	J/mol/K	8.314

CHAPTER 7

Economic Analysis of wood chip pyrolysis

A preliminary stage economic analysis of production of bio-oil using an auger reactor for pyrolysis will be considered in this chapter. The wood chip pyrolysis plant is operating at a feed rate of 2000 tons/day of ground wood chips at 50% moisture content. Also the sensitivity of the price of bio-oil with respect to cost of feedstock and return on investment will be discussed.

7.1 Design basis and Process Description

Bio oil is produced from fast pyrolysis process of wood chips in an auger based reactor. Figure 7.1 explains the schematic of fast pyrolysis process. Different processing areas which are important in the bio-oil production are as follows:

- Feed handling and drying

- Pyrolysis

- Char and gas combustion

- Bio-oil recovery

In the feed handling section, the wood chips enter the rotary dryer with 50% moisture by weight and they are dried to 10% moisture. These dried wood chips are then subjected to grinding in a ball mill grinder where the wood chips are reduced in size to less than 0.5mm. It is then sent to pyrolysis where a staged temperature pyrolysis of bio oil occurs. An auger reactor is divided into three different temperature zones to facilitate the collection of pyrolysis oils of three different major components of wood namely, cellulose, hemicellulose and lignin, at different zone temperatures. Vapors produced during the pyrolysis are immediately quenched through a

condenser (shell and tube heat exchanger) to maximize the yield of the bio-oil. Char is subjected to combustion in a combustor to provide heat of pyrolysis reaction. Excess char, if any after partially used to supplement the heat for the pyrolysis of wood chips in the auger reactor, can be sold a product and this will be a value addition to the process. Uncondensed gas and natural gas are burned in a combustor to dry the wood chips in a rotary dryer. The facility is assumed to operate continuously for 24 hrs a day for 330 days in a year; the remaining days are utilized for maintenance operations of the plant.

Figure 7. 1: Fast Pyrolysis flow of diagram

The data during the calculation of economics was taken from various sources. Table 7.1 summarizes the key design parameters and their sources.

Table 7.1 Design Basis

Parameter	Value	Source
Feedstock		
Type	Wood chips	Engineering judgment
Moisture Content	50%	
Cost	$30/ wet ton	NREL report, 2006
Throughput	2000 tons/day (50% moisture)	
Feedstock Composition (wt%, dry)		
Carbon	50.93%	Elemental Analysis of
Hydrogen	6.05%	Wood from Galbraith
Oxygen	41.93%	laboratory
Nitrogen	0.17%	
Pyrolysis Design		
Pyrolysis Type	Auger reactor	Engineering judgment
Temperature	250, 350 & 450 ^{o}C respectively for three different zones	Model (see Chapter 5)
Feed Moisture Content	10%	Model (see Chapter 5)
Ground Particle Size	< 0.5 mm	Refer to Table 3.1
Yields (Dry Basis)		
Oil	50%	(see Chapter 5)
Char and ash	20%	
Gas	20%	
Water	10%	
Oil Representative Components		
Refer to Table 6.1		
Projected Overall bio-oil		
Composition (wt. %)		
Carbon	58.90%	Refer to Table 4.4
Hydrogen	6.43%	
Oxygen	33.84%	
Nitrogen	<0.5%	

Table 7.1 continued		
Parameter	Value	Source
Target Overall bio-oil composition (wt%)		
Carbon	55-58%	BridgeWater et. al. (2002)
Hydrogen	5.5-7.0%	
Oxygen	35-40%	
Gas composition		Refer to Table 6.6

The compositions of these major streams is highly variable and are highly dependent upon, kinetic scheme of reaction, rate constant values, and reactor operating parameters. The product yields, based on Shafizadeh et. al (1977) kinetic scheme of pyrolysis, is assumed to be similar to micro reactor yields.

7.2 Material and Energy Balance results

7.2.1 Material Balance

All the calculations are based on 2000 tons/day of wet wood chips having 50% moisture entering the dryer. Therefore, feed rate of dry ground wood chips into the auger reactor is (having 10% moisture) 1100 tons/day. Material balance (based on hourly basis) around the auger reactor (refer to Table 7.1 and Figure 7.1) is as follows:

- Feed rate of ground wood chips = (83.3*0.5 + 4.63) = 46.28 tons/hr

- Bio-oil = 83.3*0.50*0.50 = 20.825 tons/hr

- Non-condensable gas = 83.3*0.50*.20 = 8.33 tons/hr

- Char = 83.3*0.50*0.20= 8.33 tons/hr

- Water = 4.63 + 83.3*0.5*0.1 = 8.795 tons/hr

Material balance for the wood chip pyrolysis plant is given in Table 7.2

Table 7.2: Mass balance around the wood chip pyrolysis facility (ton/hr)

Feed rate of wood chips (50% moisture)	*83.3*
Water	8.795
Bio-oil	20.825
Non-combusted char	4.223
Natural gas required for drying	6.182
Exhaust (Combusted natural gas and non-condensable gas, water evaporated from wet wood chips)	55.639

7.2.2 Energy Balance

Energy requirements for the wood chip pyrolysis are based on material balance around the wood chip pyrolysis facility given in Table 7.2. The data used in the calculations of energy requirements are summarized in Table 7.3. Refer to chapter 6 for further details.

Table 7.3: Data used for energy calculations

Specific heat of bio-oil (MJ/ton/K)	2.4346
Heat of Vaporization of bio-oil (MJ/ton)	609.931
Heat of combustion of gas (MJ/ton)	18270
Heat of combustion of char (MJ/ton)	26400
Specific heat capacity of char (MJ/Kg/K)	1.956
Heat of Pyrolysis (MJ/ton)	1640
Heat of combustion of Natural gas (MJ/ton)	54000
CP of water (MJ/ton/K)	4.1806
Latent heat of vaporization of water (MJ/ton)	2322.8
CP of water vapor (MJ/ton/K)	2.13

Energy requirements for different unit operations in wood chip pyrolysis based on Table 7.2 and Table 7.3 are given Table 7.4.

Table 7.4: Energy requirements for different unit operations (MJ/hr)

Energy required to dry wood chips (MJ/hr) in rotary dryer	97200
Energy required to grind biomass (MJ/hr) in ball mill	6250
Energy required for pyrolysis (MJ/hr) in an auger reactor	75900
Cooling duty required for shell and tube heat exchanger (MJ/hr)	64000

Note that the exhaust from combustion of char used to provide heat for the auger reactor has some heat capacity and can be utilized to provide some of the heat requirement to dry the wood chips in the rotary dryer. These calculations are not considered in the above table and may be considered later.

7.3 Economic analysis

There are two main components for economic analysis that are calculated separately in this section. They are Total Permanent Investment (TPI) and Operating cost (OC).

7.3.1 Total Permanent Investment

7.3.1.1 Total Permanent Investment Basis

Using the material and energy balance discussed in Tables 7.2 and 7.4, all the major unit operations were sized and the total bare module cost was determined using standard sizing procedures mentioned in Perry's Chemical Engineer's Handbook (1997), Product and Process design principles by Seider et al.(2009), Plant Design and Economics for Chemical Engineers by Peters et al. (2003). For non standard equipment, the pyrolysis reactor and dryer, references and comparison from other reports (Ringer et. al, 2006) were used.

The total bare module cost of the equipment for every unit operation was calculated from the procedure given in Product and Process design principles by Seider et al(2009). This includes equipment purchase price, field materials used for installation, direct labor used for installation and indirect module expenses. After estimating the equipment costs, a contingency factor of 20% was applied to the total equipment costs. This conservative contingency factor was designed to account for any miscellaneous equipment left out of the analysis, uncertainty in the analysis due to its early stage of development, and the conceptual nature of the analysis.

Using the total equipment cost, the total project investment (TPI) was projected using a factored method based on the methodology used in the NREL Techno-Economic Analysis of Fast pyrolysis of oil (2006). Table 7.5 outlines the factors used.

Table 7.5: Total Permanent Investment Factors (TPI)

Component	Basis
Total Equipment bare module cost	Literature
Warehouse	1.5% of bare module cost
Site Development	10% of bare module cost
Total Installed Cost (TIC)	Sum of above
Indirect Costs	
Field Expenses	20% of TIC
Home, office & Construction Fee	25% of TIC
Project Contingency	3% of TIC
Total Depreciable Capital (TDC)	Sum of the above
Other Costs (Startup)	10% of TDC
Total Permanent Investment (TPI)	Sum of the above

7.3.1.2 Total permanent Investment Results

A majority of the equipment costs were determined using the standard methods described in Seider et. al (2009). Calculation of the individual equipment cost is given in appendix C. Table 7.6 estimates the individual equipment bare module cost for every unit operation.

Table 7.6: Individual and total bare module cost for process equipement

Unit operation	Installed equipment cost ($ Million)
Rotary Dryer	8.93
Ball mill grinder	2.96
Shell and tube heat exchanger	0.41
Pyrolysis reactor	8.25
Combustor	8.48
Vacuum pump	0.08
Equipment contingency-20%	5.82
Total installed equipment cost	**34.94**

Using the installed equipment costs and the factors outlined in Table 7.5, the Total Permanent Investment (TPI) was estimated at $ **63.43** million. These results are provided in Table 7.7.

Table 7.7: Total Permanent Investment

Component	Cost ($ Million)
Total Equipment bare module cost	34.94
Warehouse	0.52
Site development	3.49
Total Installed Cost(TIC)	38.96
Indirect costs	
Field Expenses	7.79
Home Office and Construction Fee	9.74
Project contingency	1.17
Total Depreciable Capital (TDC)	57.66
Other Costs(Startup)	5.77
Total Permanent Investment (TPI)	**63.43**

7.3.2 Operating cost

7.3.2.1 Operating cost basis

Annual costs were projected for both variable and fixed operating costs. Variable operating costs are incurred for feedstock (wood chips) and utilities such as cooling water, electricity and natural gas. Feed stock cost was obtained from NREL studies. Unit costs for the cooling water, electricity and natural gas are obtained from Seider et al(2009). Table 7.8 summarizes the unit costs associated with these items.

Table 7.8: Unit costs

Input	Unit cost
Wood chip (50% moisture) ($/ton)	30
Cooling Water($/m^3)	0.02
Natural gas ($/m^3)	0.14
Electricity ($/KW-hr)	0.06

Fixed operating costs, composed of labor, maintenance, overhead, taxes and insurance, were also determined. The labor cost and the number of workers required to run the plant was estimated based on the method described in Seider et. al (2009). Refer to appendix D for detailed estimate of labor cost and electricity requirements for the wood chip pyrolysis facility. Table 7.9 summarizes the different components used in the calculation of operating cost and their basis.

Table 7.9: Total operating cost factors

Cost Factor	Basis
Feed stock (Raw materials)	
Utilities	
Operations (Labor related)	
Direct Wages and Benefits (DW&B)	35$/hr
Direct salaries and Benefits	15% of DW&B
Operating supplies and services	6% of DW&B
Maintenance (M)	
Wages and benefits (MW&B)	2% of TDC
Salaries and benefits	25% of MW&B
Materials and Services	100% of MW&B
Maintenance overhead	5% of MW&B
Operating overhead	22.8% of M&O S-W&B
Property tax and insurance	2% of TDC
Depreciation	10% of TDC
Total operating cost	Sum of the above

7.3.2.2 Operating cost results

Annual variable operating costs were determined from the material and energy balance. The largest variable operating cost, by far is the feedstock at $21.89 million annually. Second highest variable operating cost is natural gas at $9.32 million annually. Electricity and water have relatively negligible costs. Overall annual variable operating costs are thus estimated at $31.30 million annually. Table 7.10 summarizes the variable operating cost.

Table 7.10: Annual Variable Operating Cost (Million $/yr)

Feed stock (Raw materials)	(Million $/yr)
Wood chips (50% moisture)	19.79
Utility	
Electricity	0.86
water	0.35
Natural gas	10.31
Total	31.30

Labor costs were estimated as outlined in appendix D and resulted in a direct labor cost of $7.28 million. Using the variable operating costs, labor costs, Total Permanent Investment (TPI) and the factors outlined in Table 7.6, the Total annual operating cost was estimated at $ **51.92** million. These results are provided in Table 7.11.

Table 7.11: Total Annual Operating cost

Cost Factor	Annual Cost(Million $)
Feed stock (Raw materials)	19.79
Utilities	11.51
Operations (Labor related)	
Direct Wages and Benefits (DW&B)	7.28
Direct salaries and Benefits	1.09
Operating supplies and services	0.44
Maintenance (M)	
Wages and benefits (MW&B)	1.15
Salaries and benefits	0.29
Materials and Services	1.15
Maintenance overhead	0.06
Operating overhead	2.24
Property tax and insurance	1.15
Depreciation	5.77
Total operating cost	**51.92**

7.4 Financial analysis

Following are the factors considered in estimation of the cost of bio oil:

- There are two products namely bio-oil and non- combusted char than can be sold as a product. The selling price of char is fixed at $ 250/ton which approximately half the cost of activated carbon (Lu et. al, 2006).

- A tax of approximately 40% is applied on the profit made by the plant (Seider et. al, 2006).

- A return on Investment of 10% is assumed in the cost calculation and the life of the plant is assumed to be around 20 years.

The higher heating value of bio-oil is 17.9 MJ/Kg and the density of the bio-oil is 4.55Kg/gal (Mullaney et.al, 2002) and the energy density of No. 2 heating oil is 140,000 BTU/gal (http://www.eia.doe.gov/oil_gas/petroleum/info_glance/petroleum.html, 2010).

The plant is estimated to run for 20 years. The selling price of the bio-oil is projected to be **$328/ton or $1.49/gal or $18.33/GJ**.

Bio-oil is considered as substitute for No.2 heating oil. The cost of the heating oil is $2.44/gal or $ 16.57/GJ. Cost per unit energy of bio-oil is slightly greater than No.2 heating oil. The market for heating oil is significant. In 2009, over 22,900 million gallons of heating oil was purchased in the United States. (http://www.eia.gov/dnav/pet/pet_pri_dist_dcu_nus_m.htm).

Although this analysis is portraying bio-oil as a substitute for No.2 heating oil, it is critical to note that the pyrolysis oils are not fungible with petroleum fuels. A separate fuel handling and transport system must thus be developed.

7.5 Sensitivity studies

The ratio of annual operating cost to annualized capital cost obtained from Table 7.7 and 7.11 respectively is approximately 16. This indicates that the cost of bio-oil is extremely sensitive to variations in operating cost (for example, cost of feed stock) and is not significantly affected by the variations in capital cost. This fact is clearly illustrated by the sensitivity study of the price of bio-oil tabulated in Table 7.12.

Table 7.12: Bio-oil Sensitivity study

Sensitivity Study	Resulting bio-oil cost ($/gal)
Actual cost	1.49
Reduce the feed stock cost to 20$/ton	1.31
Increase the feed stock cost to 40$/ton	1.68
Reduce contingency factor to 10%	1.45
Increase facility size to 4000 wet tons/day	1.41
Cost of char reduced to 125$/ton	1.61
20% ROI	1.78
0% ROI	1.20

From Table 7.12 we can infer the following:

- A reduction of 33% in the cost of feed stock leads to a 13% reduction in the cost of bio-oil, an increase of 33% in the cost of feed stock leads to a 13% increase in the cost of bio-oil. Hence the cost of feedstock is the most important factor that can significantly impact the selling price of bio-oil.

- An increase of 100% in the processing facility of wet wood chips from 2000 wet ton/day to 4000 wet tons/day led to a 5% reduction in the selling price of bio-oil indicating weak influence of capital investment on cost of bio-oil as discussed earlier. Exponential factor of 0.6 is considered in the sizing of the plant.

- The cost of bio-oil which leads to 0% Return on Investment is 1.25 $/gal. Hence, the cost of production of bio-oil for the given operating conditions is 1.25$/gal.

- A decrease of 50% in the contingency factor of the production facility lead to 3% decrease in the selling price of bio-oil indicating the weak influence of contingency factor on cost of bio-oil.

- A reduction of 50% in the selling price of char increased the selling price of bio-oil by 8%. Hence, selling price of char plays a significant role in determining the selling price of bio-oil.

- The selling price of bio-oil according to the 20% Return on Investment (ROI) is projected to be around 1.78 $/gal. A 100% increase on the Return on Investment increased the selling price of bio-oil by 19%.

7.6 Limitations of Analysis

- Lack of current data on the kinetics of pyrolysis in an auger reactor could not predict precise product yields. Hence, the product yields were assumed to match micro-reactor yields.

- Fungibility issues and the resulting storage and distribution system requirements of the bio-oil have not been addressed.

- Large contingency factors due to large uncertainty

7.7 Summary and Conclusions

The potential of bio-oil as a substitute for heating oil and cost margin between bio-oil selling price and current No. 2 fuel oil selling prices are the main driving forces for fast pyrolysis of wood chips at a large scale.

The selling price of the bio-oil according to the cost calculation (refer to section 7.4) is projected to be $1.49/gal. The cost of feedstock is the most important factor that can significantly impact the selling price of bio-oil. A reduction of 33% in the cost of feed stock leads to 13% reduction in the cost of bio-oil. The cost of bio-oil (according to the values used in Chapter 7) has to be greater than $1.20/gal for the pyrolysis plant to yield profit. A 50% increase on the Return on Investment increased the selling price of bio-oil by 19%. A decrease of 50% in the contingency factor of the production facility leads to 3% decrease in the selling price of bio-oil. A reduction of 50% in the selling price of char increased the selling price of bio-oil by 8%. Hence cost of the feed stock and selling price of char play a crucial role in determining the selling price of bio-oil.

Bio-oil may be an acceptable substitute for No. 2 fuel oil as long as customers understand that bio-oil is not fungible with No. 2 fuel oil and that separate burners, feeding systems and storage are required.

CHAPTER 8

CONCLUSIONS AND RECOMMENDATIONS

8.1 Conclusions

8.1.1 Experimental Investigation

It can be concluded that:

- The usage of either thin or thick thermocouple in a tubular pyrolysis reactor does not significantly impact the measurement of actual temperature of the wood to an extent that the measured temperature is considerably different from the pyrolysis temperature.

- The flow rate of nitrogen does not lead to significant cooling of the sample on the surface. The temperature difference caused due to cooling by flow of nitrogen in the range of pyrolysis temperature (250-450^{0}C) is approximately 15°C.

- Radiation is the dominant mode of heat transfer in the tubular pyrolysis reactor which leads to significant heating of the woody biomass and can offset the measured temperature of the thermocouple measurement by a huge margin when placed on the surface the wood. During pyrolysis, when the thermocouple is placed on the surface of the wood, the temperature measured by the thermocouple is 35% more than the actual temperature of the wood.

- The best position of the thermocouple to minimize external effects like cooling due to the flow of nitrogen gas and radiation is to be inserted into the middle of the wood (schematic 3).

- Addition of catalyst to wood increases the percentage of char. Percentage of char increased from 21% to 28% when the wood sample was impregnated with different catalysts based on same mole ratio.

- The percentage of char is almost the same for all the catalysts when they are added on same molar ratio basis (moles of cat./gr. of wood). Approximately 28% of char was obtained for different catalysts when the same mole ratio of catalyst to wood is added.

8.1.2 System modeling

It can be concluded that:

- The kinetic parameters (depending on experimental set up) play a crucial role in determining the yield of oil

- Variations in temperature of zone 3 play a crucial role in varying the output yield of oil whereas variations in temperatures of zones 2 and 1 do not significantly impact output oil yield. For example, if we consider the reactor operating conditions at P equal to 0.3 and t_d equal to 30 seconds, a 5% increase in the temperature of zone 3 from 703 K is increasing the yield of bio-oil by 42% whereas, an increase of 5% in the temperature of zone 2 from 603K increases the yield of bio-oil by 5% and a 8 % increase in the temperature of zone 1 from 503 k increases the yield of bio-oil by less than 0.5%. These results were studied within a 10% variation from the actual temperature of zone 1(523 K), zone 2(623K) and Zone 3 (723K).

- For a given kinetic scheme of the pyrolysis reactions, the calculated values of the pre-exponential factor (A_i) (assuming that the energy of activation is known) is not sensitive to the variations in the RTD parameters due to experimental error. Hence, experimental

141

error in calculating the RTD parameters (P and td) did not significantly change the calculated value of pre-exponential factor.

- Errors in calculation of the pre-exponential factors (assuming that the energy of activation is known) caused by errors in measurement of RTD parameters does not significantly change the calculated value of output oil yield at low values of t_d

- Experimental error in calculation of the RTD parameters can induce error in the calculation of the Arrhenius constants but these values can still predict the yield of products accurately for a single component kinetic scheme of pyrolysis.

- The mean specific heat capacity and the mean latent heat of vaporization of bio-oil are not sensitive to the exact composition of organic components in the bio-oil. Any variation in composition of organic components of the bio-oil within the bounds (given by Diebold. et al., 1999) does not significantly change the mean heat capacity and the mean latent heat of vaporization of the bio-oil.

- The cooling duty required (per ton of oil produced) to cool the oil from the reactor exit temperature to room temperature does not change significantly with operating conditions. Variation of the calculated value of cooling duty per ton of oil produced is within 0.2%.

8.1.3 Economic Analysis

It can be concluded that:

- The selling price of the bio-oil according to the 10% Return on Investment (ROI) is projected to be $1.49/gal. However, the selling price of bio-oil according to the 20% Return on Investment (ROI) is projected to be around $1.78/gal. A 100% increase on the Return on Investment increased the selling price of bio-oil by 19%.

- The cost of feedstock is the most important factor that can significantly impact the selling price of bio-oil. A reduction of 33% in the cost of feed stock leads to 13% reduction in the selling price of bio-oil. This result was according to the expectations as the yield of bio-oil from feed stock is 50%.

- The production cost of bio-oil is $1.20/gal. Decreases of 50% in the contingency factor of the production facility lead to a 3% decrease in the selling price of bio-oil. A reduction of 50% in the selling price of char increased the selling price of bio-oil by 8%. Hence, the cost of bio-oil is extremely sensitive to variations in operating cost and is not significantly affected by the variations in capital cost.

8.2 Future work

Recommendations for future work are as follows:

- Although a screw extruder is a good system for performing a staged temperature pyrolysis of ground pine in a continuous process to extract pyrolysis vapors of cellulose, hemicelluloses and lignin separately, more work needs to be done on the vapor collection system for efficient collection of vapors from pyrolysis of pine at different temperatures. There is a need for design of a better condenser so that bio-oil vapors formed during pyrolysis of woody biomass do not condense on the walls of the condenser and are efficiently collected in the condenser vessel.

- Based on the experimental results obtained from the staged temperature pyrolysis of pine in the extruder, kinetic parameters for single component reaction kinetic scheme for three main components of wood; cellulose, hemicellulose and lignin can be estimated separately.

143

- The single component reaction scheme of the three main components of wood can be implemented in the model developed to predict the yield of products at different reactor operating conditions. These results can be compared to actual experimental results for better understanding of the reaction mechanism in the auger reactor.

- Also, the single component reaction scheme of three main components of wood can be lumped together to represent the scheme given by Shafizadeh et al. (1977). The values of the kinetic rate constants hence obtained can be compared to the actual data in the literature for the same reactor configuration. This will enable us to understand the significance of predicting a reaction scheme and estimate the error caused to prediction of lumped reaction kinetics. Further, the sensitivity of these lumped rate constants with respect to error in estimation of 3 component reaction kinetic scheme and the operating conditions of the reactor can be analyzed.

- Economic analysis of a catalyst impregnated wood chip pyrolysis plant can be performed and the cost sensitivity of bio-oil selling price with respect to yield of the oil and cost of the catalyst can be pursued. Effect on selling price of bio-oil with respect to percentage recovery of catalyst can also be studied.

APPENDIX A

PROGRAMMING CODE

A.1 Matlab code to measure the yield of products for given RTD, Temperature, Kinetics

```
******************************************************************

A.1.1 Main code

***********************************

% Main program to calculate the optimum values of P & td.



d= 0.108;
% bins represents the number of partitions of P
i = 0;  bins = 10;
td_val = 10:5:40;
P_val = linspace(0.1,0.9,bins);
Zee=bins*length(td_val);

% final yield including P and td
Final_C = zeros(Zee,6);

% TD DEPENDS ON THE TIME FRAME GIVEN IN THE PREVIOUS CONC CODE

idx = 0;
idxt = 0;

  for idtd = 1:length(td_val);
      idx = idx + 1;
      td = td_val(idtd);
 for idP = 1:bins
```

```matlab
    P = P_val(idP);
            i=i+1;
         C_zone1 = zonez1(P,td,d);
         C_zone2 = zonez2(P,td,C_zone1,d);
         C_zone3 = zonez3(P,td,C_zone2,d);
         C_zone3 = (C_zone3)';
         Final_C(i,1) = P;
         Final_C(i,2) = td;
         %c1 is gas, c2 is tar, c3 is char, c4 is biomass
         Final_C(i,3) = C_zone3(1);
         Final_C(i,4) = C_zone3(2);
         Final_C(i,5) = C_zone3(3);
         Final_C(i,6) = C_zone3(4)
  end

   end


   figure(1)
C1 = zeros(length(P_val),idx);
for idpp = 1:idx
   C1(:,idpp) = Final_C((idpp - 1)*bins + 1:idpp*bins,4);
   if idpp == 1
       leg = sprintf('''Tau_D = %d'',',td_val(idpp));
   else
       lega = sprintf('''Tau_D = %d'',',td_val(idpp));
       leg = [leg,lega]; %#ok<AGROW>
   end
end
preleg = 'legend(';
leg(:,end) = ')';
runleg = [preleg,leg];
plot(P_val,C1),eval(runleg)
xlabel('parameter P');
ylabel('yield of oil');
title('plot of oil conc vs P for a given td');

   Final_C;


 ***********************************************
```

A.1.2 Zone yield functions

****

\-

A.1.2.1 Zone 1 yield

\-

```matlab
% Simpsons Integration Fomula

function yield1 = corc12(k1,k2,k3,co,td,P,d)



h=0.01;
% T REPRESENTS THE TOTAL TIME IN SECONDS WHERE REACTION RUNS
time= 300;
t = 0:h:time;
i=0;
t = t';
M = (time/h)+1;
C = zeros(M,1);
c = zeros(M,1);
RTD_val = zeros(M,1);
Fsum = 0;
Gsum = 0;



for i = 1:1:M
    % c(i) is the amount of biomass reacted
    c(i) = co*exp(-(k1+k2+k3)*t(i));

    if (t(i)>= P*td)
        RTD_val(i) = RTD(d,P,t(i),td);
    else
        RTD_val(i) = 0;
    end
    RTD_val(i);
    C(i) =  h*c(i)*RTD_val(i);
     Fsum = Fsum + C(i);
```

147

```matlab
end
 for i = 2:1:M-1
    if (t(i)>= P*td)
        RTD_val(i) = RTD(d,P,t(i),td);
    else
        RTD_val(i) = 0;
    end
     if (mod(i,2)==0)
        Gsum = Gsum + 2*RTD_val(i);
     else
        Gsum = Gsum + 4*RTD_val(i);
     end
end


Gsum = Gsum + RTD_val(M);


Gsum = (h/3)*Gsum;
if Gsum >1
    Gsum =1;
end


Gsum;
%yield of reacted biomass
  CBF = co- Fsum;




% C1 is gas, C2 is biooil, C3 is char
% In zone 1 only primary reactions take place, so oil does not decompose
% into gas and char, CBis the biomass conc after it exits zone 1
C1 = (((k1)/(k1+k2+k3))*(CBF));
C2 = (((k2)/(k1+k2+k3))*(CBF));
C3 =  (((k3)/(k1+k2+k3))*(CBF));


yield1 = [C1 C2 C3 Fsum];0
---------------------------------------------------------
```

A.1.2.2 Zone 2 yield

```matlab
--------------------------------------------------------------

% Simpsons Integration Fomula
```

```matlab
function yield2 = corc22(k1,k2,k3,td,P,C1_vec,d)

% let the intial conc of products from zone 2 be ca0,cb0,cc0,cd0,ce0,cB0.

h = 0.01;
time2= 300;
t = 0:h:time2;
t = t';
M = (time2/h)+1;
ca0 = C1_vec(1);
cb0 = C1_vec(2);
cc0 = C1_vec(3);
%cd0 = 0;
%ce0 = 0;
cB0 = C1_vec(4);
C = zeros(M,1);
c = zeros(M,1);
%D = zeros(M,1);
%de = zeros(M,1);
RTD_val = zeros(M,1);
Fsum = 0;
Gsum = 0;
%Hsum = 0;


%d = 0.108;
% need to calculate hsum for some cb calculations

  for i = 1:1:M
    % c(i) is the amount of biomass reacted
    c(i) = cB0*exp(-(k1+k2+k3)*t(i));
    %de(i) = ((cb0)*exp(-(k4+k5)*t(i))) + (((k2)/(k1+k2+k3-k4-k5))*cB0*(exp(-
(k4+k5)*t(i)) - exp(-(k1+k2+k3)*t(i))));

    if (t(i)>= P*td)
        RTD_val(i) = RTD(d,P,t(i),td);
    else
        RTD_val(i) = 0;
    end
    RTD_val(i);
    C(i) =  h*c(i)*RTD_val(i);
```

149

```matlab
    %D(i) =  h*de(i)*RTD_val(i);
     Fsum = Fsum + C(i);
     %Hsum = Hsum + D(i);
  end


for i = 2:1:M-1
    if (t(i)>= P*td)
        RTD_val(i) = RTD(d,P,t(i),td);
    else
        RTD_val(i) = 0;
    end
     if (mod(i,2)==0)
        Gsum = Gsum + 2*RTD_val(i);
     else
        Gsum = Gsum + 4*RTD_val(i);
     end
end


Gsum = Gsum + RTD_val(M);
Gsum = (h/3)*Gsum;
if Gsum >1
    Gsum =1;
end
%yield of reacted biomass
  CBF = cB0- Fsum;



%ca gas, cb oil, cc char, cd gas from oil due to secondary rxns, ce char
%from oil due to secondary reactions
ca = (ca0) + (((k1)/(k1+k2+k3))*(CBF));
cc = (cc0) + (((k3)/(k1+k2+k3))*(CBF));


%Yield of reacted bio oil
cb = (cb0) + (((k2)/(k1+k2+k3))*(CBF));


%cd = ((cd0) + (((k4)/(k4+k5))*cb));
%ce = ((ce0) + (((k5)/(k4+k5))*cb));



yield2 = [ca cb cc Fsum];
```

A.1.2.3 Zone 3 yield

```matlab
% Simpsons Integration Fomula

function yield2 = corc32(k1,k2,k3,td,P,C1_vec,d)

% let the intial conc of products from zone 2 be ca0,cb0,cc0,cd0,ce0,cB0.

h = 0.01;
time3= 300;
t = 0:h:time3;
t = t';
M = (time3/h)+1;
ca0 = C1_vec(1);
cb0 = C1_vec(2);
cc0 = C1_vec(3);
%cd0 = 0;
%ce0 = 0;
cB0 = C1_vec(4);
C = zeros(M,1);
c = zeros(M,1);
%D = zeros(M,1);
%de = zeros(M,1);
RTD_val = zeros(M,1);
Fsum = 0;
Gsum = 0;
%Hsum = 0;

%d = 0.108;
% need to calculate hsum for some cb calculations

  for i = 1:1:M
    % c(i) is the amount of biomass reacted
    c(i) = cB0*exp(-(k1+k2+k3)*t(i));
    %de(i) = ((cb0)*exp(-(k4+k5)*t(i))) + (((k2)/(k1+k2+k3-k4-k5))*cB0*(exp(-
(k4+k5)*t(i)) - exp(-(k1+k2+k3)*t(i))));

    if (t(i)>= P*td)
```

151

```matlab
        RTD_val(i) = RTD(d,P,t(i),td);
    else
        RTD_val(i) = 0;
    end
    RTD_val(i);
    C(i) =  h*c(i)*RTD_val(i);
    %D(i) =  h*de(i)*RTD_val(i);
     Fsum = Fsum + C(i);
     %Hsum = Hsum + D(i);
  end


for i = 2:1:M-1
    if (t(i)>= P*td)
        RTD_val(i) = RTD(d,P,t(i),td);
    else
        RTD_val(i) = 0;
    end
     if (mod(i,2)==0)
        Gsum = Gsum + 2*RTD_val(i);
     else
        Gsum = Gsum + 4*RTD_val(i);
     end
end


Gsum = Gsum + RTD_val(M);
Gsum = (h/3)*Gsum;
if Gsum >1
    Gsum =1;
end
%yield of reacted biomass
  CBF = cB0- Fsum;




%ca gas, cb oil, cc char

ca = (ca0) + (((k1)/(k1+k2+k3))*(CBF));
cc = (cc0) + (((k3)/(k1+k2+k3))*(CBF));

%Yield of reacted bio oil
cb = (cb0) + (((k2)/(k1+k2+k3))*(CBF));
```

```
%cd = ((cd0) + (((k4)/(k4+k5))*cb));
%ce = ((ce0) + (((k5)/(k4+k5))*cb));


yield2 = [ca cb cc Fsum];
```

A.1.3 Zone kinetic rate parameters

A.1.3.1 Zone 1 kinetic parameters

....

```
% Optimization of screw extruder performance

% Zone 1
% Variable declaration

% Units of E in J/mol and Units of A in 1/s

function C1_vec = zonez1(P,td,d)

% C1 is gas, C2 is biooil, C3 is char

A = [1.11*10^11;
     9.28*10^9;
     3.05*10^7];
E = [177*10^3;
     149*10^3;
     125*10^3];


% A = [0.0143*10^6
```

```matlab
%      4.1250*10^6
%      0.7377*10^6];
% E   =[ 88.6*10^3;
%       112.7*10^3;
%       106.5*10^3];


R = 8.314;
% Temperature in zone 1
T = 573;
C0 = 1000000;


% Main Program


% Rate constants definitions


for i = 1:3
    k(i) = A(i)*exp ((-E(i))/(R*T)));
end



C1_vec = corc12(k(1),k(2),k(3),C0,td,P,d);
```

A.1.3.2 Zone 2

```matlab
% Optimization of screw extruder performance


% Zone 2
% Variable declaration


% Units of E in J/mol and Units of A in 1/s


function C2_vec = zonez2(P,td,C1_vec,d)


A = [1.11*10^11;
     9.28*10^9;
     3.05*10^7];
E = [177*10^3;
```

```matlab
    149*10^3;
    125*10^3];
% A = [0.0143*10^6
%      4.1250*10^6
%      0.7377*10^6];
% E  =[ 88.6*10^3;
%       112.7*10^3;
%       106.5*10^3];
R = 8.314;
% Temperature in Zone 2
T = 673;



% Main Program


% Rate constants definitions


for i = 1:3
    k(i) = A(i)*exp ((-E(i))/(R*T));
end


k;


C2_vec = corc22(k(1),k(2),k(3),td,P,C1_vec,d);
```

A.1.3.3 Zone 3

```matlab
% Optimization of screw extruder performance

% Zone 3
% Variable declaration

% Units of E in J/mol and Units of A in 1/s

function C3_vec = zonez3(P,td,C2_vec,d)

A = [1.11*10^11;
```

```matlab
    9.28*10^9;
    3.05*10^7];
E = [177*10^3;
    149*10^3;
    125*10^3];



% A = [0.0143*10^6
%     4.1250*10^6
%     0.7377*10^6];
% E  =[ 88.6*10^3;
%      112.7*10^3;
%      106.5*10^3];
R = 8.314;
% Temperature in Zone 2
T = 773;




% Main Program

% Rate constants definitions

for i = 1:3
    k(i) = A(i)*exp ((-E(i))/(R*T));
end

k;

C3_vec = corc32(k(1),k(2),k(3),td,P,C2_vec,d);


 ----------------------------------------
A.1.4 RTD module
----------------------------------------
function restime = RTD(d,P,t,td)


restime = (1/((1-d)*(1-P)*td))*exp(-(t-P*td)/((1-d)*(1-P)*td));


end
```

156

```
*********************************************************************
```

A.2 Matlab code to measure the sensitivity of products yields with respect to zone temperature

```
***********************************************************************
```

A.2.1 Temperature variations in zone 1

```
*******************************************
```

```matlab
% Main program to calculate the optimum values of P & td varying t1

 clear all;
 clc;
i = 0;j = 0;k = 0;
%P = 0.1:0.1:1;
% td = 30
% td represents a vector of time and ntd is the no of time partitions
P = 0.3;ntd = 25;d =0.108;
td = linspace(5,30,ntd);
% T1, T2 & T3 are temp of zone 1,2 &3 resp.
%T1 = 573;
T2= 623;
T3= 723;
Tbins = 5;
T1 = linspace(503,543,Tbins);
Final_C = zeros((ntd*length(T1)),9);

for n = 1:length(T1);
   for h = 1:ntd;

        C_zone1 = zone1(P,td(h),d,T1(n));
        C_zone2 = zone2(P,td(h),d,T2,C_zone1);
        C_zone3 = zone3(P,td(h),d,T3,C_zone2);
        C_zone3 = (C_zone3)';
        i = i+1;
        Final_C(i,1) = P;
```

157

```matlab
        Final_C(i,2) = td(h);
        Final_C(i,3) = C_zone3(1);
        Final_C(i,4) = C_zone3(2);
        Final_C(i,5) = C_zone3(3);
        Final_C(i,6) = C_zone3(4);
        Final_C(i,7) = T1(n);
        Final_C(i,8) = T2;
        Final_C(i,9) = T3;
        C2_zone3(i,1) = P;
        C2_zone3(i,2) = td(h) ;
        C2_zone3(i,3) = Final_C(i,4);
    end
end



figure(1)
C1 = zeros(ntd,length(T1));
for idpp = 1:length(T1)
   C1(:,idpp) = Final_C((idpp - 1)*ntd + 1:idpp*ntd,4);
   if idpp == 1
       leg = sprintf('''T1 = %d'',',T1(idpp));
   else
       lega = sprintf('''T1 = %d'',',T1(idpp));
       leg = [leg,lega]; %#ok<AGROW>
   end
end
preleg = 'legend(';
leg(:,end) = ')';
runleg = [preleg,leg];
plot(td,C1),eval(runleg)
xlabel('parameter td');
ylabel('yield of oil(kg/hr)');
title('plot of oil conc vs td for a given T1');
```

A.2.2 Temperature variations in zone 2

```matlab
% Main program to calculate the optimum values of P & td varying t2
```

```matlab
 clear all;
 clc;
i = 0;j = 0;k = 0;
%P = 0.1:0.1:1;
% td = 30
% td represents a vector of time and ntd is the no of time partitions
P = 0.3;ntd = 25;d =0.104;
td = linspace(5,30,ntd);
% T1, T2 & T3 are temp of zone 1,2 &3 resp.
T1 = 523;
%T2= 673;
T3= 723;
Tbins = 5;
T2 = linspace(603,643,Tbins);
Final_C = zeros((ntd*length(T2)),9);


for n = 1:length(T2);
   for h = 1:ntd;

        C_zone1 = zone1(P,td(h),d,T1);
        C_zone2 = zone2(P,td(h),d,T2(n),C_zone1);
        C_zone3 = zone3(P,td(h),d,T3,C_zone2);
        C_zone3 = (C_zone3)';
        i = i+1;
        Final_C(i,1) = P;
        Final_C(i,2) = td(h);
        Final_C(i,3) = C_zone3(1);
        Final_C(i,4) = C_zone3(2);
        Final_C(i,5) = C_zone3(3);
        Final_C(i,6) = C_zone3(4);
        Final_C(i,7) = T1;
        Final_C(i,8) = T2(n);
        Final_C(i,9) = T3;
        C2_zone3(i,1) = P;
        C2_zone3(i,2) = td(h) ;
        C2_zone3(i,3) = Final_C(i,4);
   end
end
```

159

```matlab
figure(1)
C1 = zeros(ntd,length(T2));
for idpp = 1:length(T2)
    C1(:,idpp) = Final_C((idpp - 1)*ntd + 1:idpp*ntd,4);
    if idpp == 1
        leg = sprintf('''T2 = %d''',',',T2(idpp));
    else
        lega = sprintf('''T2 = %d''',',',T2(idpp));
        leg = [leg,lega]; %#ok<AGROW>
    end
end
preleg = 'legend(';
leg(:,end) = ')';
runleg = [preleg,leg];
plot(td,C1),eval(runleg)
xlabel('parameter td');
ylabel('yield of oil (kg/hr)');
title('plot of oil conc vs td for a given T2');
```

```
****************************
```

A.2.3 Temperature variations in Zone 3

```matlab
% Main program to calculate the optimum values of a & td.

 clear all;
 clc;
i = 0;j = 0;k = 0;
%P = 0.1:0.1:1;
% td = 30
% td represents a vector of time and ntd is the no of time partitions
P = 0.3;ntd = 35;d =0.104;
td = linspace(5,40,ntd);
% T1, T2 & T3 are temp of zone 1,2 &3 resp.
T1 = 573;
T2= 673;
%T3= 673;
Tbins = 5;
T3 = linspace(723,773,Tbins);
```

```matlab
Final_C = zeros((ntd*length(T3)),9);
T3vec = zeros(ntd*length(T3),1);
for n = 1:Tbins;
    for h = 1:ntd;

        C_zone1 = zone1(P,td(h),d,T1);
        C_zone2 = zone2(P,td(h),d,T2,C_zone1);
        C_zone3 = zone3(P,td(h),d,T3(n),C_zone2);
        C_zone3 = (C_zone3)';
        i = i+1;
        Final_C(i,1) = P;
        Final_C(i,2) = td(h);
        Final_C(i,3) = C_zone3(1);
        Final_C(i,4) = C_zone3(2);
        Final_C(i,5) = C_zone3(3);
        Final_C(i,6) = C_zone3(4);
        Final_C(i,7) = T1;
        Final_C(i,8) = T2;
        Final_C(i,9) = T3(n);
        C2_zone3(i,1) = P;
        C2_zone3(i,2) = td(h) ;
        C2_zone3(i,3) = Final_C(i,4);
        T3vec(ntd*(n-1) + h) = T3(n);
    end
end


figure(1)
C1 = zeros(ntd,length(T3));
for idpp = 1:length(T3)
    C1(:,idpp) = Final_C((idpp - 1)*ntd + 1:idpp*ntd,4);
    if idpp == 1
        leg = sprintf('''T3 = %d'',',T3(idpp));
    else
        lega = sprintf('''T3 = %d'',',T3(idpp));
        leg = [leg,lega]; %#ok<AGROW>
    end
end
preleg = 'legend(';
leg(:,end) = ')';
runleg = [preleg,leg];
plot(td,C1),eval(runleg)
```

161

```matlab
xlabel('parameter td');
ylabel('yield of oil');
title('plot of oil conc vs td for a given T3');


% Get heat of pyrolysis, HT OF COMBUSTION in J/gr& exenergy in j/hr


htcomb_char = 26.4*10^3;



heats = heatpyro(Final_C(:,3),Final_C(:,4),Final_C(:,5),T3vec);


Final_C = [Final_C,heats];


exenergy = Final_C(:,5)*htcomb_char - Final_C(:,10);


Final_C = [Final_C,exenergy];


figure(2)
C2 = zeros(ntd,length(T3));
for idpp = 1:length(T3)
    C2(:,idpp) = Final_C((idpp - 1)*ntd + 1:idpp*ntd,11);
    if idpp == 1
        leg = sprintf('''T3 = %d''',',T3(idpp));
    else
        lega = sprintf('''T3 = %d''',',T3(idpp));
        leg = [leg,lega]; %#ok<AGROW>
    end
end
preleg = 'legend(';
leg(:,end) = ')';
runleg = [preleg,leg];
plot(td,C2),eval(runleg)
xlabel('parameter td');
ylabel('Excess energy in j/hr');
title('plot of excess energy(j/hr) vs td for a given T3');



 *************************************
```

162

A.3 Sensitivity of product yields with respect to variations in RTD parameters

```matlab
% Main program to calculate the optimum values of P & td.
 % P is the fraction of PFR volume, can vary from 0-1 but the best range is
 % 0.3-0.7 for the optimum result
 % THERE ARE SEVERAL VALUES OF d, but average values of d from the paper are
 % taken




 close all;
 clc;
 clear;




d= 0.108;
% bins represents the number of partitions of P
i = 0;  bins = 20;
td_val = 10:5:30;
P_val = linspace(0.3,0.7,bins);
Zee=bins*length(td_val);
iteration = 1000;


% final yield including P and td
Final_C = zeros(Zee,6);
Iter_C = zeros(iteration,4);


% TD DEPENDS ON THE TIME FRAME GIVEN IN THE PREVIOUS CONC CODE

idx = 0;
idxt = 0;
j=0;

  for idtd = 1:length(td_val);
      idx = idx + 1;
      td = td_val(idtd);

 for idP = 1:bins
  P = P_val(idP);
```

```matlab
    for itr = 1:iteration

        j=j+1;
        C_iter1 = zonez1(P,td,d);
        C_iter2 = zonez2(P,td,C_iter1,d);
        C_iter3 = zonez3(P,td,C_iter2,d);
        C_iter3 = (C_iter3)';
        %c1 is gas, c2 is tar, c3 is char, c4 is biomass
        Iter_C(j,1) = C_iter3(1);
        Iter_C(j,2) = C_iter3(2);
        Iter_C(j,3) = C_iter3(3);
        Iter_C(j,4) = C_iter3(4);
    end


        i=i+1;
        Final_C(i,1) = P;
        Final_C(i,2) = td;
        %c1 is gas, c2 is tar, c3 is char, c4 is biomass
        Final_C(i,3) = mean(Iter_C(:,1));
        Final_C(i,4) = mean(Iter_C(:,2));
        Final_C(i,5) = mean(Iter_C(:,3));
        Final_C(i,6) = mean(Iter_C(:,4));
        Final_C(i,7) = std(Iter_C(:,1));
        Final_C(i,8) = std(Iter_C(:,2));
        Final_C(i,9) = std(Iter_C(:,3));
        Final_C(i,10) = std(Iter_C(:,4));

    end



    end


    figure(1)
C1 = zeros(length(P_val),idx);
for idpp = 1:idx
    C1(:,idpp) = Final_C((idpp - 1)*bins + 1:idpp*bins,4);
    if idpp == 1
        leg = sprintf('''Tau_D = %d'',',td_val(idpp));
    else
```

```matlab
        lega = sprintf('''Tau_D = %d''',',',td_val(idpp));
        leg = [leg,lega]; %#ok<AGROW>
    end
end
preleg = 'legend(';
leg(:,end) = ')';
runleg = [preleg,leg];
plot(P_val,C1),eval(runleg)
xlabel('parameter P');
ylabel('Mean yield of oil');
title('plot of oil conc vs P for a given td');

 figure(2)
C2 = zeros(length(P_val),idx);
for idpp = 1:idx
    C2(:,idpp) = Final_C((idpp - 1)*bins + 1:idpp*bins,8);
    if idpp == 1
        leg = sprintf('''Tau_D = %d''',',',td_val(idpp));
    else
        lega = sprintf('''Tau_D = %d''',',',td_val(idpp));
        leg = [leg,lega]; %#ok<AGROW>
    end
end
preleg = 'legend(';
leg(:,end) = ')';
runleg = [preleg,leg];
plot(P_val,C1),eval(runleg)
xlabel('parameter P');
ylabel('Standard deviation of  yield of oil');
title('plot of std of oil conc vs P for a given td');

  ***********************************
```

A.4 Calculation of Arrhenius parameters from product yield

```matlab
% Main program to calculate the optimum values of P & td.
 % P is the fraction of PFR volume, can vary from 0-1 but the best range is
 % 0.3-0.7 for the optimum result
```

```matlab
% THERE ARE SEVERAL VALUES OF d, but average values of d from the paper are
% taken




close all;
clc;
clear;




d= 0.108;
% bins represents the number of partitions of P
i = 0;  bins = 20;
td_val = 10:5:30;
P_val = linspace(0.3,0.7,bins);
Zee=bins*length(td_val);
iteration = 1000;


% final yield including P and td
Final_C = zeros(Zee,6);
Iter_C = zeros(iteration,4);


% TD DEPENDS ON THE TIME FRAME GIVEN IN THE PREVIOUS CONC CODE

idx = 0;
idxt = 0;
j=0;

  for idtd = 1:length(td_val);
      idx = idx + 1;
      td = td_val(idtd);

 for idP = 1:bins
  P = P_val(idP);


  for itr = 1:iteration


       j=j+1;
        C_iter1 = zonez1(P,td,d);
        C_iter2 = zonez2(P,td,C_iter1,d);
```

```matlab
        C_iter3 = zonez3(P,td,C_iter2,d);
        C_iter3 = (C_iter3)';
        %c1 is gas, c2 is tar, c3 is char, c4 is biomass
        Iter_C(j,1) = C_iter3(1);
        Iter_C(j,2) = C_iter3(2);
        Iter_C(j,3) = C_iter3(3);
        Iter_C(j,4) = C_iter3(4);
    end


        i=i+1;
        Final_C(i,1) = P;
        Final_C(i,2) = td;
        %c1 is gas, c2 is tar, c3 is char, c4 is biomass
        Final_C(i,3) = mean(Iter_C(:,1));
        Final_C(i,4) = mean(Iter_C(:,2));
        Final_C(i,5) = mean(Iter_C(:,3));
        Final_C(i,6) = mean(Iter_C(:,4));
        Final_C(i,7) = std(Iter_C(:,1));
        Final_C(i,8) = std(Iter_C(:,2));
        Final_C(i,9) = std(Iter_C(:,3));
        Final_C(i,10) = std(Iter_C(:,4));

 end



  end


  figure(1)
C1 = zeros(length(P_val),idx);
for idpp = 1:idx
   C1(:,idpp) = Final_C((idpp - 1)*bins + 1:idpp*bins,4);
   if idpp == 1
       leg = sprintf('''Tau_D = %d'',',td_val(idpp));
   else
       lega = sprintf('''Tau_D = %d'',',td_val(idpp));
       leg = [leg,lega]; %#ok<AGROW>
   end
end
preleg = 'legend(';
leg(:,end) = ')';
```

```matlab
runleg = [preleg,leg];
plot(P_val,C1),eval(runleg)
xlabel('parameter P');
ylabel('Mean yield of oil');
title('plot of oil conc vs P for a given td');


 figure(2)
C2 = zeros(length(P_val),idx);
for idpp = 1:idx
   C2(:,idpp) = Final_C((idpp - 1)*bins + 1:idpp*bins,8);
   if idpp == 1
       leg = sprintf('''Tau_D = %d'',',td_val(idpp));
   else
       lega = sprintf('''Tau_D = %d'',',td_val(idpp));
       leg = [leg,lega]; %#ok<AGROW>
   end
end
preleg = 'legend(';
leg(:,end) = ')';
runleg = [preleg,leg];
plot(P_val,C1),eval(runleg)
xlabel('parameter P');
ylabel('Standard deviation of  yield of oil');
title('plot of std of oil conc vs P for a given td');
```

A.5 Total energy requirements

A.5.1 Main function

```matlab
% Main program to calculate the optimum values of P & td.
 % P is the fraction of PFR volume, can vary from 0-1 but the best range is
 % 0.3-0.7 for the optimum result
 % THERE ARE SEVERAL VALUES OF d, but average values of d from the paper are
 % taken
```

```matlab
 close all;
 clc;
 clear;



d= 0.108;
% bins represents the number of partitions of P
i = 0;  bins = 5;
td_val = 10:5:30;
P_val = linspace(0.3,0.7,bins);
Zee=bins*length(td_val);


% final yield including P and td
Final_C = zeros(Zee,6);


% TD DEPENDS ON THE TIME FRAME GIVEN IN THE PREVIOUS CONC CODE

idx = 0;
idxt = 0;

  for idtd = 1:length(td_val);
      idx = idx + 1;
      td = td_val(idtd);
 for idP = 1:bins
  P = P_val(idP);
        i=i+1;
      C_zone1 = zonez1(P,td,d);
      C_zone2 = zonez2(P,td,C_zone1,d);
      C_zone3 = zonez3(P,td,C_zone2,d);
      C_zone3 = (C_zone3)';
      Final_C(i,1) = P;
      Final_C(i,2) = td;
      %c1 is gas, c2 is tar, c3 is char, c4 is biomass
      Final_C(i,3) = C_zone3(1);
      Final_C(i,4) = C_zone3(2);
      Final_C(i,5) = C_zone3(3);
      Final_C(i,6) = C_zone3(4);


  end
```

```matlab
    end

  figure(1)
C1 = zeros(length(P_val),idx);
for idpp = 1:idx
   C1(:,idpp) = Final_C((idpp - 1)*bins + 1:idpp*bins,4);
   if idpp == 1
       leg = sprintf('''Tau_D = %d'',',td_val(idpp));
   else
       lega = sprintf('''Tau_D = %d'',',td_val(idpp));
       leg = [leg,lega]; %#ok<AGROW>
   end
end
preleg = 'legend(';
leg(:,end) = ')';
runleg = [preleg,leg];
plot(P_val,C1),eval(runleg)
xlabel('parameter P');
ylabel('yield of oil');
title('plot of oil conc vs P for a given td');
%
  Final_C;


  %Section where all energy utilities are defined Get heat of pyrolysis, HT
OF COMBUSTION in MJ/ton& exenergy in MJ/hr


htcomb_char = 26.4*10^3;
htcomb_gas = 18.3*10^3;
energy_grinding = 2812.5;  %based on 83.3ton/hr of biomass), MJ/hr
energy_drying = 91100; %based on 83.3ton/hr of biomass), MJ/hr
conc_biomass = 41.65; %based on 83.3ton/hr of biomass),ton
htcomb_natgas = 54*10^3; %(MJ/ton)
cp_char = 1.956; %MJ/ton/c


% Energy required for drying, MJ/hr
Final_C(:,7) = energy_drying;


%Energy required for grinding MJ/hr
```

```matlab
Final_C(:,8) = energy_grinding;


% heat required to do pyrolysis; heat of rxn only (HHV)MJ/hr
heats = heatpyro(Final_C(:,3),Final_C(:,4),Final_C(:,5));


Final_C = [Final_C,heats];


%heat required to cool oil from 500 to 25 degrees centigrade, MJ/ton, per
%ton of oil produced
oilheat = cooloil(Final_C(:,3),Final_C(:,4));


Final_C = [Final_C,oilheat];


%Energy available from heat of combustion, MJ/hr
tothtcomb = Final_C(:,5)*htcomb_char + Final_C(:,3)*htcomb_gas;


Final_C = [Final_C,tothtcomb];


% Energy available from combustion of natural gas, MJ/ton


Final_C(:,12)= htcomb_natgas;


% this section deals with energy balance(as we have additional energy all
% the time

extranergy = Final_C(:,11)- (Final_C(:,9));
Final_C = [Final_C,extranergy];


% Char not combusted tons/hr
wtchar_notcomb = Final_C(:,5)-(((Final_C(:,9))-
Final_C(:,3)*htcomb_gas*0.70)/(htcomb_char*(0.70)));
Final_C = [Final_C,wtchar_notcomb];


%energy from remaining char is completely combusted for drying, MJ/hr
energy_deficitdry = Final_C(:,7)- (Final_C(:,14)*htcomb_char)*(0.40);
Final_C = [Final_C,energy_deficitdry];


% energy from gas and char is completely used to dry the woody biomass,
% energy left
energy_excessdry = Final_C(:,11)*(.20)- Final_C(:,7);
```

```matlab
Final_C = [Final_C,energy_excessdry];



%heat available from heat of combustion of gas (j/gr)
%
% htgascomb=18273;
% gascomb= Final_C(:,3)*htgascomb;
% Final_C = [Final_C,gascomb];



% Final_C 3=GAS, 4=OIL,5=CHAR,6=BIOMASS,7=HT REQ TO DO PYROLYSIS,8= EXCESS
% ENERGY AVAILABLE AFTER USED FOR PYROLYSIS,9= ENERGY REQUIRED TO COOL OIL,
%10= HT AVAILABLE FROM GAS COMBUSTION



 figure(2)
C2 = zeros(length(P_val),idx);
for idpp = 1:idx
   C2(:,idpp) = Final_C((idpp - 1)*bins + 1:idpp*bins,13);
   if idpp == 1
       leg = sprintf('''Tau_D = %d'',',td_val(idpp));
   else
       lega = sprintf('''Tau_D = %d'',',td_val(idpp));
       leg = [leg,lega]; %#ok<AGROW>
   end
end
preleg = 'legend(';
leg(:,end) = ')';
runleg = [preleg,leg];
plot(P_val,C2),eval(runleg)
xlabel('parameter P');
ylabel('Additional energy available from pyrolysis if gas and char are
completely combusted (MJ/hr)');
title('plot of excess energy(MJ/hr) vs P for a given td');

figure(3)
C3 = zeros(length(P_val),idx);
for idpp = 1:idx
   C3(:,idpp) = Final_C((idpp - 1)*bins + 1:idpp*bins,14);
   if idpp == 1
       leg = sprintf('''Tau_D = %d'',',td_val(idpp));
```

```matlab
        else
            lega = sprintf('''Tau_D = %d'',',td_val(idpp));
            leg = [leg,lega]; %#ok<AGROW>
        end
    end
    preleg = 'legend(';
    leg(:,end) = ')';
    runleg = [preleg,leg];
    plot(P_val,C3),eval(runleg)
    xlabel('parameter P');
    ylabel('Weight of char as a product (Tons/hr) after partially used for
    combustion');
    title('plot of excess char (Tons/hr) vs P for a given td');


    figure(4)
    C4 = zeros(length(P_val),idx);
    for idpp = 1:idx
        C4(:,idpp) = Final_C((idpp - 1)*bins + 1:idpp*bins,10);
        if idpp == 1
            leg = sprintf('''Tau_D = %d'',',td_val(idpp));
        else
            lega = sprintf('''Tau_D = %d'',',td_val(idpp));
            leg = [leg,lega]; %#ok<AGROW>
        end
    end
    preleg = 'legend(';
    leg(:,end) = ')';
    runleg = [preleg,leg];
    plot(P_val,C4),eval(runleg)
    xlabel('parameter P');
    ylabel('Heat removal to cool biooil (MJ/ton)');
    title('plot of heat removal(MJ/ton) to cool bio oil per ton of oil produced
    vs P for a given td');
    %
    % mean(Final_C(:,9));
    % std(Final_C(:,9));

    figure(5)
    C5 = zeros(length(P_val),idx);
    for idpp = 1:idx
        C5(:,idpp) = Final_C((idpp - 1)*bins + 1:idpp*bins,15);
```

173

```matlab
    if idpp == 1
        leg = sprintf('''Tau_D = %d''',',td_val(idpp));
    else
        lega = sprintf('''Tau_D = %d''',',td_val(idpp));
        leg = [leg,lega]; %#ok<AGROW>
    end
end
preleg = 'legend(';
leg(:,end) = ')';
runleg = [preleg,leg];
plot(P_val,C5),eval(runleg)
xlabel('parameter P');
ylabel('Net deficit energy required after  hot char is completely combusted
for drying(MJ/hr)');
title('plot net deficit energy after remaining hot char is completely
combusted for drying(MJ/hr) vs P for a given td');


figure(6)
C6 = zeros(length(P_val),idx);
for idpp = 1:idx
    C6(:,idpp) = Final_C((idpp - 1)*bins + 1:idpp*bins,16);
    if idpp == 1
        leg = sprintf('''Tau_D = %d''',',td_val(idpp));
    else
        lega = sprintf('''Tau_D = %d''',',td_val(idpp));
        leg = [leg,lega]; %#ok<AGROW>
    end
end
preleg = 'legend(';
leg(:,end) = ')';
runleg = [preleg,leg];
plot(P_val,C6),eval(runleg)
xlabel('parameter P');
ylabel('Net excess energy left after  hot char and gas is completely
combusted for drying(MJ/hr)');
title('plot of net excess energy remaining hot char and gas is completely
combusted for drying(MJ/hr) vs P for a given td');


A.5.2 Mean specific heat and latent heat of vaporization of oil


% Heat of cooling oil


function heatoilcool
```

```matlab
s = load('C:\Documents and Settings\agoteti3\My
Documents\MATLAB\Energy\oilparameters');
r = load('C:\Documents and Settings\agoteti3\My
Documents\MATLAB\Energy\hvoil');
p = load('C:\Documents and Settings\agoteti3\My
Documents\MATLAB\Energy\gcm');


oil_parameters = s.oil_parameters;
hvoil = r.hvoil;
gcm = p.gcm;



    function cpaveoil = cpcalc
        ncomp = size(oil_parameters,1);
        oilcomp = (oil_parameters(:,2) - oil_parameters(:,1)).*rand(ncomp,1)
+ oil_parameters(:,1);
        oilcomp = oilcomp/sum(oilcomp);
        cpmassbased = (oil_parameters(:,4)./oil_parameters(:,3));
        cpaveoil = sum(cpmassbased.*oilcomp);
    end
ncomp = size(oil_parameters,1);
tb = zeros(ncomp,1);
tc = zeros(ncomp,1);
pc = zeros(ncomp,1);
hv = zeros (ncomp,1);
% R is in J/mol/K
R = 8.314;
%hv in MJ/ton, cp is in MJ/ton/k

    function hvaveoil = hvcalc
        ncomp = size(oil_parameters,1);
        oilcomp = (oil_parameters(:,2) - oil_parameters(:,1)).*rand(ncomp,1)
+ oil_parameters(:,1);
        oilcomp = oilcomp/sum(oilcomp);
    for i = 1: ncomp
        tb(i) = 198 + sum(gcm(3,:).*hvoil(i,:));
        tc(i) = tb(i)/((0.576)+ (sum(gcm(1,:).*hvoil(i,:)))-
(sum(gcm(1,:).*hvoil(i,:)))^2);
        pc(i)= oil_parameters(i,3)/(0.34+ sum(gcm(2,:).*hvoil(i,:)))^2;
        tbr(i) = tb(i)./tc(i);
        hv(i) = (1.093*R*tc(i)*tbr(i)*(log(pc(i))-1))/(0.930-tbr(i));
    end
```

```
      hvgrbased= hv./oil_parameters(:,3);
       hvaveoil = sum(hvgrbased.*oilcomp);
    end
iter = 100000;
cpiter = zeros(iter,1);
for j = 1:iter
    cpiter(j) = cpcalc;
    hviter(j) = hvcalc;
end

Cpave = mean(cpiter)
Cpstd = std(cpiter)
hvave = mean(hviter)
hvstd = std(hviter)

figure(1)
plot(cpiter)

figure(2)
plot(hviter)

end
```
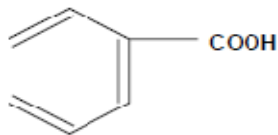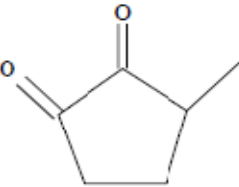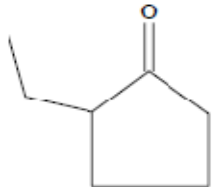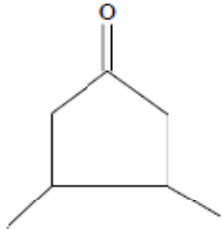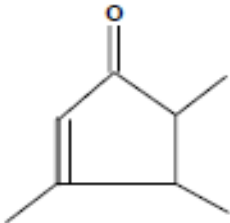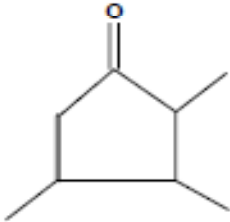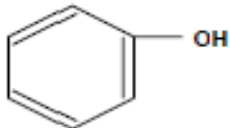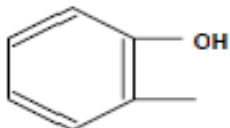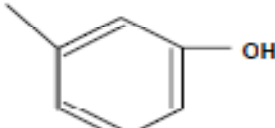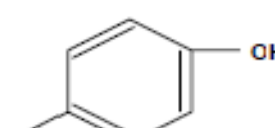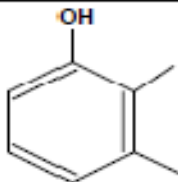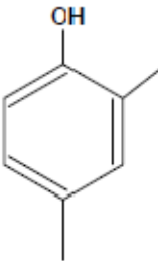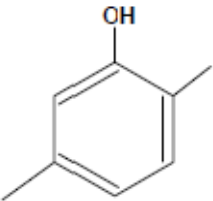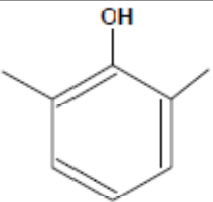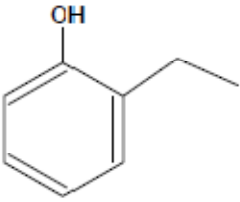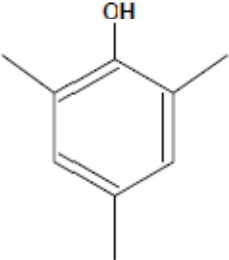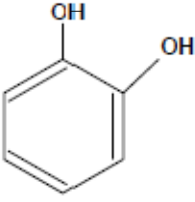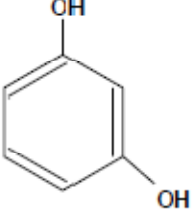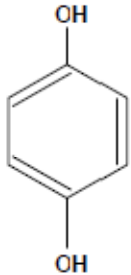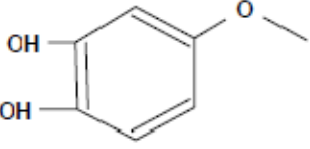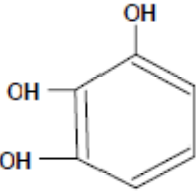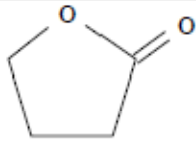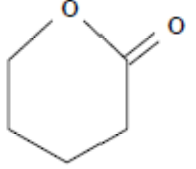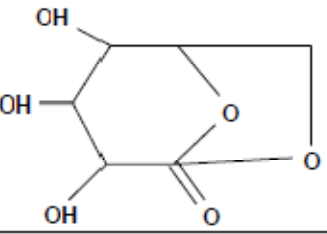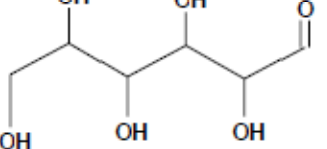
APPENDIX B

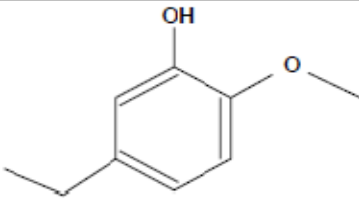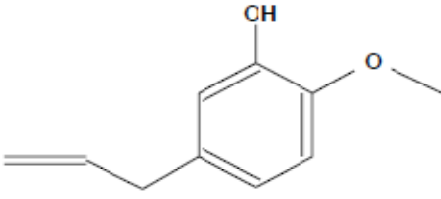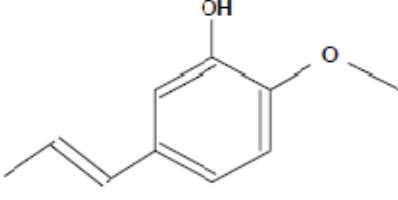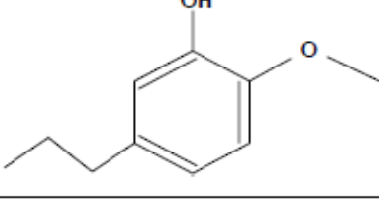## B.1 Atomic Structures and Formulas for Components in Bio-oil
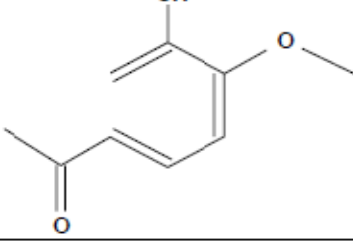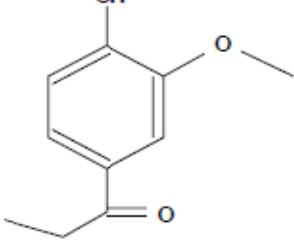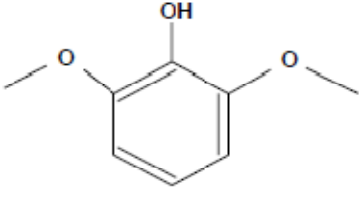
1	Formic acid	H-COOH	CH_2O_2
2	Acetic acid	CH_3-COOH	$C_2H_4O_2$
3	Propanoic acid	CH_3-CH_2-COOH	$C_3H_3O_2$
4	Hydroxyacetic acid	OH-CH_2-COOH	$C_2H_4O_3$
5	Butanoic acid	CH_3-$(CH_2)_2$-COOH	$C_4H_8O_2$
6	Pentanoic acid	CH_3-$(CH_2)_3$-COOH	$C_5H_{10}O_2$
7	4-Oxypentanoic acid	CH_3-CO-$(CH_2)_2$-COOH	$C_5H_8O_3$
8	Hexanoic acid	CH_3-$(CH_2)_4$-COOH	$C_6H_{12}O_2$
9	Benzoic acid		$C_7H_6O_2$
10	Heptanoic acid	CH_3-$(CH_2)_5$-COOH	$C_7H_{14}O_2$
11	Methanol	CH_3-OH	CH_4O
12	Ethanol	CH_3-CH_2-OH	C_2H_6O
13	Ethylene Glycol	OH-CH_2-CH_2-OH	$C_2H_6O_2$
14	Acetone	CH_3-CO-CH_3	C_3H_6O
15	2-Butanone	CH_3-CO-CH_2-CH_3	C_4H_8O
16	2,3-Pentenedione	CH_3-CO-CO-CH_2-CH_3	$C_5H_8O_2$
17	3Me2cyclopenten2ol1one		$C_6H_8O_2$
18	2-Et-cyclopentanone		$C_7H_{12}O$
19	Dimethylcyclopentanone		$C_7H_{12}O$

177
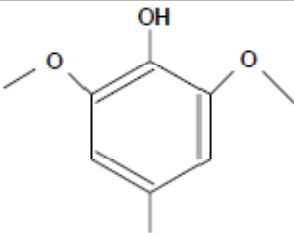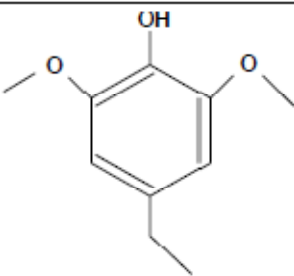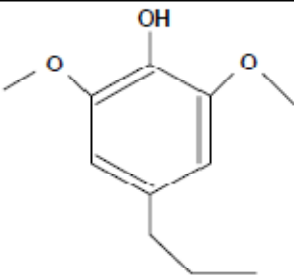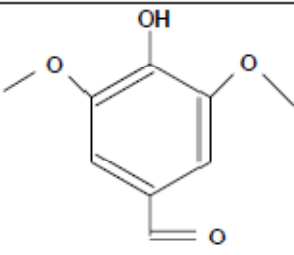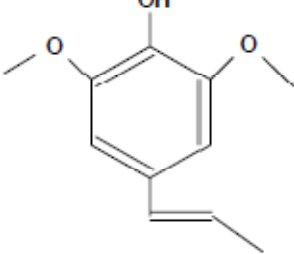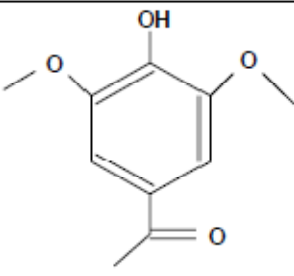
20	Trimethylcyclopentenone		$C_8H_{12}O$
21	Trimethylcyclopentanone		$C_8H_{14}O$
22	Formaldehyde	H-CHO	CH_2O
23	Acetaldehyde	CH_3-CHO	C_2H_4O
24	2-Propenal	CH_2=CH-CHO	C_3H4O
25	2-Methyl-2-butenal	CH_3-CH=C(CH_3)-CHO	C_5H_8O
26	Pentanal	CH_3-(CH_3)$_3$-CHO	$C_5H_{10}O$
27	Ethanedial	CHO-CHO	$C_2H_2O_2$
28	Phenol		C_6H_6O
29	2-Methyl Phenol		C_7H_8O
30	3-Methyl Phenol		C_7H_8O
31	4-Methyl Phenol		C_7H_8O
32	2,3 Dimethyl Phenol		$C_8H_{10}O$

33	2,4 Dimethyl Phenol		$C_8H_{10}O$
34	2,5 Dimethyl Phenol		$C_8H_{10}O$
35	2,6 Dimethyl Phenol		$C_8H_{10}O$
36	2-Ethylphenol		$C_8H_{10}O$
37	2,4,6 TriMe Phenol		$C_9H_{12}O$
38	1,2 DiOH Benzene		$C_6H_6O_2$
39	1,3 DiOH Benzene		$C_6H_6O_2$
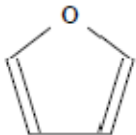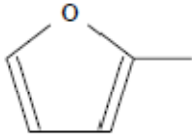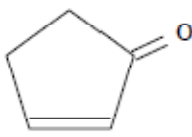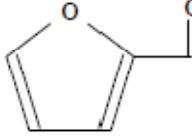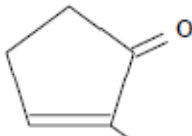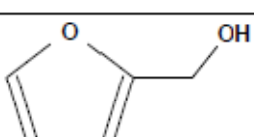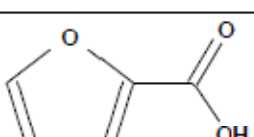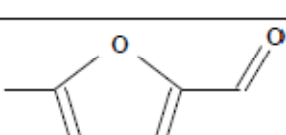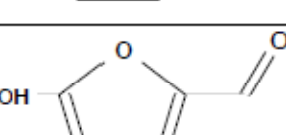
40	1,4 DiOH Benzene		$C_6H_6O_2$
41	4-Methoxy Catechol		$C_7H_8O_3$
42	1,2,3 Tri-OH-Benzene		$C_6H_6O_3$
43	Methyl Formate	$CH_3-O-CHO$	$C_2H_4O_2$
44	Butyrolactone		$C_4H_6O_2$
45	Valerolactone		$C_5H_8O_2$
46	Angelicalactone		$C_5H_6O_2$
47	Levoglucosan		$C_6H_{10}O_5$
48	Glucose		$C_6H_{12}O_6$
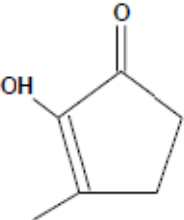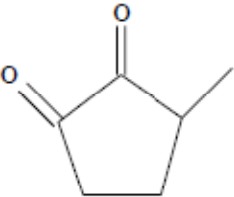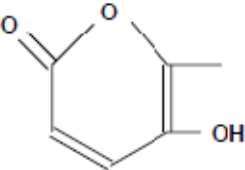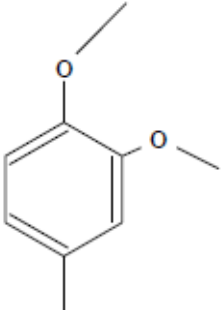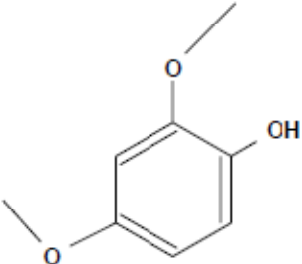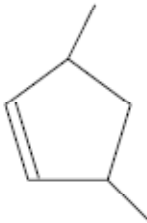
49	Fructose		$C_6H_{12}O_6$
50	D-Xylose		$C_5H_{10}O_5$
51	D-Arabinose		$C_5H_{10}O_5$
52	Cellobiosan		$C_{12}H_{20}O_{10}$
53	1,6 Anhydroglucofuranose		$C_6H_{10}O_5$
54	2-Methoxy Phenol		$C_7H_8O_2$
55	4-Methyl Guaiacol		$C_8H_{10}O_2$
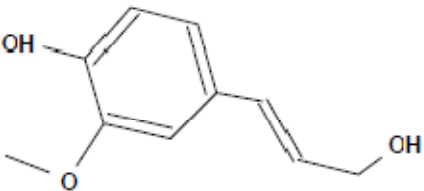
56	Ethyl Guaiacol		$C_9H_{12}O_2$
57	Eugenol		$C_{10}H_{12}O_2$
58	Isoeugenol		$C_{10}H_{12}O_2$
59	4-Propylguaiacol		$C_{10}H_{14}O_2$
60	Acetoguaiacone		$C_9H_{10}O_3$
61	Propioguaiacone		$C_{10}H_{12}O_3$
62	2,6-DiOMe Phenol		$C_8H_{10}O_3$

63	Methyl Syringol		$C_9H_{12}O_3$
64	4-Ethyl Syringol		$C_{10}H_{14}O_3$
65	Propyl Syringol		$C_{11}H_{16}O_3$
66	Syringaldehyde		$C_9H_{10}O_4$
67	4-Propenyl Syringol		$C_{11}H_{14}O_3$
68	4-OH-3,5-DiOMe Phenyl Ethanone		$C_{10}H_{12}O_4$

69	Furan		C_4H_4O
70	2-Methyl Furan		C_5H_6O
71	2-Furanone		$C_4H_4O_2$
72	Furfural		$C_5H_4O_2$
73	3-Methyl-2(3h) Furanone		$C_5H_6O_2$
74	Furfural alcohol		$C_5H_6O_2$
75	Furoic Acid		$C_5H_4O_3$
76	5-Methyfurfural		$C_6H_6O_2$
77	5-OH-Methyl-2-Furfural		$C_6H_6O_3$
78	Hydroxyacetaldehyde	$OH-CH_2-CHO$	$C_2H_4O_2$
79	Acetol	$CH_3-CO-CH_2-OH$	$C_3H_6O_2$
80	Acetal	$(C_2H_5O)CH-CH_3$	$C_6H_{14}O_2$
81	Acetyloxy-2-propanone	$CH_3-CO-O-CH_2-CO-CH_3$	$C_5H_8O_3$

82	2-OH-3-Me-2-cyclopentene-1-one		$C_6H_8O_2$
83	Methyl Cyclopentenolone		$C_6H_8O_2$
84	1-Acetyloxy-2-Propanone	$CH_3-CO-O-CH_2-CO-CH_3$	$C_5H_8O_3$
85	2-Methyl-3-hydroxy-2-pyrone		$C_6H_6O_3$
86	2-Methoxy-4-methylanisole		$C_9H_{12}O_2$
87	4-OH-3 methoxybenzaldehyde		$C_8H_8O_3$
88	Dimethylcyclopentene		C_7H_{12}

89	Pyrolytic Lignin		C$_7$H$_9$O$_3$

B.2 Property values of different functional groups (Reid et. al, 1977)

Property values	Non Ring groups									
	(-CH3)	(-CH2-)	(>CH-)	(>C<)	(=CH2)	(=CH-)	(=C<)	(=C=)	(≡CH)	(≡C-)
Del T	0.02	0.02	0.012	0	0.018	0.018	0	0	0.005	0.005
Del P	0.227	0.227	0.21	0.21	0.198	0.198	0.198	0.198	0.153	0.153
Gi	23.58	22.88	21.74	18.25	18.18	24.96	24.14	26.15	9.2	27.38
	Ring groups									
	(-CH2-)	(>CH-)	(>C<)	(=CH-)	(=C<)	(=C=)				
Del T	0.013	0.012	-0.007	0.011	0.011	0.011				
Del P	0.184	0.192	0.154	0.154	0.154	0.154				
Gi	27.15	21.78	21.32	26.73	31.01	0				
	Oxygen groups									
	(-OH (alco	(-OH (phe	(-O- (nonr	(-O- (ring)	(>C=O (no	(>C=O (rin	(O=CH- (a	(-COOH (a	(-COO- (e	(=O (rest)
Del T	0.082	0.031	0.021	0.014	0.04	0.033	0.048	0.085	0.047	0.02
Del P	0.06	-0.02	0.16	0.12	0.29	0.2	0.33	0.4	0.47	0.12
Gi	92.88	76.34	22.42	31.22	76.75	94.97	72.24	169.09	81.1	-10.5

TOTAL BARE MODULE COST OF INSTALLED EQUIPMENT

Total bare module cost of standard equipment is estimated from "Product and Process Design Principles by *Seider, Seader, Lewin and Widagdo (SSLW),* 3rd edition". A general algorithm to calculate the total bare module cost of standard equipment in a unit operation is described as follows:

Evaluate the energy and mass balance around the unit operation

Calculate the size factor (S) used in the cost correlation

Calculate the equipment purchase cost from Table 22.33 of SSLW-3rd edition.

Calculate the current CE index, material factor (F_M) and bare module factor from Chapter 22 of SSLW-3rd edition

Calculate the current bare module cost of the equipment
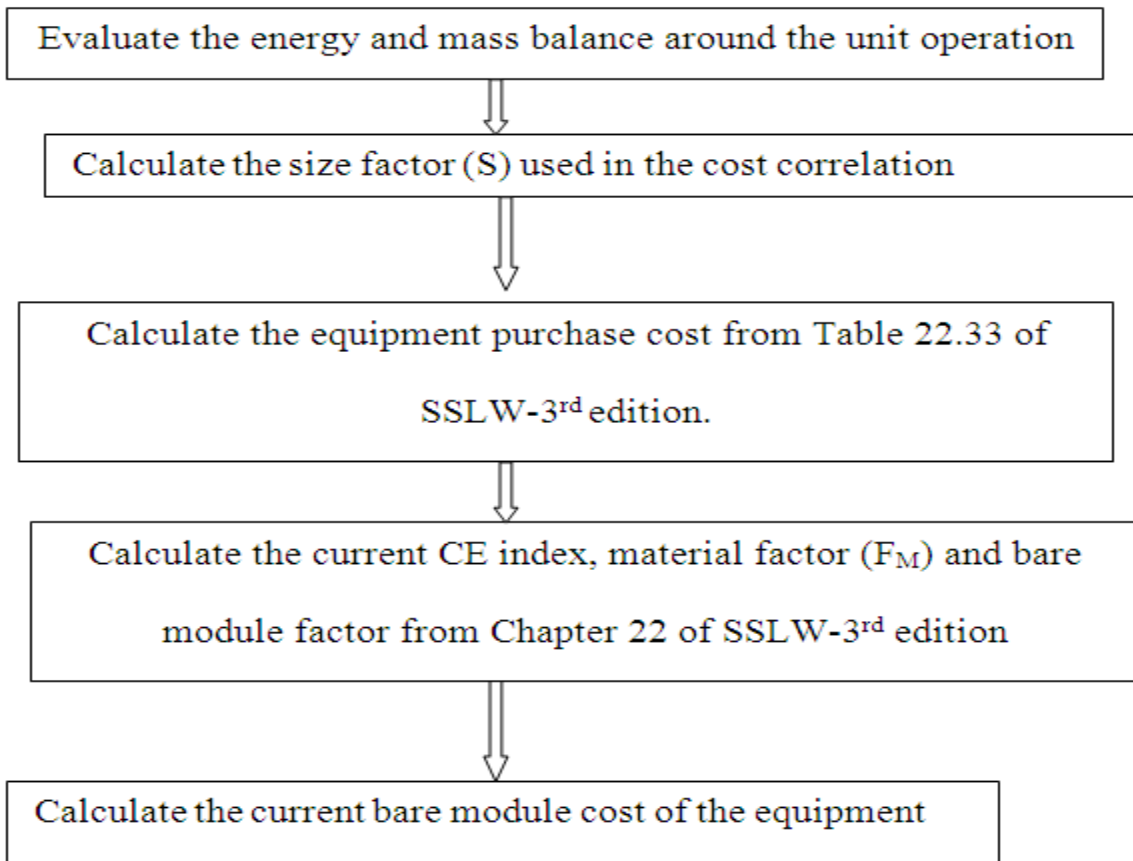
Figure C. 1: Flow chart to calculate the bare module cost of equipment

The factors considered in the total bare module cost calculations are equipment purchase cost, field material cost, direct field labor cost, indirect module expenses (Freight, contractor engineering expenses). Calculation of non standard equipment like the dyer and pyrolysis reactor, are based on some assumptions and data taken from commercial units.

Pyrolysis reactor

Main components of pyrolysis reactor are the screw conveyor and the fired heater used for supplying heat for pyrolysis reaction. Cost of screw conveyor is a function of conveyor length and diameter. Cost of fired heater is a function of heat duty.

A.) Conveyor cost: Flow rate and residence time of solids in the extruder are assumed and the volume is calculated. Diameter of the screw root is assumed and length of the conveyer is calculated based on the total area. This process is iterated so that the length to diameter of the screw ratio is less than 20. Our calculations resulted in 6 parallel auger units.

B.) Fired heater cost: Total heat load is divided between 6 units and the total cost is estimated from standard procedure given in Seider (2009).

The sum of total bare module cost of these six parallel units is approximated as the cost of pyrolysis reactor. Table C1 summarizes the total bare module cost of the auger reactor.

Table C. 1: Cost components and sizing of the auger reactor

Initial Sizing						
	Use ground up wood (same as batch pretreater)					
	Density of dry chips		0.5	g/cc	bulk + cells	
	Water		1	g/cc		
	assume 90% solids		0.9			
	Average density		0.55	g/cc		
	Pick mass flow in		7,638,889	g/h		
	Pick residence time		2	min		
	Volume rate in		13888889	cc/h		
	Volume of reactor		462963	cc		
	3X volume		1388889	cc		
	call it		1388889	cc		
	assume D screw root		40	cm		
	assume D barrel		60	cm		
	area		1570	cm^2		
	length		885	cm		
	length + 5 %		931	cm	for screw flights	
	L/D		16			
energy balance						
	Tin, C	25	298	K		
	Tmax, C	500	773	K		
	Heat of Reaction		1640	kJ/kg	Van de Velden, et al, 2010	
	Cp for wood		0	kJ/kg/K	Van de Velden, et al, 2010	
	Heat up		0	kJ/h	0	BTU/h
	Pyrolysis		11,275,000	kJ/h	10,687,204	BTU/h
	Total		11,275,000	kJ/h	10,687,204	BTU/h
	No of units		6			
	wood flow rate		7,639	kg/h	183.3333333	tons/day
			7,638,889	g/h	Per single conveyor	
	CE Index	500				
Screw Conveyor						
Cost (1 unit), $		12,522	p. 595 in SSLW, 3rd edition, wo drive, wo heaters			
Total cost	75,132		Six parallel conveyors			
Current CE INDEX	615					
Actual cost (2009)	92,457					
Bare module factor	1.61					
Total bare module cost	148856.56					
Reaction rate k		A	34,700	s-1	Van de Velden, et al, 2010	
		del H	68.4	kj/mol	Van de Velden, et al, 2010	
		R	8.314	J/mol		
		k	0.828145078	s-1	at 400 C	
Fired heater for pyrolysis cost						
Efficiency of heat transfer	0.7					
$		428,316	p. 592 in SSLW, 3rd edition		500,000,000	BTU/h max
Total cost	2,569,893		Six parallel heaters			
Current CE INDEX	615					
Actual cost (2009)	3,162,511					
Stainles steel material factor	1.17					
Bare module factor	2.19					
Total bare module cost	8,103,301					
Total Reactor cost (million $)	8.252					

Rotary dryer

Dryer was sized from a pilot scale dryer designed by Meza. et.al (2008) to reduce the moisture content of the wood chips from 50% to 10%. The total surface area required to dry the wood chips from 50% moisture content to 10% moisture content is around 1560 m^2. Based on the total area of the dryer, the cost of the dryer is estimated as $ 16.57 million. A quote from the Matches (http://www.matche.com/) estimated the cost of dryer to be around $ 8.93 million. This is considered as the total bare module cost as the cost information given in SSLW is not applicable in the range of area of the dryer.

Grinder

The cost of grinder was tabulated from standard procedure from SSLW and it is tabulated in Table C2.

Table C. 2: Total bare module cost of Grinder

Grinding parameters		
Feed rate to ball mill (ton/hr)	49.98	Includes motor and drive
CE Index	500	
Cost of one unit ($)	595784	1-30 ton/hr
Cost of second unit($)	450076	
Total cost ($)	1045859	
CE Index (2009)	615	
Actual cost(2009) ($)	1287035	
Bare module factor	2.3	
Total bare module cost (million $)	**2.96**	

Combustor

The combustor is used to burn the natural gas and non-condensable gas from the pyrolysis to supply the heat energy required from drying wood chips. The cost of combustor evaluated using standard approach is $ 34.60 million as tabulated in Table C3. This was considered to be too expensive and a quote from Matches (http://www.matche.com/) which estimated the cost of the combustor for the given duty to be around $ **8.48** million is used instead.

Table C. 3: Total bare module cost of combustor

Heat load for dryer (MJ/hr)	91100
Efficiency of rotary dryer	0.2
Heat load for combustor (MJ/hr)	455500
Heat load (million BTU/hr)	432
CE Index	500
Cost of combustor (million $)	6.42
Cost factor for stainless steel	2
CE Index(2009)	615
Bare module factor	2.19
Total bare module cost (million $)	34.60

Shell and tube heat exchanger

Standard approach from SSLW is followed for the total bare module cost and the result is tabulated in Table C4.

Table C. 4: Total Bare module cost of Shell and Tube heat exchanger

Condenser parameters	
Heat duty of the shell and tube heat exchanger (MJ/hr)	63993
Inlet water temperature (^{0}c)	25
Exit water temperature (^{0}c)	35
Efficiency of heat transfer (%)	70
CP of water (MJ/ton/C)	4.1806
Flow rate of water (ton/hr)	2187
Inlet temperature of vapor (^{0}C)	500
Outlet temperature of oil	35
Log mean temperature diff	119
Mean average heat transfer coefficient (W/m^{2}K)	400 (Table 14.5, Peter et al., 2003)
Area of the heat exchanger (m^2)	375
Area of the heat exchanger (ft^2)	4034
CE index	500
Base cost (CB)	26645
FM	4.00
Length of condenser (ft)	20
FL	1
Pressure on shell side (psig)	90
FP	0.99
Total base cost ($)	106232
CE index (2009)	615
Actual cost ($)	130729
Bare module factor ($)	3.17
Total bare module cost (million $)	**0.414**

APPENDIX D

Labor operating cost

The Direct wages and Benefit (DW&B) cost related to the labor operations is estimated from "Product and Process Design Principles by *Seider, Seader, Lewin and Widagdo (SSLW),* 3rd edition".

From Table 22.3 of SSLW, number of operators required for a 2000ton/day of feedstock is 20. The annual cost of DW &B is obtained from:

DW&B, $/yr = (operators/shift)*(5 shifts)*(2,080 hr/yr operator)*($ 35/hr)   (D1)

Using equation D1, the direct wages and benefit cost is estimated to be $ 7.28 million. Note that the plant is operate for 330 days in a year and the rest is utilized for maintenance.

Electricity utility

The power consumption of standard rotary dryer and ball mill grinder are obtained from commercial manufacturing companies (Dusk drying system Inc. and SBM China Inc). The dryers and grinders are scaled and the power requirements are calculated accordingly. These units are assumed to operate at 60% efficiency of their ratings. The power consumption for

dryer and grinder is 1000KW and 800KW respectively. Hence, the total power consumption of these units operations is approximately 1800KW. Hence the total power consumption is approximately 3000KW. The sources used for the estimation of power requirements are as follows:

http://www.sbmchina.com/product/grinding/ball-mill/ball_mill.php (last viewed, July 2010)

http://www.duskedryingsystems.com/drying-systems.htm (last viewed, July 2010)

Natural gas utility

The natural gas is combusted to supply heat for the dryer. Based on the energy calculations, after the gas produced from pyrolysis of wood chips is combusted to provide the energy to dryer, there is a deficit of approximately 67,000 MJ/hr. This deficit is supplied by combustion of natural gas from external source. Accounting for 20% efficiency of drying, the amount of natural gas to provide additional energy is 6.2 ton/hr. Annual volumetric consumption is approximately $72*10^6$ m^3/yr.

REFERENCES

Abdullah, H. and Wu, H.,2009, "Biochar as a Fuel: 1. Properties and Grindability of Biochars Produced from the Pyrolysis of Mallee Wood under Slow-Heating Conditions" *Energy and Fuels*, 23, PP. 4174-4181

Adam, J., Blazso´, M., Me´sza´ros, E., Sto¨cker, M., Nilsen, M. H., Bouzga, A., Hustad, J. E., Grønli, M., Øye, G., 2005, "Pyrolysis of Biomass in the Presence of Al-MCM-41 Type Catalysts", *Fuel*, 84(12-13), PP. 1494-1502

Atutxa, A., Aguado, R., Gayubo, A. G., Olazar, M., and Bilbao, R., 2005, "Kinetic Description of the Catalytic Pyrolysis of Biomass in a Conical Spouted Bed Reactor", *Energy Fuels, 19*(3), PP. 765-774

Bahng, M., Mukarakate, C., Robichaud, D., and Nimlos, M., 2009, "Current Technologies for Analysis of Biomass Thermochemical Processing: A Review", Analytica Chimica Acta, 651(2), PP. 117-138

Biomass as Feedstock for a Bioenergy and Bioproducts Industry: The Technical Feasibility of Billion-Ton Annual Supply, Technical Report, USDA (U.S. Department of Agricultural-Forestry Service), April 2005 (available at: http://feedstockreview.ornl.gov/pdf/billion_ton_vision.pdf)

Blackledge, R. D., 1992, "Application of Pyrolysis Gas Chromatography in Forensic Science", Forensic Science Reviews, 4(1), PP. 1-16

Bridgewater, A. V., Meier, D., and Radlein, D., 1999, "An Overview of Fast Pyrolysis of Biomass", *Organic Geochemistry*, 30, PP. 1479-1493

Bridgewater, A.V. and Peacocke, G. V. C, 2000, "Fast Pyrolysis for Biomass", *Renewable and Sustainable Energy Reviews*, 4, PP. 1-73

Bridgwater, A. V., Czernik, S., and Pikorz, J., 2003, "The Status of Biomass Fast Pyrolysis," Chapter 1, In: Bridgwater A. V., Ed., *Fast Pyrolysis of Biomass: A Handbook*. Vol. 2, New Greenham Park: CPL Scientific Publishing Services Ltd

Bridgwater, A. V., Toft, A. J., and Brammer, J. G., 2002, "A Techno-Economic Comparison of Power Production by Biomass Fast Pyrolysis with Gasification and Combustion" *Renewable & Sustainable Energy Reviews*, 6, PP. 181-248.

Bridgwater, A., Czernik, S., Piskorz, J., 2001, "An Overview of Fast Pyrolysis", in: Bridgwater, A.V. (Ed.), *Progress in Thermochemical Biomass Conversion*, Blackwell Science, London, P. 977

Bridgwater, A.V. and Kuester, J. L., 1991, *Research in Thermochemical Biomass Conversion*, Elsevier Science, London

Bridgwater, A.V., 2003, "Renewable Fuels and Chemicals by Thermal Processing of Biomass", *Chemical Engineering Journal*, 91(2-3), PP. 87-102

Brown, D. S., 1979, Abstracts of Papers of the American Chemical Society, P 9.

Daugaard, D. E. and Brown, R. C., 2003, "Enthalpy of Pyrolysis for several types of Biomass," *Energy and Fuels*, 17, PP. 934-939

Davis, S. C. Transportation Energy Data Book 18, Technical Report ORNL-6941, Oak Ridge National Laboratory, Oak Ridge, TN, September 1998 (available at: http://cta.ornl.gov/data/Index.shtml)

Dean, J. A., 1987, *Handbook of Organic Chemistry*, McGraw-Hill, New York

Demirbas, A. and Arin, G., 2002, "An Overview of Biomass Pyrolysis", *Energy Sources Part A*, 24, PP. 471-482

Di Blasi, C., 2006, "Modeling Chemical and Physical Processes of Wood and Biomass Pyrolysis", *Progress in Energy and Combustion Science*, 34, PP. 47-90

Diebold J. P., 2003, "A Review of the Chemical and Physical Mechanisms of the Storage Stability of Fast Pyrolysis Bio-Oils". In: Bridgwater A. V., Ed., *Fast Pyrolysis of Biomass: A Handbook*, Vol. 2, New Greenham Park: CPL Scientific Publishing Services Ltd

Diebold, J. and Scahill, J., 1988, in: E.J. Soltes and T.A. Milne (Eds.), In Pyrolysis Oils from Biomass: Producing, Analyzing, and Upgrading, American Chemical Society, Washington, DC, PP. 31

Energy Information Administration, "Cost of No. 2 heating oil 2010"
http://www.eia.gov/dnav/pet/pet_pri_dist_dcu_nus_m.htm Accessed 2010

Ericsson, I., 1985, "Influence of Pyrolysis Parameters on Results in Pyrolysis-Gas Chromatography", *Journal of Analytical and Applied Pyrolysis*, 8, PP. 73-86

Fukushima, K., Saito, K., Kato, T., Takamori, H., Kishimoto, T., and Yamamoto, A., 2006, "A New Analysis of the Depolymerized Fragments of Lignin Polymer in the Plant Cell Walls Using ToF-SIMS", *Applied Surface Science*, 252(19), PP. 6734-6737

Fulcheri, L. and Schwob, Y., 1995, "From Methane to Hydrogen, Carbon Black and Water", *International Journal of Hydrogen Energy*, 20(3), PP. 197-202

Garcia, L., Salvador, M. L., Arauzo, J., and Bilbao, R., 2001, "Catalytic pyrolysis of biomass: influence of the catalyst pretreatment on gas yields", *Journal of Analytical and Applied Pyrolysis, 58-59*, PP. 491-501

Goyal, H. B., Saxena, R. C., and Seal, D., 2008, "Thermochemical Conversion of Biomass to Liquids and Gaseous Fuels", in: A. Pandey (Ed.), *Handbook of Plant-Based Biofuels*, CRC Press, P. 29

Greenwood, P. F., George, S.C., and Hall, K., 1998, "Applications of Laser Micropyrolysis–Gas Chromatography–Mass Spectrometry", *Organic Geochemistry*, 29(5-7), PP. 1075-1089

http://www.duskedryingsystems.com/drying-systems.htm (last viewed, July 2010)

http://www.matche.com/, accessed July, 2010

http://www.sbmchina.com/product/grinding/ball-mill/ball_mill.php (last viewed, July 2010)

Kovac, R. J., O'Neil, D. J., 1989, "The Georgia Tech Entrained Flow Pyrolysis Process, Pyrolysis and Gasification", in: G.L. Ferrero, K. Maniatis, A. Buekens, A.V. Bridgwater (Eds.), *Pyrolysis and Gasification*, Elsevier, Amsterdam, PP. 169-179

Lede, J.; 1999, "Solar Thermochemical Conversion of Biomass", *Solar Energy*, 65, PP. 3-13

Levy, R. L., Wolf, C. J., and Fanter, D.L., 1972, "Temperature Rise Time and True Pyrolysis Temperature in Pulse Mode Pyrolysis Gas Chromatography", *Analytical Chemistry*, 44, PP. 38-42

Ling Zhang, 2004, "Sunlight Ancient and Modern: The Relative Energy Efficiency of Hydrogen from Coal and Current Biomass", MS Thesis, Georgia Institute of Technology

Liu, R., 1999, "Experimental Research on Rotating Cone Reactor for Biomass Flash Pyrolysis", *Proceedings of 99 International Conference on Agricultural Engineering,* Beijing, China

Lu. *et. al*, 2006, Expanding Market for Activated Carbon from Corn-to-Ethanol By-Products, Research Report, Illinois council of food and agricultural research (http://www.ilcfar.org/research/display.cfm?project_id=479, last viewed July, 2010).

Luo, Z., Wang, S., Liao, Y.F., Zhou, J.S., Gu, Y.L., Cen, K.F., 2004, "Research on Biomass Fast Pyrolysis for Liquid Fuel", *Biomass Bioenergy*, 26(5), PP. 455-462

Meruva, N. K., Metz, L. A., Goode, S. R., and Morgan, S. L., 2004, "UV Laser Pyrolysis Fast Gas Chromatography/Time-of-Flight Mass Spectrometry for Rapid Characterization of Synthetic Polymers: Instrument Development", *Journal of Analytical and Applied Pyrolysis*, 71(1), PP. 313-325

Meza, J., Gil, C. and Gonzales, A., 2008, "Drying Costs of Woody Biomass in a Semi-Industrial Experimental Rotary Dryer", *16th European Conference & Exhibition on Biomass for Energy*

Mohan, D., Pittman, C. U., and Steele, P. H., 2006, "Pyrolysis of Wood/Biomass for Bio-oil: A Critical Review ", *Energy Fuels*, 20, PP. 848-889

Mullaney, H. 2002, *Technical, Environmental and Economic Feasibility of Bio-Oil in New Hampshire's North Country,* Durham, NH: University of New Hampshire

Muzzy, J., *et. al.,* 2008, Biomass Pyrolysis, Stabilization and Characterization, Chevron Annual Report, Georgia Institute of Technology

Muzzy, J., *et. al.,* 2009, Biomass Pyrolysis, Stabilization and Characterization, Chevron Annual Report, Georgia Institute of Technology

Muzzy, J., *et. al.,* 2009, Biomass Pyrolysis, Stabilization and Characterization, Chevron Annual Report, Georgia Institute of Technology

Muzzy, J., *et. al*., 2010, Biomass Pyrolysis, Stabilization and Characterization, Chevron First Quarter Report, Georgia Institute of Technology

Muzzy, J., *et. al.,* 2010, Biomass Pyrolysis, Stabilization and Characterization, Chevron Second Quarter Report, Georgia Institute of Technology

Perry, R. H. and Green, D. W, Eds., 1997, *Perry's Chemical Engineer's Handbook*, 7th Edition, PP. 2-347 - 2-348

Peter, M., S., Timmerhaus, K., D., and West, R., E., "Plant Design and Economics for Chemical Engineers", 5th edition, McGraw Hill Inc., 2003

Reid, R., Prausnitz, J., and Sherwood, T., K., "The Properties of Gases and Liquids", 3rd edition, McGraw Hill Inc., 1977

Rowell, R. M., 1984, *The Chemistry of Solid Wood*, American Chemical Society: Washington DC

Seider, W., Seader, J. D., Lewin, D., and Widagdo, S., 2009, *Product and Process Design Principles- Synthesis, Analysis and Evaluation*, 3rd Edition, John Wiley Inc.

Shafizadeh, F. and Chin, P. P. S., 1977, *ACS Symposium*, Ser. No. 43, P. 57

Tang, L. and Huang, H., 2005, "Plasma Pyrolysis of Biomass for Production of Syngas and Carbon Adsorbent", *Energy Fuels*, 19(3), PP. 1174-1178

Thurner, F., and Mann, U., 1981, "Kinetic Investigation of Wood Pyrolysis", Industrial and Engineering Chemistry Process Design and Development, 20(3), PP. 482-488

Van de Velden, M., Baeyens, J., Brems, A., Janssens, B., and Dewil, R., 2010, "Fundamentals, Kinetics and Endothermicity of the Biomass Pyrolysis Reaction," *Renewable Energy*, 35, PP. 232-242

Wagenaar, B. M., Kuipers, J.A.M., Prins, W., Swaaij van, W.P.M., 1994, Energy fromBiomass, in: *Progress in Thermochemical Conversion*

Wagenaar, B., M., Prins, W., and Van Swaaij, W., P., M., 1994, "Flash Pyrolysis Kinetics of Pine Wood," *Fuel Processing Technology*, 36, PP. 291–302

White, R. L., 1991, "Microfurnace Pyrolysis Injector for Capillary Gas Chromatography", *Journal of Analytical and Applied Pyrolysis*, 18(3-4), PP. 269-276

Williams, P. T. and Horne, P. A., 1994, "Characterization of Oils from the Fluidized bed Pyrolysis of Biomass with Zeolite Catalyst Upgrading", *Biomass Bioenergy,* 7(1-6), PP. 223-236

Yaws, C. L., 1997, "Handbook of Chemical Compound Data for Process Safety: Comprehensive Safety and Health-Related Data for Hydrocarbons and Organic Chemicals: Selected Data for Inorganic Chemicals", Houston, TX

Yeh, A. and Jaw, Y.,1999, "Predicting residence time distributions in a single screw extruder from operating conditions," *Journal of Food Engineering*, 39, PP. 81-89